Studies on Triplet Energy Migration-based Photon Upconversion in Self-Assembled Molecular Systems

小川, 卓

https://doi.org/10.15017/1931868

出版情報：Kyushu University, 2017, 博士（工学）, 課程博士
バージョン：
権利関係：

Studies on Triplet Energy Migration-based Photon Upconversion in Self-Assembled Molecular Systems

Taku Ogawa

Department of Chemistry and Biochemistry
Graduates School of Engineering
KYUSHU UNIVERSITY

2018

Table of contents

Chapter 1 General introduction

1-1 Triplet-triplet annihilation based photon upconversion

Photon upconversion (UC), converting low-energy photons to higher-energy photons, is a key method for overcoming the efficiency limits of sunlight-powered devices, including photovoltaic cells and photochemical hydrogen production. Conventional methods, such as second harmonic generation and multi-step excitation of lanthanides, require light intensities that are orders of magnitude higher than the solar irradiance, and their low conversion efficiencies detract from their appeal.[1] However, a promising strategy developed in the last decade is workable with non-coherent, low-intensity light sources; namely, the sensitized triplet-triplet annihilation-based photon upconversion (TTA-UC) in multi-component donor (D)-acceptor (A) systems (Fig. 1-1-1).[2-13] This mechanism starts with the generation of donor (sensitizer) triplets (^{3}D*) by intersystem crossing (ISC) from the photogenerated singlet state (^{1}D*) and succeeding D-to-A triplet-triplet energy transfer (TET) to form optically dark, metastable acceptor triplets (^{3}A*). The subsequent diffusion and collision of two excited acceptor triplets generate a higher energy excited singlet state (^{1}A*) through TTA,[14] from which the upconverted fluorescence is emitted.

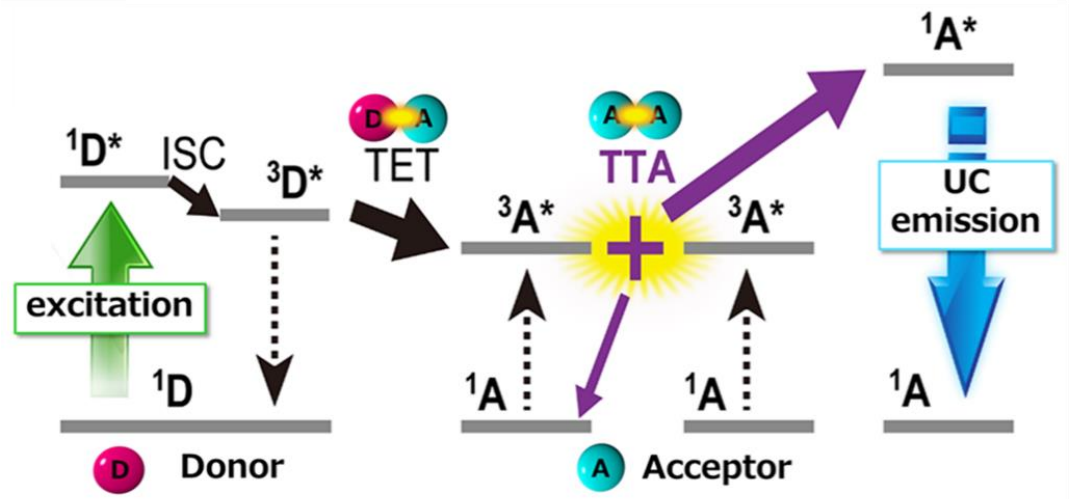

Figure 1-1-1. Scheme for the mechanism of TTA-UC. A triplet state of donor ^{3}D*, formed by intersystem crossing (ISC) from the photo-excited (green arrow) singlet state ^{1}D*, experiences triplet-triplet energy transfer (TET) to an acceptor triplet ^{3}A*. Two acceptor excited triplets annihilate to form a higher singlet energy level ^{1}A*, which consequently produces upconverted delayed fluorescence (blue arrow).

The finding of TTA phenomena dates back to the 1960s[15] but until recently, TTA process has been recognized as one of the deactivation processes to reduce the photocurrent in organic photovoltaic devices. However, there has been renewed attention in this decade by the demonstration of efficient TTA-UC under weak solar excitation.[2,4,16]

1-2 Requirement for application of TTA-UC

Because of the advantages mentioned in the previous section, TTA-UC is highly expected to be applied to the renewable energy production technologies or medical fields such as optogenetics. For applications of TTA-UC to the real world, there are several factors needed to be evaluated;

(i) Conversion wavelength
(ii) Upconversion quantum yield
(iii) Excitation intensity

For basic understanding and optimization of the TTA-UC mechanisms, these fundamental issues have been studied mainly in solution system. In this section, we overview recent investigations of TTA-UC studies from the viewpoint of these three factors.

1-2-1 Conversion wavelength

In the study of TTA-UC, the conversion wavelength is important for real-world applications. Especially, near-infrared (NIR) to visible (vis) and vis to ultra-violet (UV) upconversion are much coveted from the practical applications such as energy conversion devices or medical applications. Based on these demands, various types of donor and acceptor combination have been developed. Among these progresses, a novel triplet sensitization strategy arises and attracts much attention. This strategy aims to minimize the energy loss during S_1 to T_1 intersystem crossing of triplet donor molecules, which is fatal for NIR-to-vis or vis-to-UV UC.[17] One of the solution is to directly generate the triplet state of donor molecules with small or no energy loss. Thermally activated delayed fluorescence (TADF) molecules,[18-20] chalcogenide nanocrystals[20-24] or direct S-T absorption metal complexes[25,26] are typical candidates of this strategy. By utilizing these novel triplet sensitizers, moderately high UC quantum yield of several percents have been achieved for both NIR-to-vis and vis-to-UV UCs. Meanwhile, it is known that these donor molecules have short triplet lifetimes as compared with typical aromatic compounds. Therefore, to realize efficient TET, it is necessary to adopt a specific approach different from the conventional method which depends on molecular diffusion (Fig. 1-2-1).

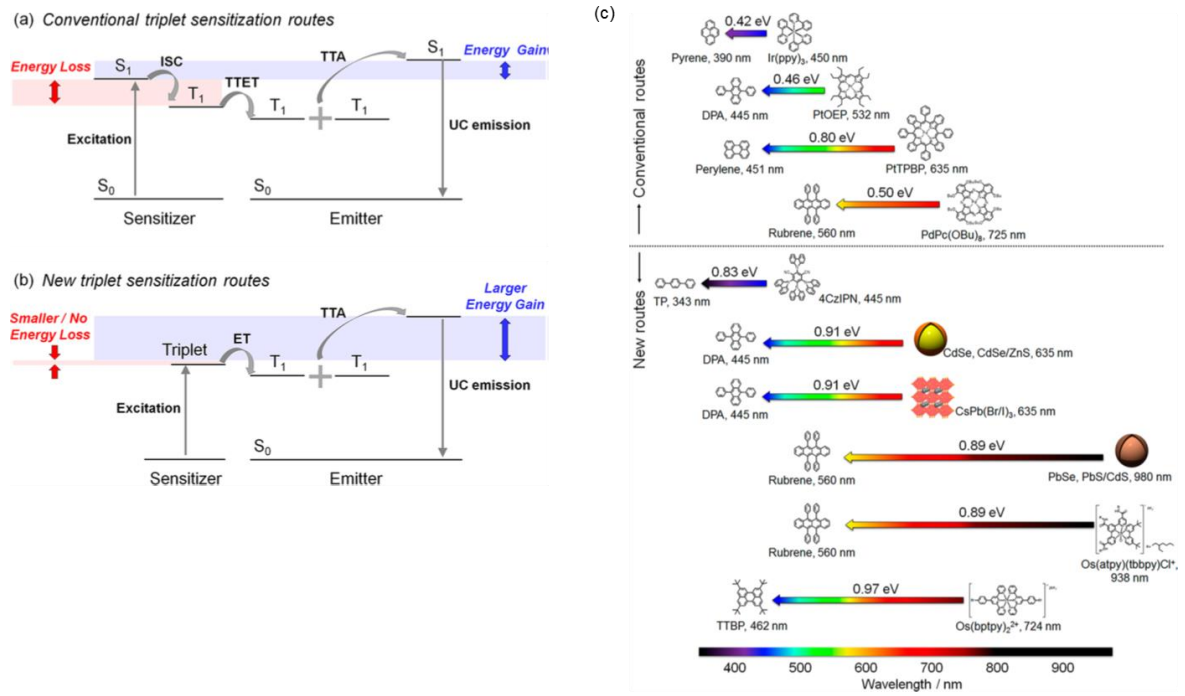

Figure 1-2-1. (a) Scheme for TTA-UC via conventional triplet sensitization routes that involve energy loss during sensitizer S_1-to-T_1 ISC. (b) Scheme for TTA-UC via new triplet sensitization routes that contain small or no energy loss due to the sensitizer ISC. (c) Representative combinations of sensitizer and emitter and their respective excitation and emission wavelengths. The widths of the anti-Stokes shift are also shown.[17]

1-2-2 Upconversion quantum yield

In general, a quantum yield is defined as the ratio of absorbed photons to emitted photons, and thus the maximum quantum yield (Φ_{UC}) for the bimolecular TTA-UC process is 50%. However, many reports multiply this value by 2 to set the maximum quantum yield at 100%. To avoid the confusion between these different definitions, the UC quantum yield is written as Φ_{UC}' (= $2\Phi_{UC}$) when the maximum efficiency is normalized to 100%. Φ_{UC}' is represented by the following equation,

$$\Phi_{uc}' = f\,\Phi_{ISC}\,\Phi_{ET}\,\Phi_{TTA}\,\Phi_{A} \qquad (1\text{-}2\text{-}1)$$

where Φ_{ISC}, Φ_{ET}, Φ_{TTA}, and Φ_{A} represent the quantum efficiencies of donor ISC, donor-to-acceptor TET, TTA, and acceptor emission.[11,27] The parameter f is the statistical probability for obtaining a singlet excited state after the annihilation of two triplet states. As can be seen from this equation, the improvement of the quantum yield of each process is important to achieve high Φ_{UC}'.

First, Φ_{ISC} mainly depends on the performance of the donor. As aforementioned in the previous section, the donor molecules can create their triplet state with high efficiency mainly thanks to the spin-orbital coupling promoted by the heavy atom effect, respectively.[17,27] In typical solution systems in which energy transfer process relies on the diffusion of molecules, Φ_{ET} can be quantitative because of the sufficiently long triplet lifetime of the donor molecules under optimal concentration conditions. The parameter Φ_{TTA} varies depending on the concentration of excited triplet acceptor species in the system. It increases as the excitation light is intensified, and theoretically, reaches to 1. The requirement of reducing the excitation light intensity necessary for achieving Φ_{TTA} of 1 will be described later. Regarding Φ_{A}, effects of reabsorption by the donor molecules and concentration quenching should take into account when the sample conditions are optimized.

Finally, the parameter *f* is the statistical probability for obtaining a singlet excited state after the annihilation of two triplet states. The possible energy levels involved in transition process are mainly S_1, T_2, and quintet Q. Among them, the energy transferred to T_2 and Q is immediately inactivated and go back to the ground state, lowering *f* factor. However, since Q is actually located at a very high energy level, its formation probability can be considered to be zero. Therefore, only S_1 and T_2 are taken into consideration in practice. Since T_2 is triply degenerated, the theoretical maximum value of *f* was initially considered to be 2/5 when considering the transition probabilities to S_1 and T_2 are equivalent.[3,28] However, from recent experimental facts, Monguzzi and colleagues reported that $f = 1$ could be achieved by using an appropriate acceptor molecule for the relationship between T_2 and $2T_1$ levels.[29] According to this study, since the energy of T_2 in utilized acceptor molecule, perylene, is larger than that of the sum of $2T_1$ and thermal energy, the energy after TTA-UC all transits to S_1, resulting in $f = 1$ (Fig. 1-2-2). Along with this fact, UC emission quantum yield Φ_{UC} also reported the highest value of 0.38 so far.

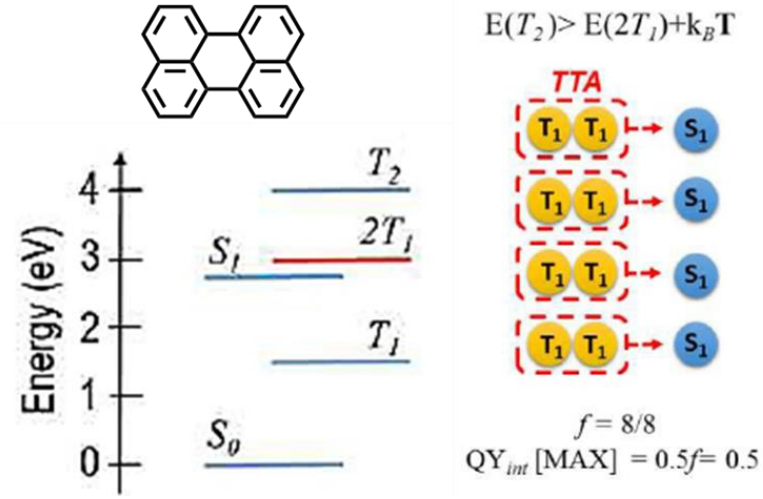

Figure 1-2-2. Molecular structure and energy levels of perylene. The right column shows the sketch of the TTA process involving four triplet pairs. In this case, where the T_2 level is not energetically accessible, the collision of four triplet pairs produces four singlet excited states. Thus $f = 8/8 = 1$, with a predicted maximum internal quantum yield as 0.5.[29]

1-2-3 Excitation intensity

In the practical applications of UC light emission, lower excitation intensity for ideal UC efficiency is preferable if the same UC quantum yield can be obtained. For example, from the viewpoint of utilizing sunlight, the sum of the energy irradiated from the sun is about 100 mW cm^{-2}, and this value is naturally reduced in a specific wavelength region.[16] Also, in biological applications, it should be avoided to irradiate a human body with a strong coherent laser. To evaluate the excitation light intensity necessary for efficient TTA process, a figure-of-merit parameter called threshold excitation intensity, I_{th}, is proposed.[30] I_{th}, is the excitation light intensity at which Φ_{TTA} is 0.5, which is derived from the relationship between the UC emission intensity and the excitation light intensity. When the UC emission intensity is plotted against the excitation light intensity as a double-logarithmic chart, I_{th} value is provided as a changing point of the slope from 2 to 1, which is derived from the following rate equations:[30]

$$\partial T_D/\partial t = \alpha(E)I_{exc} - k_D^T T_D - k_{tr}T_D \qquad (1\text{-}2\text{-}2a)$$

$$\partial T_A/\partial t = k_{tr}T_D - k_A^T T_A - \gamma_{TTA}T_A^2 \qquad (1\text{-}2\text{-}2b)$$

$$\partial S_A/\partial t = 0.5f\gamma_{TTA}T_A^2 - k_A^S S_A \qquad (1\text{-}2\text{-}2c)$$

where T_D and T_A represent the population of the donor and acceptor excited triplets, respectively and S_A shows acceptor excited singlets. The α(E) and I_{exc} show the absorption coefficient of the donor and excitation intensity. γ_{TTA} is the rate constant of the TTA, and k is the decay rate constant, and the subscripts D, A represent donor and acceptor, respectively. Equation (1-2-2) can be used to solve the steady-state conditions. When the excitation light intensity is weak, it can be regarded as $k_A^T T_A \gg \gamma_{TTA}T_A^2$ because the thermal deactivation of the acceptor triplet is dominant, and SA can be described as;

$$S_A = 0.5f\frac{\gamma_{TTA}}{k_A^S}\left[\frac{k_{tr}/k_A^T}{k_D^T + k_{tr}}\right]^2 [\alpha(E)I_{\mathrm{exc}}]^2 \propto I_{exc}^2 \qquad (1\text{-}2\text{-}3)$$

where the UC emission intensity is proportional to the square of the excitation light intensity. Therefore, the slope of the double logarithmic plot becomes 2. On the other hand, under conditions where the excitation light intensity is sufficiently strong, T_A becomes large and it can be regarded as $k_A^T T_A \ll \gamma_{TTA}T_A^2$ because T_A spices immediately causing TTA with the neighboring T_A. Then the equation (1-2-2) can be solved as;

$$S_A = 0.5f\frac{1}{k_A^S}\left[\frac{k_{tr}}{k_D^T + k_{tr}}\right]\alpha(E)I_{\mathrm{exc}} \propto I_{exc} \qquad (1\text{-}2\text{-}4)$$

where the UC emission intensity is directly proportional to the excitation light intensity, leading to the slope of the logarithmic plot becomes 1.

I_{th} value is obtained from the intersection of these two lines with slopes 2 and 1, and that is finally represented by:

$$I_{th} = (\alpha(E)\Phi_{ET}8\pi D_T a_0 {\tau_T}^2)^{-1} \qquad (1\text{-}2\text{-}5)$$

where τ_T is the lifetime of the acceptor triplet and triplet diffusion constant D_T is described as $\gamma_{TT} = \sqrt{8\pi D_T}$ for three-dimensional diffusion systems.To understand the meaning of I_{th} value, it is noteworthy that diffusion constant D_T is included in the equation. Considering the applied approximate expression, it is apparent that I_{th} can be minimized when the value of D_T becomes large. This can be understood because the faster the molecular diffusion, the larger the probability of molecular collisions. From this viewpoint, low I_{th} is expected for TTA-UC exhibiting fast molecular diffusion in a low-viscosity solvent. In the THF solution system using PtOEP as a donor molecule and 9,10-diphenylanthracene (DPA) as an acceptor molecule, a considerably low value of I_{th} = 0.3 mWcm^{-2} has been reported.[11]

As mentioned above, TTA-UC in solution has been studied so far by taking advantage of the fast diffusion of component molecules. As chromophores utilized for TTA in solutions usually exhibit less intermolecular interactions, it is possible to make use of the inherent high emission quantum yield under the molecularly dispersed condition. Moreover, the fast molecular diffusion in a low viscous solvent (typically D_T of ~10^{-5} cm^{2}s^{-1} order)[31] can efficiently cause the molecular collision process. However, for the most of applications of TTA-UC to the real-world devices, solid-state systems are highly preferable since they are free from volatile and toxic organic solvents. In such solid systems, molecules involved in TTA would not be able to diffuse freely as the ones in solution. Therefore, in order to achieve the ideal conditions as discussed in this section, a strategy different from the conventional way is required.

1-3 Energy migration-based TTA-UC

To achieve solid-state TTA-UC, several strategies to overcome the fundamental issues have been proposed in current TTA-UC studies. One is described as molecular diffusion-based TTA-UC in rubbery polymer matrices. Castellano, Weder, Kim, and coworkers have reported highly efficient TTA-UC by dispersing donor and acceptor dyes in soft rubbery polymers,[9,32-34] but the inevitably slow molecular diffusion in the solid-state remains as an essential challenge for further improvement.

On the other hand, a few groups have proposed the triplet energy migration-based photon upconversion mechanism (TEM-UC) for solid-state upconverters. In these systems, donor molecules ared doped in acceptor assemblies, thus promoting TET from the donor to the adjacent acceptor molecules and consequent triplet energy migration in densely aligned acceptor arrays (Fig. 1-2-3).[35-41] In this section, the merits and challenges of TEM-UC in current studies will be provided.

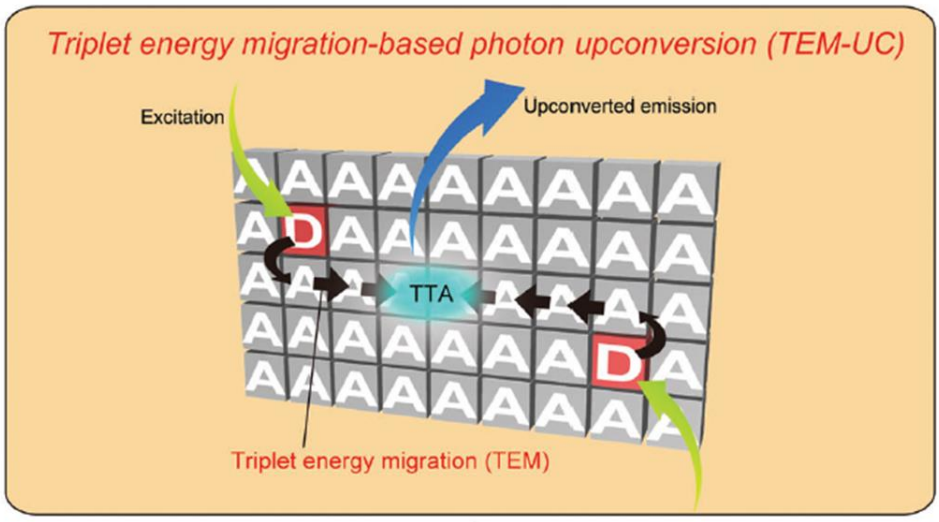

Figure 1-2-3. Scheme of the concept of triplet energy migration-based photon upconversion (TEM-UC). The objects marked D and A represent triplet donor and acceptor molecules, respectively. In this system, excitation (green arrow) of donor molecules is followed by a sequence of TET, TEM in the acceptor arrays, TTA between the excited acceptors, and higher energy UC emission (blue arrow).[39]

1-3-1 Advantages of TEM-UC

Oxygen barrier property

The UC emission is sensitive to air because the triplet excited state is readily quenched by molecular oxygen and this is inevitable in ambient solution systems. In recent year, several methods to avoid this situation have been proposed. One strategy is to introduce active oxygen-consuming materials into the system. The consumption of oxygen by chemical reaction lowers the oxygen concentration around the upconverter and makes it possible to observe stable UC emission even under ambient conditions. For example, oleic acid and linoleic acid with unsaturated double bonds[42,43] and hyperbranched unsaturated polyphosphate[33,44] are typical examples employed in this strategy. However, considering the fact that the scavenger is gradually consumed by the chemical reaction, the long-term stability of these systems remains unclear.

Another strategy is to suppress penetration and diffusion of oxygen by dispersing chromophores in a rigid or a highly viscous medium. In the former case, by designing an acceptor molecule to form an amorphous glass phase, oxygen concentration in the system can be reduced.[36] In latter case, the introduction of non-covalent intermolecular interactions such by hydrogen bonding in matrixes improves their cohesive energy density, and consequently the diffusion of oxygen can be suppressed.[9,32,45,46] This has been achieved with hydrogen bonding polymers with high glass transition temperatures and non-covalent gels.

The TEM-UC system can make full use of the advantages of such a rigid medium. This is because the application of TEM makes it possible to realize expect efficient TTA-UC even in a rigid medium due to the triplet diffusion being independent from the molecular diffusion. In fact, TEM-UC in the gel utilizing non-covalent bonding showed both high oxygen stability and good I_{th} value at the same time (Fig. 1-3-1).[45]

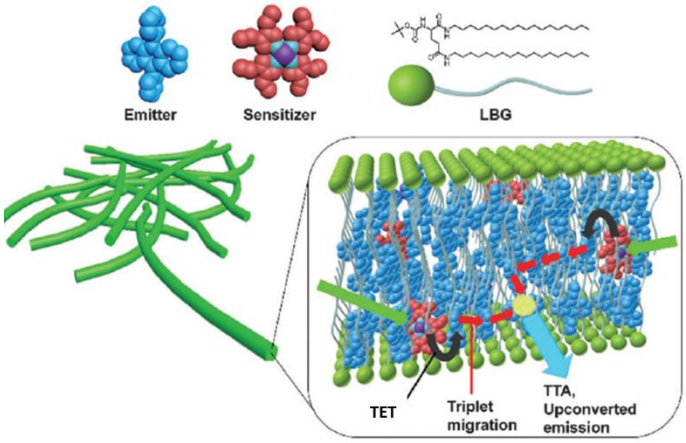

Figure 1-3-1. A schematic representation of the unit supramolecular structure of the upconversion gel system. Donor (red) and acceptor (blue) molecules are incorporated in the LBG nanofibers as extended domains. The donor molecules are excited by long-wavelength light, followed by a sequence of TTET, TEM, TTA and delayed fluorescence from the upconverted singlet state of acceptor molecules.

Triplet diffusion coefficient

In the TEM-UC system, the triplet energy transfer does not occur via molecular diffusion, but rather the diffusion of triplet energy itself. The triplet energy transfer occurs via the electron exchange mechanism, so sufficient overlap of wave functions is required between the donor and acceptor for TET, and also in-between acceptors for TEM. The typical Dexter radius is considered to be less than 1 nm.[31] In condensed materials, especially in single crystals, very fast triplet diffusion occurs if such proper conditions are satisfied.[47] For example, the triplet diffusion coefficient D_T of (0.5–2) × 10^{-4} for anthracene single crystals[48,49] or 1.3 × 10^{-4} for pyrene single crystals[50] have been reported. In such media, it is to note that μm-order-triplet diffusion lengtsh have been achieved.

Although low I_{th} is observed in the solution system, the intensity of the excitation light for exerting the maximum Φ_{UC}' is typically one order of magnitude larger than I_{th}. However, in the solution system, as the diffusion of molecules determines the triplet diffusion coefficient, further improvement in I_{th} under conditions of realistic acceptor concentration cannot be expected. On the other hand, if high triplet diffusion coefficient as mentioned above is realized in the TEM-UC system, it has the potential to maximize the quantum yield under an extremely low excitation light intensity, which has been difficult in the past solution system.

For the TEM-UC-based researches in recent years, Kamada, Hanson, and Kimizuka groups have reported low I_{th} values typically in ca. 10 mWcm^{-2}.[38,40,51] These values are actually still insufficient, but the researches pointed at the right direction for TEM-UC study.

Triplet lifetimes

As another point of view, triplet lifetime is a significant parameter which affects I_{th}. The reason can be understood as their quadratic dependence of I_{th} on the triplet lifetime of the acceptor molecules, which described in Equation (1-2-5). Generally, in solution media, the rate constant for nonradiative deactivation of the triplet species increases due to the thermal relaxation processes including rotation and vibration between covalent bonds, resulting in shorter triplet lifetimes. On the other hand, owing to the suppression of such motions in the solid state, it is expected that a very long triplet lifetime is realized as compared with that in solution. For example, the triplet lifetime of 20-22 ms for anthracene single crystals has been reported[52] whereas that value was reduced to ca. 1.7 ms in diluted solutions.[53]

1-3-2 Challenging issues for TEM-UC

As mentioned in the previous section, the potential of TEM-UC could not be fully extended with the conventional molecular diffusion-based TTA-UC systems. Meanwhile, there exist some challenging issues needed to be overcome with the TEM-UC system. These problems arise mainly because two different molecules, donor, and acceptor, should coexist in the condensed media for TTA-UC. In this section, these issues will be summarized.

Phase separation

The donor and acceptor molecules used for TTA-UC exert inherent structural differences and accordingly they show different optical characteristics such as absorption and emission regions. In particular, the difference is remarkable in the new type of donor molecules recently developed for NIR-to-vis and vis-to-UV UCs. Therefore, in the TEM-UC system, especially for a crystalline media in which fast and efficient triplet energy diffusion is expected, it is necessary to avoid phase separation between the donor and acceptor molecule. In fact, phase separation has been observed in typical chromophore combination for TTA-UC (9,10-diphenylanthracene (DPA) and platinum octaethylporphyrin (PtOEP) or their derivatives), which resulted in a decrease in the energy transfer efficiency and subsequently decrease in the UC quantum yield. The system using molecular crystals reported by Monguzzi and coworker (Fig. 1-3-2a)[11] or chromophore-blanched copolymer system developed by Weder and Simon et al (Fig. 1-3-2b)[54] are typical examples. In these systems, they did not mention the UC yields probably because the values were too low to be determined.

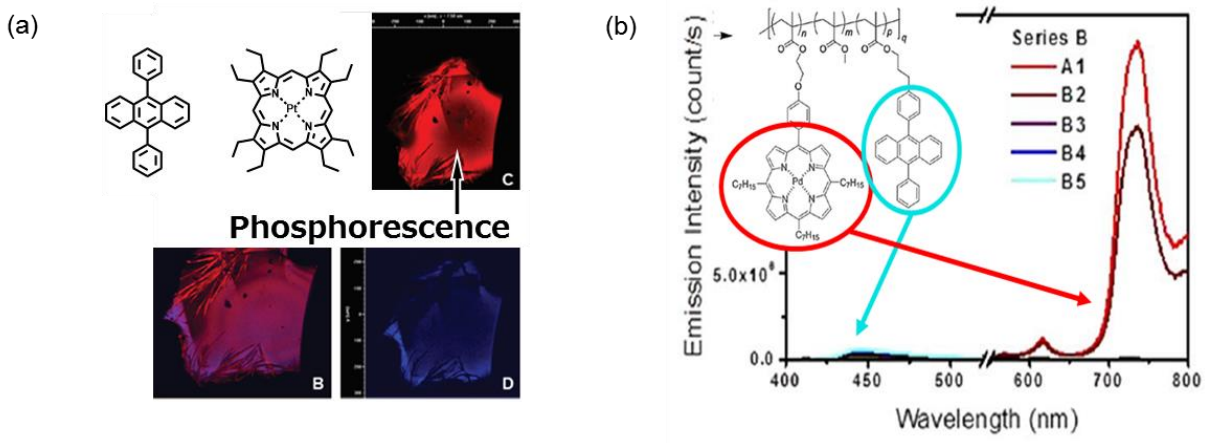

Figure 1-3-2. Photoluminescence from TTA-UC pairs in condensed media. (a) DPA-PtOEP molecular crystal system and (b) chromophore-blanched copolymer system. In both cases, strong phosphorescence from donor molecules has been observed.

Deactivation pathways for upconverted energy

In recent years, a few strategies have been reported to overcome the phase separation problem in crystalline TEM-UC systems. For example, the modification of acceptor units with flexible alkyl chains can create room for donor molecules to be accommodated in acceptor crystals.[38] This strategy, unfortunately, resulted in detracting the advantages of crystalline systems; the reduction of crystal regularity was necessary for homogeneous donor accommodation, which inhibited the rate and efficiency of energy diffusion. In such condition, defects caused by disordered structures were suspected to act as quenching sites for excitons and largely reduced the UC efficiency.

In another point of view, owing to the condensed material characteristics of TEM-UC in the solid state, some specific deactivation pathways exist through which the UC quantum yield degrades. Although the large orbital overlap among acceptor moieties is required for the fast triplet energy migration, it often decreases the acceptor fluorescence efficiency through various non-radiative deactivation pathways in the assembled state. In addition, since the donor and acceptor molecules are highly condensed, a certain part of the upconverted singlet energy is consumed by undesirable back energy transfer from the acceptor to the donor. The last issue should become more serious for new triplet donors such as semiconductor nanocrystals and singlet-to-triplet (S-T) absorption metal complexes, that are recently developed for NIR-to-vis TTA-UC, due to the large overlapping between the donor absorption and the acceptor emission.[17,21-24,26,55] Therefore, development of a rational strategy is highly desired to solve these issues based on the understanding of exciton behaviors in the condensed state.

1-4 Survey of this thesis

The main purpose of this thesis is to establish a rational design for the triplet energy migration-based photon upconversion systems by introducing the molecular self-assembly concept.

Chapter 2 describes that the first supramolecular triplet-energy-harvesting system that shows energy-migration-based TTA-UC instead of the conventional molecular-diffusion-based mechanism. A newly developed lipophilic 9,10-diphenylanthracene-based emitter molecule functionalized with multiple hydrogen-bonding moieties spontaneously coassembled with a triplet sensitizer in organic media, showing efficient triplet sensitization and subsequent triplet energy migration among the preorganized chromophores. This supramolecular light-harvesting system shows the high UC quantum yield of 30% optimized at low excitation power in deaerated conditions. Significantly, the UC emission largely remains even in an air-saturated solution, and this approach is facilely applicable to organogel and solid-film systems.

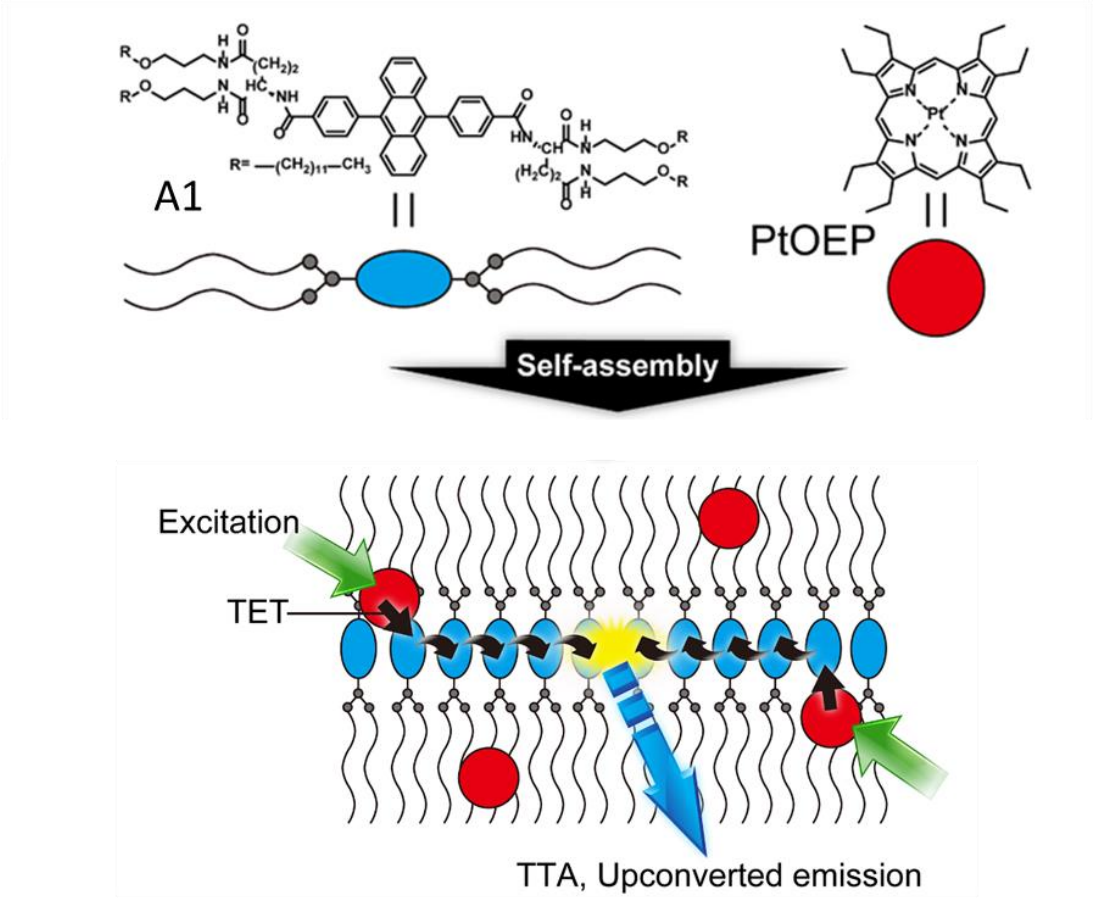

Figure 1-4-1. A graphical abstract for Chapter 2, entitled ''*Highly Efficient Photon Upconversion in Self-Assembled Light-Harvesting Supramolecular Systems*''.

Chapter 3 describes that a kinetically-controlled crystal growth approach which improved the dispersibility of donors in acceptor crystals and consequently increased the efficiency of TEM-UC. We applied the kinetic control concept to improve the miscibility of donor PtOEP and acceptor DPA in nanocrystals. For this, we adopted a colloid chemistry approach; different condition of tetrahydrofuran (THF) solutions of DPA-PtOEP were injected into aqueous cetyltrimethylammonium bromide (CTAB). Upon the diffusion of injected THF solution into the aqueous phase, nucleation of water-insoluble aromatic crystals occured. Absorption of CTAB molecules on the resulting crystal surfaces during the crystal growing process would reduce their interfacial energy, thus enhancing the dispersion stability of the crystals. It was found that increasing the concentration of DPA-PtOEP caused faster crystallization of DPA, which allowed the PtOEP molecules to be kinetically trapped in the DPA crystals with improved dispersibility.

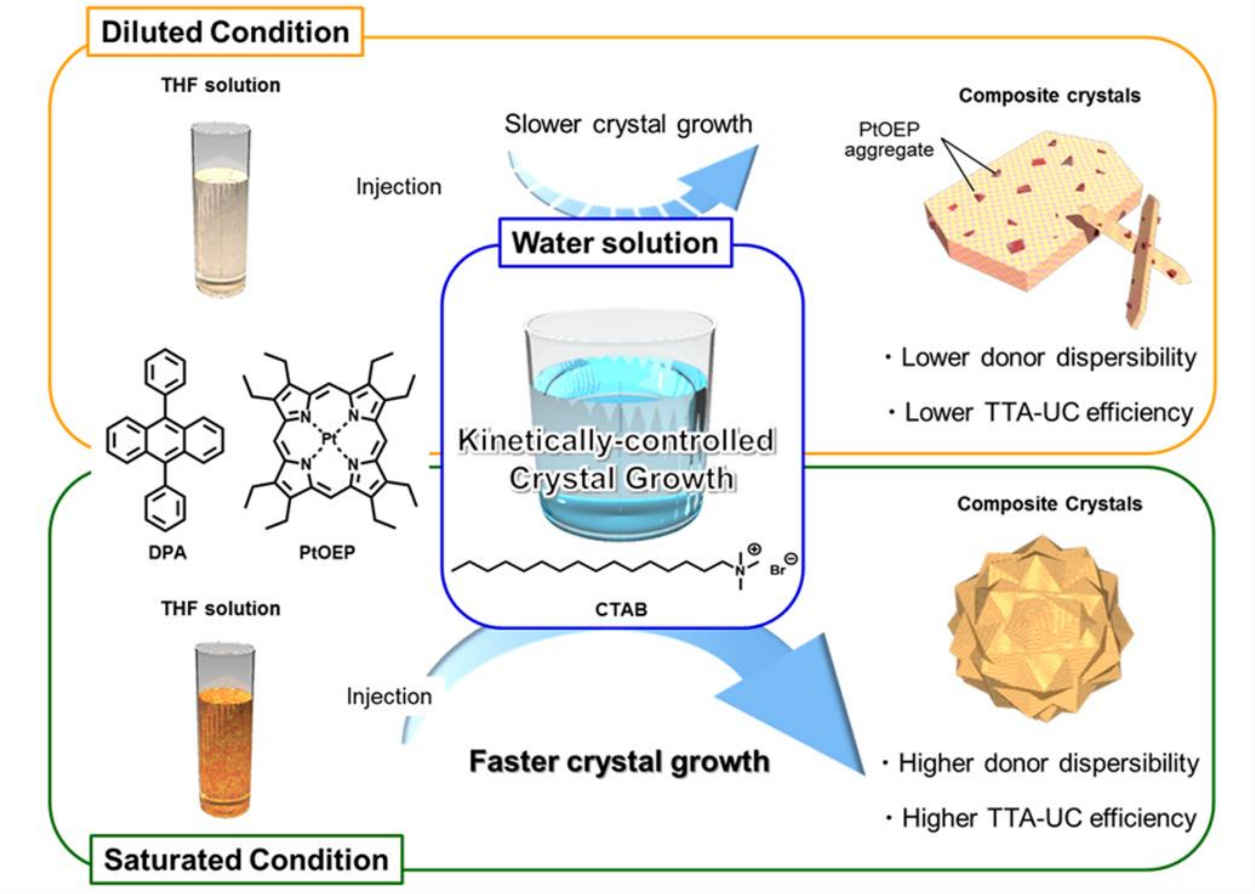

Figure 1-4-2. A graphical abstract for Chapter 3, entitled "*Kinetically-Controlled Crystal Growth Approach to Enhance Triplet Energy Migration-based Photon Upconversion*".

Chapter 4 describes that ionic interactions can realize aggregation-free dispersion of donor molecules in acceptor ionic crystals without losing the high crystal regularity. As a proof-of-concept, one of the simplest anionic acceptors 9,10-anthracenedicarboxylate (ADC) was combined with dicyclohexyl ammonium (DCA) cations to form ionic crystals (DCA)2ADC. When the ionic crystals were prepared in the presence of an anionic donor, palladium mesoporphyrin (PdMesoP), the donor molecules were successfully introduced into the crystals. Remarkably, accommodated donor molecules were found to be molecularly dispersed, resulting in quantitative donor-to-acceptor TET. The impact of the crystal defects upon TTA-UC properties was proven for the first time by comparing the UC efficiency and the emission decay profiles of single crystals and mechanically-ground powder samples. This work offers a clear answer to the long-standing questions; what makes the UC efficiency in crystalline systems low, and how to rationally achieve efficient UC in solid crystals.

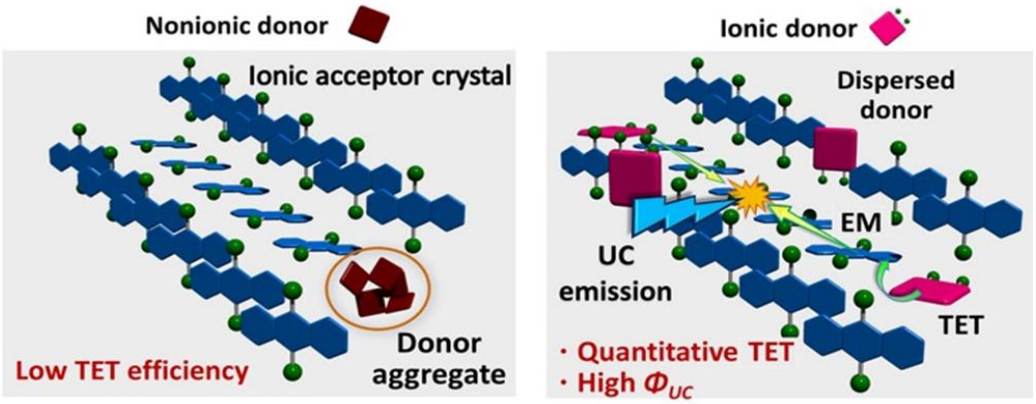

Figure 1-4-3. A graphical abstract for Chapter 4, entitled ‘‘*Rational Strategy for Photon Upconversion Crystals: Aggregation-free Sensitizer Accommodation in Ionic Crystals with Less Defects*’’.

Chapter 5 describes that the UC efficiency can be largely improved by the introduction of a third component, highly fluorescent singlet energy collector, to the lipophilic acceptor A2 and PtOEP combination for improving the fluorescence quantum yield and avoiding the back energy transfer to the donor. In this work, we introduced, 2,5,8,11-tetra-*tert*-butylperylene (TTBP) an energy collector, whose absorption has a larger spectral overlapping with the acceptor fluorescence than that of the donor-acceptor two-component system. By the addition of TTBP, the UC efficiency was successfully improved from 4.2% to 9.0%. To understand this observation, we carried out various experiments to study the basic behavior of excitons in the condensed films. By analyzing the dynamics of acceptor singlet state, we found that the delocalized singlet excitons with a long lifetime of 29.7 ns give a significantly long singlet diffusion length of 26.1 nm. Furthermore, since the donor PtOEP and the collector TTBP are fixed in a spatially separated manner in the A2 film, the singlet back energy transfer from TTBP to PtOEP was completely suppressed, which has been difficult to achieve with the previous donor-acceptor two-component systems.

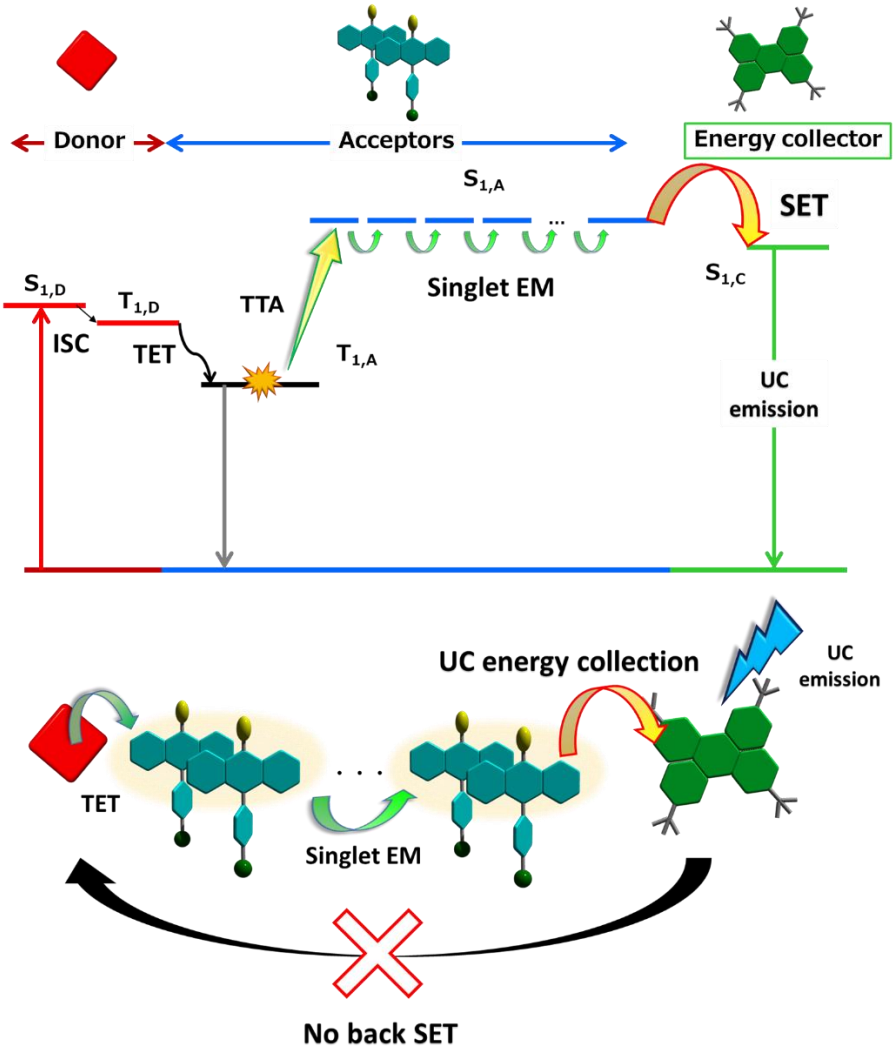

Figure 1-4-3. A graphical abstract for Chapter 5, entitled ‘‘*Donor-Acceptor-Collector Ternary Crystalline Films for Efficient Solid-State Photon Upconversion*’’.

References

(1) F. Auzel, *Chem. Rev.*, 2004, **104**, 139-173.

(2) S. Baluschev, T. Miteva, V. Yakutkin, G. Nelles, A. Yasuda and G. Wegner, *Phys. Rev. Lett.*, 2006, **97**, 143903.

(3) Y. Y. Cheng, B. Fuckel, T. Khoury, R. G. C. R. Clady, M. J. Y. Tayebjee, N. J. Ekins-Daukes, M. J. Crossley and T. W. Schmidt, *J. Phys. Chem. Lett.*, 2010, **1**, 1795-1799.

(4) T. N. Singh-Rachford and F. N. Castellano, *Coordin. Chem. Rev.*, 2010, **254**, 2560-2573.

(5) W. H. Wu, H. M. Guo, W. T. Wu, S. M. Ji and J. Z. Zhao, *J. Org. Chem.*, 2011, **76**, 7056-7064.

(6) M. Haring, R. Perez-Ruiz, A. Jacobi von Wangelin and D. D. Diaz, *Chem. Commun.*, 2015, **51**, 16848-16851.

(7) Z. Y. Huang and M. L. Tang, *J. Am. Chem. Soc.*, 2017, **139**, 9412-9418.

(8) Y. C. Simon and C. Weder, *J. Mater. Chem.*, 2012, **22**, 20817-20830.

(9) J. H. Kim, F. Deng, F. N. Castellano and J. H. Kim, *Chem. Mater.*, 2012, **24**, 2250-2252.

(10) Q. Liu, T. S. Yang, W. Feng and F. Y. Li, *J. Am. Chem. Soc.*, 2012, **134**, 5390-5397.

(11) A. Monguzzi, R. Tubino, S. Hoseinkhani, M. Campione and F. Meinardi, *Phys. Chem. Chem. Phys.*, 2012, **14**, 4322-4332.

(12) H. Ono, T. Hosokawa, K. Ichii, S. Matsuo, H. Nasu and M. Yamada, *Opt. Express*, 2015, **23**, 27405-27418.

(13) V. Gray, D. Dzebo, M. Abrahamsson, B. Albinsson and K. Moth-Poulsen, *Phys. Chem. Chem. Phys.*, 2014, **16**, 10345-10352.

(14) B. B. Song, H. Zhang, Y. P. Miao, W. Lin, J. X. Wu, H. F. Liu, D. L. Yan and B. Liu, *Opt. Express*, 2015, **23**, 15372-15379.

(15) C. A. Parker, C. G. Hatchard and T. A. Joyce, *Nature*, 1965, **205**, 1282-1284.

(16) T. F. Schulze and T. W. Schmidt, *Energy Environ. Sci.*, 2015, **8**, 103-125.

(17) N. Yanai and N. Kimizuka, *Acc. Chem. Res.*, 2017, **50**, 2487-2495.

(18) T. C. Wu, D. N. Congreve and M. A. Baldo, *Appl Phys Lett*, 2015, **107**.

(19) N. Yanai, M. Kozue, S. Amemori, R. Kabe, C. Adachi and N. Kimizuka, *J. Mater. Chem. C*, 2016, **4**, 6447-6451.

(20) M. Tabachnyk, B. Ehrler, S. Gelinas, M. L. Bohm, B. J. Walker, K. P. Musselman, N. C. Greenham, R. H. Friend and A. Rao, *Nat. Mater.*, 2014, **13**, 1033-1038.

(21) Z. Y. Huang, X. Li, M. Mahboub, K. M. Hanson, V. M. Nichols, H. Le, M. L. Tang and C. J. Bardeen, *Nano Lett.*, 2015, **15**, 5552-5557.

(22) Z. Y. Huang, D. E. Simpson, M. Mahboub, X. Li and M. L. Tang, *Chem. Sci.*, 2016, **7**, 4101-4104.

(23) K. Okumura, K. Mase, N. Yanai and N. Kimizuka, *Chem. -Eur. J.*, 2016, **22**, 7721-7726.

(24) C. Mongin, S. Garakyaraghi, N. Razgoniaeva, M. Zamkov and F. N. Castellano, *Science*, 2016, **351**, 369-372.

(25) S. Amemori, Y. Sasaki, N. Yanai and N. Kimizuka, *J. Am. Chem. Soc.*, 2016, **138**, 8702-8705.

(26) Y. Sasaki, S. Amemori, H. Kouno, N. Yanai and N. Kimizuka, *J. Mater. Chem. C*, 2017, **5**, 5063-5067.

(27) T. W. Schmidt and F. N. Castellano, *J. Phys. Chem. Lett.*, 2014, **5**, 4062-4072.

(28) Y. Y. Cheng, T. Khoury, R. G. C. R. Clady, M. J. Y. Tayebjee, N. J. Ekins-Daukes, M. J. Crossley and T. W. Schmidt, *Phys. Chem. Chem. Phys.*, 2010, **12**, 66-71.

(29) S. Hoseinkhani, R. Tubino, F. Meinardi and A. Monguzzi, *Phys. Chem. Chem. Phys.*, 2015, **17**, 4020-4024.

(30) A. Monguzzi, J. Mezyk, F. Scotognella, R. Tubino and F. Meinardi, *Phys. Rev. B*, 2008, **78**, 195112.

(31) A. Monguzzi, R. Tubino and F. Meinardi, *Phys. Rev. B*, 2008, **77**, 155122.

(32) R. R. Islangulov, J. Lott, C. Weder and F. N. Castellano, *J. Am. Chem. Soc.*, 2007, **129**, 12652-12653.

(33) F. Marsico, A. Turshatov, R. Pekoz, Y. Avlasevich, M. Wagner, K. Weber, D. Donadio, K. Landfester, S. Baluschev and F. R. Wurm, *J. Am. Chem. Soc.*, 2014, **136**, 11057-11064.

(34) S. H. Lee, D. C. Thevenaz, C. Weder and Y. C. Simon, *J. Polym. Sci. A Polym. Chem.*, 2015, **53**, 1629-1639.

(35) S. Baluschev, V. Yakutkin, G. Wegner, B. Minch, T. Miteva, G. Nelles and A. Yasuda, *J. Appl. Phys.*, 2007, **101**, 023101.

(36) R. Vadrucci, C. Weder and Y. C. Simon, *J. Mater. Chem. C*, 2014, **2**, 2837-2841.

(37) H. Goudarzi and P. E. Keivanidis, *J. Phys. Chem. C*, 2014, **118**, 14256-14265.

(38) M. Hosoyamada, N. Yanai, T. Ogawa and N. Kimizuka, *Chem.-Eur. J.*, 2016, **22**, 2060-2067.

(39) N. Yanai and N. Kimizuka, *Chem. Commun.*, 2017, **53**, 655-655.

(40) K. Kamada, Y. Sakagami, T. Mizokuro, Y. Fujiwara, K. Kobayashi, K. Narushima, S. Hirata and M. Vacha, *Mater. Horiz.*, 2017, **4**, 83-87.

(41) T. Ogawa, N. Yanai, H. Kouno and N. Kimizuka, *J. Photon. Energy*, 2017, **8**, 022003.

(42) J. H. Kim and J. H. Kim, *J. Am. Chem. Soc.*, 2012, **134**, 17478-17481.

(43) Q. Liu, B. R. Yin, T. S. Yang, Y. C. Yang, Z. Shen, P. Yao and F. Y. Li, *J. Am. Chem. Soc.*, 2013, **135**, 5029-5037.

(44) M. A. Filatov, E. Heinrich, D. Busko, I. Z. Ilieva, K. Landfester and S. Baluschev, *Phys. Chem. Chem. Phys.*, 2015, **17**, 6501-6510.

(45) P. F. Duan, N. Yanai, H. Nagatomi and N. Kimizuka, *J. Am. Chem. Soc.*, 2015, **137**, 1887-1894.

(46) A. Monguzzi, F. Bianchi, A. Bianchi, M. Mauri, R. Simonutti, R. Ruffo, R. Tubino and F. Meinardi, *Adv. Energy Mater.*, 2013, **3**, 680-686.

(47) O. V. Mikhnenko, P. W. M. Blom and T. Q. Nguyen, *Energy Environ. Sci.*, 2015, **8**, 1867-1888.

(48) V. Ern, A. Suna, Tomkiewi.Y, P. Avakian and R. P. Groff, *Phys. Rev. B*, 1972, **5**, 3222-&.

(49) P. Avakian and R. E. Merrifield, *Phys. Rev. Lett.*, 1964, **13**, 541.

(50) S. Arnold, J. L. Fave and M. Schott, *Chem. Phys. Lett.*, 1974, **28**, 412.

(51) T. Dilbeck, J. C. Wang, Y. Zhou, A. Olsson, M. Sykora and K. Hanson, *J. Phys. Chem. C*, 2017, **121**, 19690-19698.

(52) Y. Lupien and D. F. Williams, *Mol. Cryst.*, 1968, **5**, 1-&.

(53) K. H. Grellmann and H. G. Scholz, *Chem. Phys. Lett.*, 1979, **62**, 64-71.

(54) S. H. Lee, D. C. Thevenaz, C. Weder and Y. C. Simon, *J. Polym. Sci. Pol. Chem.*, 2015, **53**, 1629-1639.

(55) M. F. Wu, D. N. Congreve, M. W. B. Wilson, J. Jean, N. Geva, M. Welborn, T. Van Voorhis, V. Bulovic, M. G. Bawendi and M. A. Baldo, *Nat. Photon.*, 2016, **10**, 31-34.

Chapter 2 Highly Efficient Photon Upconversion in Self-Assembled Light-Harvesting Supramolecular Systems

Abstract

To meet the world's demands on the development of sunlight-powered renewable energy production, triplet–triplet annihilation-based photon upconversion (TTA–UC) has raised great expectations. However, an ideal highly efficient, low-power, and in-air, TTA–UC has not been achieved. Here, we report a novel self-assembly approach to achieve this, which enabled highly efficient TTA–UC even in the presence of oxygen. A newly developed lipophilic 9,10-diphenylanthracene-based emitter molecule functionalized with multiple hydrogen-bonding moieties spontaneously coassembled with a triplet sensitizer in organic media, showing efficient triplet sensitization and subsequent triplet energy migration among the preorganized chromophores. This supramolecular light-harvesting system shows the high TTA-UC efficiency of 30% optimized at low excitation power in deaerated conditions. Significantly, the UC emission largely remains even in an air-saturated solution, and this approach is facilely applicable to organogel and solid-film systems.

2-1 Introduction

A promising strategy developed in the last decade is workable with non-coherent, low-intensity light sources; namely, the sensitized triplet-triplet annihilation-based photon upconversion (TTA-UC) in multicomponent donor-acceptor systems (Fig. 2-1-1).[1-12]

Although the researchers have demonstrated the proof-of-principle improvement of photovoltaic and photochemical devices by integrating TTA-UC materials,[13-16] the insufficient TTA-UC efficiency and strict deaeration process for avoiding oxygen quenching of triplet state make them far from real-world applications. To overcome this situation, there are three major challenges with TTA-UC. First, it is desired to develop UC systems that display quantum efficiencies exceeding the current record of 26%[10] (the theoretical maximum is defined as 50% for two-to-one photon conversion process[12]). Second, the rational design of molecular systems that work under low excitation light intensities is required so that the lower-energy component of sunlight can be upconverted. Third, TTA-UC systems that operate under aerobic conditions need to be developed, which requires suppressing the massive quenching of the triplet excited states by molecular oxygen. In conventional TTA-UC systems, the donor and acceptor molecules are dissolved in low-viscosity solvents, where the UC emission is largely quenched by dissolved oxygen.[3,4,10,12] To avoid this, donor and acceptor molecules have been dispersed in solid polymers[8,16,17] or viscous liquid mixtures.[9,14] However, the consequent slow diffusion of dye molecules in these matrices inevitably lowered the TET and TTA efficiencies, which necessitated the use of undesirably high excitation power.

Here, we report the first supramolecular triplet-energy-harvesting system that shows energy-migration-based TTA-UC instead of the conventional molecular-diffusion-based mechanism. In contrast to the extensive applications of singlet energy transfer and migration in supramolecular assemblies,[18,19] studies on triplet energy migration have been largely limited to the field of solid-state physics[20-22] and photofunctional polymers.[23-25] Although energy-migration-based UC emission has been recently reported by us and others[26-30], there exist no systems that fulfill all of the requirements above. To achieve these goals, it is imperative to improve the migration rate and range of triplet excitons and to develop molecular designs for reducing the collision with oxygen molecules. We have designed a novel amphiphilic acceptor **A1** (Fig. 2-1-2) that possesses a solvophobic 9,10-diphenylanthracene (DPA) unit and solvophilic ether-linked alkyl chains that are connected via L-glutamate linkers with multiple amide groups.

As a design strategy for assembled structure of the acceptor in organic solvent, both the solvophobic and solvophilic properties are carefully selected.[31] Phenyl rings in DPA moiety selected as a chromophore part may impair the molecular orientation orderliness in two-dimensional molecular structure due to the steric hindrance. So six amide groups are introduced as a hydrogen bonding functional group in order to increase the cohesive force.[32,33] Besides, in order to improve the solvophilicity, dialkyl type-alkyl chains containing flexible ether bonds are introduced.[34]

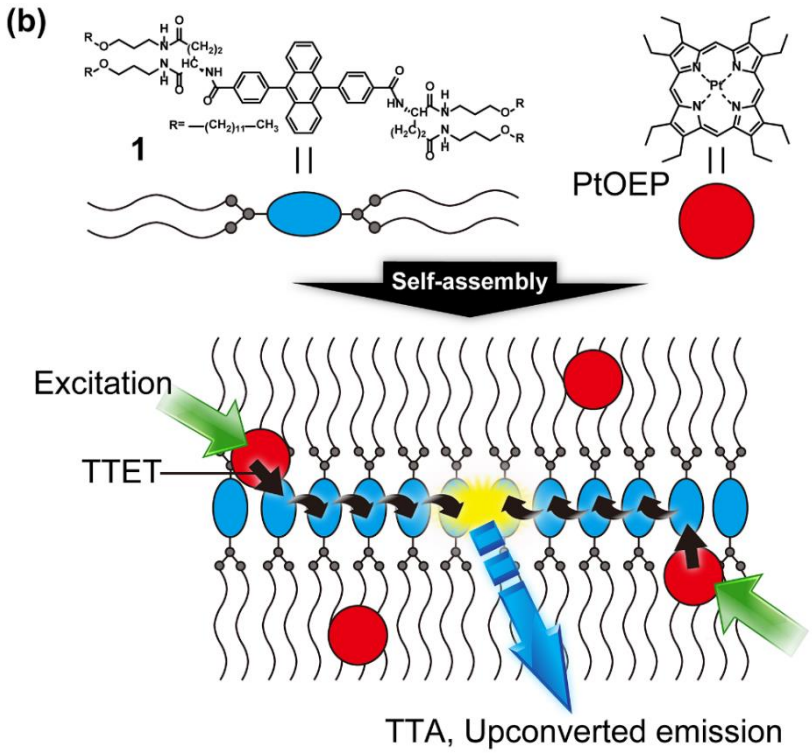

Figure 2-1-2. Schematic illustration of the basic self-assembly structure. Acceptor molecules (**A1**) spontaneously self-assemble in solution and donor molecules (PtOEP) efficiently bind to the self-assemblies by solvophobic interaction. Upon photoexcitation of donor molecules by green light, donor-to-acceptor TET is followed by triplet energy migration among the acceptor networks. It leads to efficient TTA between acceptor triplets and consequent upconverted blue emission from the acceptor excited singlets. The excited triplet species are effectively protected against the quenching by molecular oxygen in the self-assembled structures.

DPA has been employed as a benchmark acceptor in TTA-UC.[3,7,10,12] The amide group-enriched L-glutamate connector has been employed to impart chirality and hydrogen bonding networks that improve control of molecular orientation and thermal stability.[22,35,36] The acceptor **A1** self-assembles in organic media that efficiently uptake donor Pt(II) octaethylporphyrin (PtOEP) molecules, giving supramolecular donor-acceptor nanohybrids. They show efficient donor-to-acceptor TET as well as fast triplet energy migration among aligned acceptors, leading to a high UC quantum yield at low excitation power. Remarkably, the TTA-UC emission is mostly preserved even in the air-saturated condition. Furthermore, the in-air TTA-UC emission was also observed in different important material forms such as gels and solid films, demonstrating the universality of the supramolecular triplet-harvesting strategy.

2-2 Experimental section

2-2-1 General information

Materials

All reagents and solvents were used as received otherwise noted. The detailed synthetic procedure and characterizations of the new acceptor **A1** are written in the Supplementary Information. Platinum(II) octaethylporphyrin (PtOEP) was purchased from Sigma Aldrich. For spectroscopic measurements, we used analytical grade chloroform purchased from Wako Pure Chemical.

Characterizations

^{1}H NMR (300 MHz) spectra were measured on Bruker DRX-300 spectrometer using TMS as the internal standard. Elemental analysis was conducted at the Elemental Analysis Center, Kyushu University. Atomic force microscopy (AFM, tapping mode) was carried out using an Agilent PicoPlus 5500. UV-vis absorption spectra were recorded on a JASCO V-670 spectrophotometer. Luminescence spectra were measured by using a PerkinElmer LS 55 fluorescence spectrometer. The samples were excited with an incidence angle of 45º to the quartz cell surface and the fluorescence was detected along the normal. The absolute quantum yields were calculated using a Hamamatsu C9920-02G instrument. Time-resolved photoluminescence lifetime measurements were carried out by using time-correlated single photon counting lifetime spectroscopy system, HAMAMATSU Quantaurus-Tau C11367-02 (for fluorescence lifetime)/C11567-01(for delayed luminescence lifetime). The quality of the fit has been judged by the fitting parameters such as χ^2 (<1.2) as well as the visual inspection of the residuals. The upconversion luminescence emission spectra were recorded on Otsuka Electronics MCPD-7000 instrument with the excitation source using an external, adjustable 532 nm semiconductor laser.

Determination of TTA-UC Emission Quantum Efficiency

The upconversion luminescence quantum efficiency (Φ_{UC}) of a chloroform solution containing **A1** and PtOEP ([**A1**] = 10 mM, [PtOEP] = 10 μM) was determined relative to the DPA-PtOEP UC pair in deaerated tetrahydrofuran ([DPA] = 10 mM, [PtOEP] = 100 μM) according to the following equation[12]

$$\Phi_{\mathrm{UC}} = \Phi_{std}\left(\frac{A_{std}}{A_{UC}}\right)\left(\frac{I_{uc}}{I_{std}}\right)\left(\frac{P_{std}}{P_{uc}}\right)\left(\frac{\eta_{uc}}{\eta_{std}}\right)^2 \quad (3)$$

where Φ_{UC}, A_{UC}, $I_{UC,}$ P_{UC} and η_{UC} represent the quantum yield, absorbance at the excitation intensity (532 nm) integrated photoluminescence spectral profile, excitation power density, and refractive index of the medium. The corresponding terms for the subscript "*std*" are for the reference quantum counter of DPA-PtOEP pair in deaerated tetrahydrofuran at the identical excitation wavelength. The theoretical maximum UC quantum efficiency is 0.50 since the TTA-UC process uses 2 photons to produce 1 photon. The reflective index of chloroform and tetrahydrofuran are 1.44 and 1.41 at 293 K, respectively. The UC quantum yield of reference is known as 0.26 at its maximum.[10] Note that the comparison between different UC systems should be based on the careful examination of experimental conditions, since UC quantum yield of DPA-PtOEP is known to depend strongly on the experimental conditions, such as chromophore concentration, solvent, and excitation power, even if the employed donor and acceptor are identical.[12]

2-3 Synthesis of acceptor molecule A1

Acceptor molecule, **A1**, was synthesized by following scheme 1.

Scheme 1. Synthetic procedure of acceptor molecule **A1**.

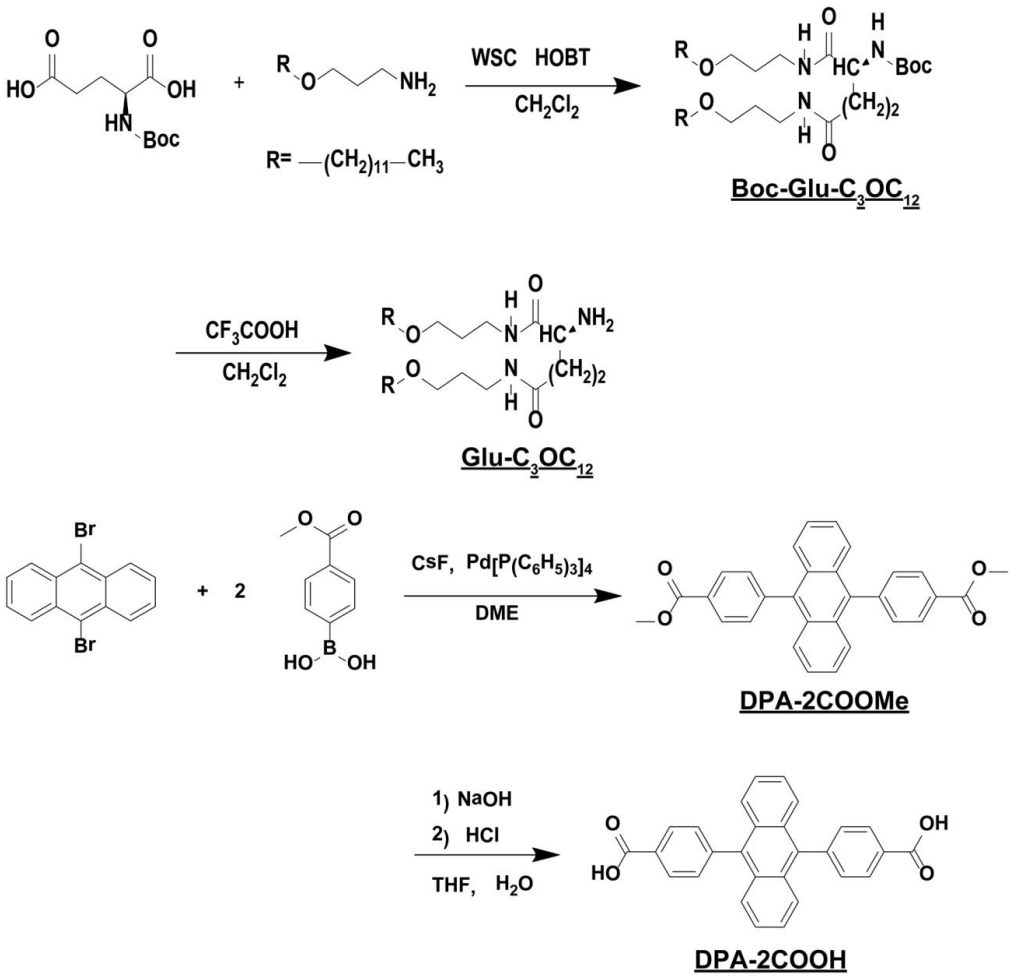

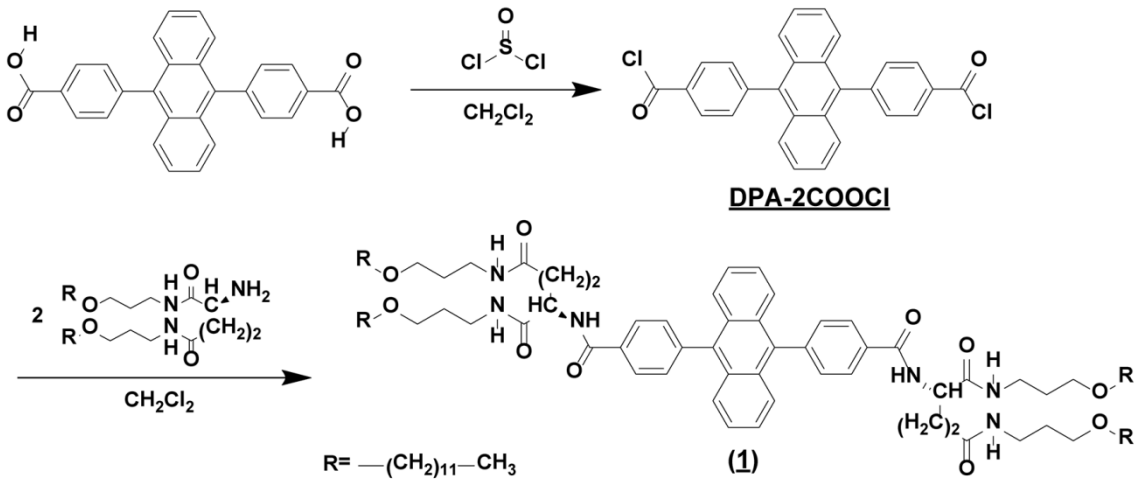

2-3-1 Synthesis of Boc-Glu-C_3OC_{12}.

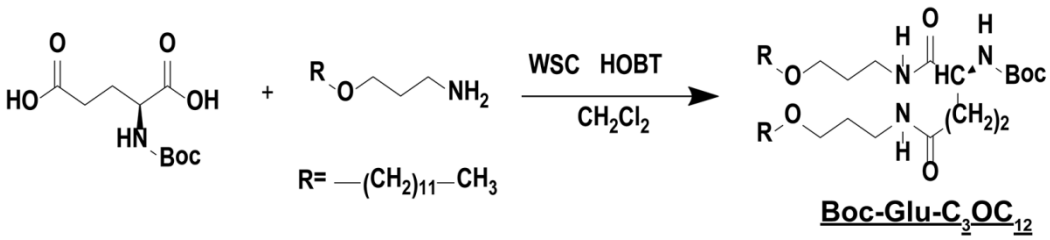

3-(dodecyloxy)propylamine 12.7 ml (0.044 mol), 1-ethyl-3-(3-dimethylaminopropyl)-carbodiimide 8.43 g (0.044 mol), and 1-hydroxybenzotriazole 5.95 g (0.044 mol) were added to N-(tert-Butoxycarbonyl)-L-glutamic acid 4.94 g (0.02 mol) in 400 ml distilled dichloromethane and reacted for 48h at the room temperature in Ar. After the reaction, the solution was washed several times with $NaHCO_3$ aqueous solution and with water, dried over anhydrous Na_2SO_4. Evaporation of the organic layer under reduced pressure followed by reprecipitation (methanol/water) and column chromatography (dichloromethane/methanol) over silica gel yielded the pure Boc-Glu-C_3OC_{12} solid (yield: 88%). ^{1}H NMR (300 MHz, $CDCl_3$): δ = 0.86-0.91 (t, 6H), 1.26 (m, 36H), 1.44 (s, 9H), 1.56-1.62 (m, 4H), 1.73-1.81 (m, 4H), 1.90-2.09 (m, 2H), 2.21-2.32 (m, 2H), 3.32-3.53 (m, 12H), 5.72-5.75 (d, 1H), 6.44 (t, 1H), 6.95 (t, 1H). ESI-MS: calculated for $C_{40}H_{79}N_3O_6$ 698.07; found 698.65 [M^+].

2-3-2 Synthesis of Glu-C_3OC_{12}

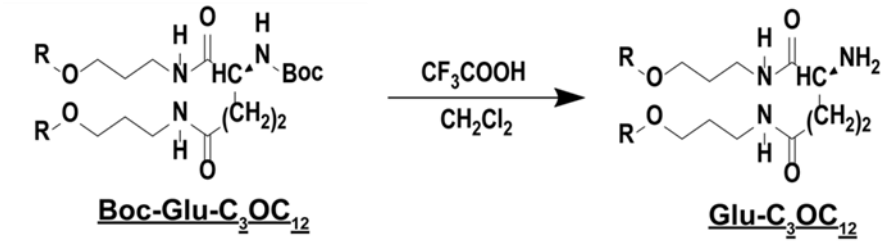

Boc-Glu-C_3OC_{12} 2.09 g (3.0 mmol) was dissolved in 150 ml of distilled dichloromethane and cooled by an ice bath. A large excess of trifluoroacetic acid (6.88 ml) was added to this solution and stirred at the room temperature for 12 h. The solvent removal by rotary evaporation gave an oily product. This product was dissolved in 10 mL THF and poured into 150 mL aqueous solution saturated with $NaHCO_3$. After filtration, the product was purified by recrystalization in methanol/ethyl acetate to give a colorless solid Glu-C_3OC_{12} (yield: 94%). ^{1}H NMR (300 MHz, $CDCl_3$): δ = 0.88-0.90 (t, 6H), 1.26 (m, 36H), 1.59 (m, 4H), 1.73-1.80 (m, 4H), 1.82-2.05 (m, 2H), 2.27-2.32 (m, 2H), 3.32-3.51 (m, 12H), 6.48 (t, 1H), 6.44 (t, 1H), 7.60 (t, 1H).

2-3-3 Synthesis of DPA-2COOMe

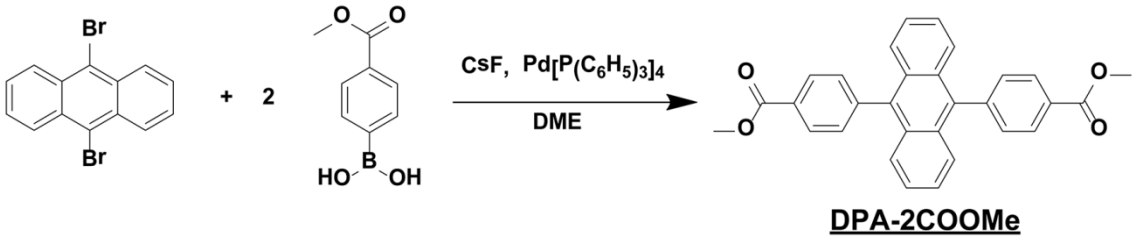

A mixture of 2.12 g (11.8 mmol) 4-methoxycarbonylphenylboronic acid, 1.80 g (5.4 mmol) 9,10-dibromo anthracene, 2.60 g (24.2 mmol) CsF and 187 mg (0.61 mmol) Tetrakis(triphenylphosphine)palladium(0) were placed in a 300 ml flask under Ar, and 100 ml of degassed 1,2-dimethoxyethane were added. After refluxing under Ar for 60 h, the solvent was removed to give a yellow residue. This obtained solid was suspended in 35 ml water and extracted with 100 ml of $CHCl_3$. After drying the organic phase over $MgSO_4$ and removing the solvent, the product was purified by column chromatography ($CHCl_3$) over silica gel to yield of a yellow powder (yield: 21 %). ^{1}H NMR (300 MHz, $CDCl_3$): δ = 4.02 (s, 6H), 7.32-7.38 (m, 4H), 7.56-7.61 (d, 4H), 7.61-7.64 (m, 4H), 8.28-8.31 (d, 4H). [37,38]

2-3-4 Synthesis of DPA-2COOH

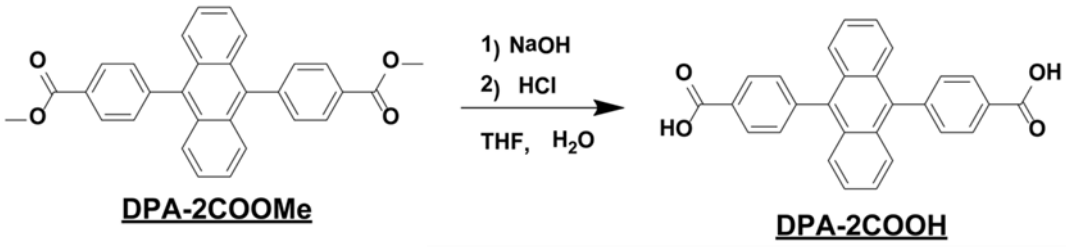

To a suspension of 288 mg (0.65 mmol) DPA-2COOMe in 75 ml 1:1 mixture of THF/MeOH, 15 ml of a 2M KOH aqueous solution was added. The mixture was allowed to reflux for 3 h. THF was removed under reduced pressure, and the resulting suspension was diluted with water. The precipitate formed by acidification with aqueous HCl (2M) was collected by filtration, washed several times with water yielding 227 mg (84 %) of a pale yellow solid. ^{1}H NMR (300 MHz, d_6-DMSO): δ = 7.44-7.49 (m, 4H), 7.51-7.58 (d, 4H), 7.60-7.67 (m, 4H), 8.21-8.32 (d, 4H) 13.16 (s, 2H). [37,38]

2-3-5 Synthesis of DPA-2(L)Glu (A1).

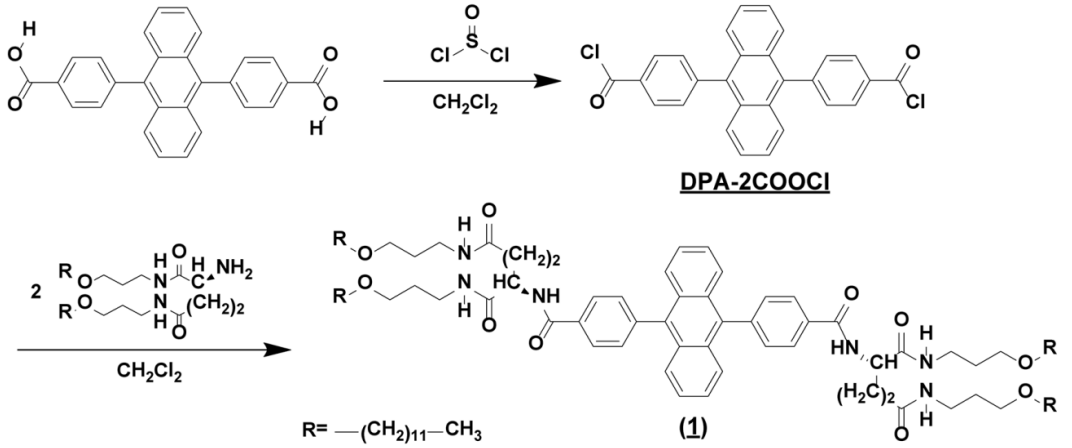

3 ml of distilled benzene and 1 ml of thionyl chloride were added to 145 mg (0.35 mmol) of DPA-2COOH placed in a 10 ml flask under Ar. This mixture was refluxed for 3 h with catalyst quantity of DMF. After removing the solvent and excess thionyl chloride under reduced pressure, residual yellow solid was dispersed into 25 ml of distilled dichloromethane, and this solution was added dropwise to 623 mg (1.04 mmol) Glu-C_3OC_{12} dissolved in 25 ml of distilled dichloromethane under Ar. This mixture was stirred at the room temperature for 2h. After the reaction, the solution was washed several times with $NaHCO_3$ aqueous solution and with water, dried over anhydrous Na_2SO_4. Evaporation of the organic layer under reduced pressure and column chromatography (chloroform/methanol) over silica gel yielded the 403 mg of pale yellow solid. ^{1}H NMR (300 MHz, $CDCl_3$): δ = 0.81-0.92 (t, 12H), 1.16-1.38 (m, 74H), 1.49-1.57 (m, 8H), 1.73-1.90 (m, 8H), 2.14-2.46 (m, 2H), 2.50-2.68 (m, 2H), 3.34-3.47 (m, 16H), 3.47-3.58 (q, 4H), 4.59-4.71 (q, 2H) 6.45-6.52 (t, 2H), 7.17-7.25 (t, 2H), 7.30-7.40 (q, 4H), 7.55-7.61 (d, 4H), 7.61-7.67 (q, 4H), 8.13-8.20 (d, 4H) 8.44-8.51 (d, 2H). Elemental analysis: calculated for H 9.96 C 74.58 N 5.32; found H 9.93 C 74.40 N 5.25.

2-4 Results and discussion

2-4-1 Assembled structure of A1

The new acceptor **A1** was synthesized and fully characterized, and its assembled structure in chloroform was studied by ^{1}H NMR spectroscopy, absorption spectroscopy, and atomic force microscopy (AFM) measurements. ^{1}H NMR spectra of **A1** in deuterated chloroform (10 mM) showed amide proton signals at around 8.5, 7.2, and 6.6 ppm at 298 K, which shifted to a higher magnetic field upon heating to 333 K (Fig. 2-4-1). This result indicates the presence of hydrogen bonding interactions between the amide groups at 298 K, which were weakened by heating. Meanwhile, the ^{1}H NMR peaks of the DPA unit did not show noticeable shifts upon changing the temperature, suggesting the absence of strong π-stacking interactions, which is ascribed to the steric hindrance imposed by the two out-of-plane phenyl rings. These considerations were further supported by the absorption spectra of **A1** in chloroform (Fig. 2-4-2), in which ^1B_b and ^1L_a absorption peaks of the anthracene chromophore did not show changes upon heating.

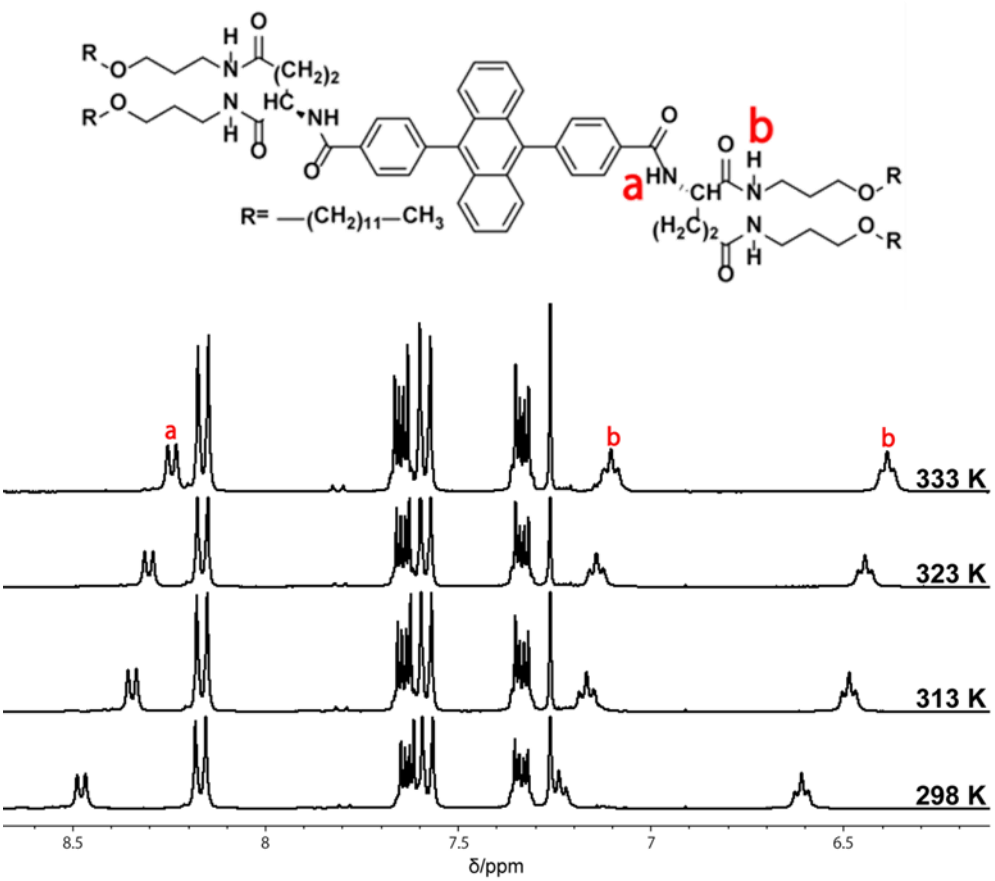

Figure 2-4-1. ^{1}H NMR spectra of **A1** (10 mM in $CDCl_3$, 300 MHz) at different temperatures. The protons attributable to the b position are split into two regimes because of their chiral environment.

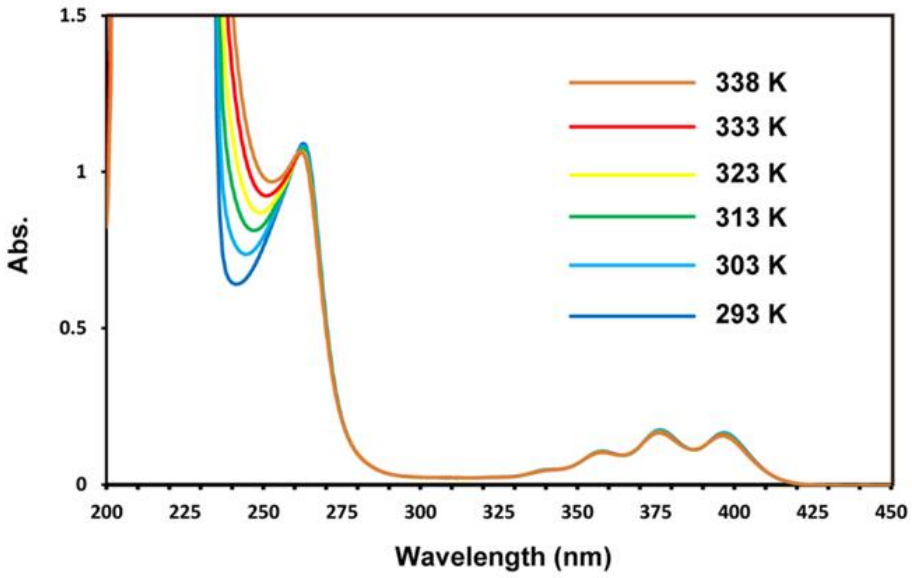

Figure 2-4-2. Temperature-dependent absorption spectra of **A1** in chloroform ([**A1**] = 20 μM) between 293 K and 338 K. No large changes of the DPA absorption bands were observed with increasing the temperature. Similar results were observed by using 1 mM chloroform solution of **A1**. These observations agree with the temperature dependent NMR results that suggest the absence of strong intermolecular interaction between the DPA moieties.

The AFM image of **A1** drop cast of 1 mM solution on a highly oriented pyrolytic graphite (HOPG) surface exhibited tape-like nanostructures with an average width and height of around 20 and 2 nm, respectively (Fig. 2-4-3a and 2-4-3b). The latter value corresponds to the molecular length of a single acceptor molecule **A1**, and thus **A1** spontaneously self-assembles in chloroform to give developed monolayer membranes. Interestingly, the similar nanofiber structure was observed when a diluted solution ([**A1**] = 20 μM) was used to cast, suggesting the structural stability against the dilution (Fig. 2-4-3c).

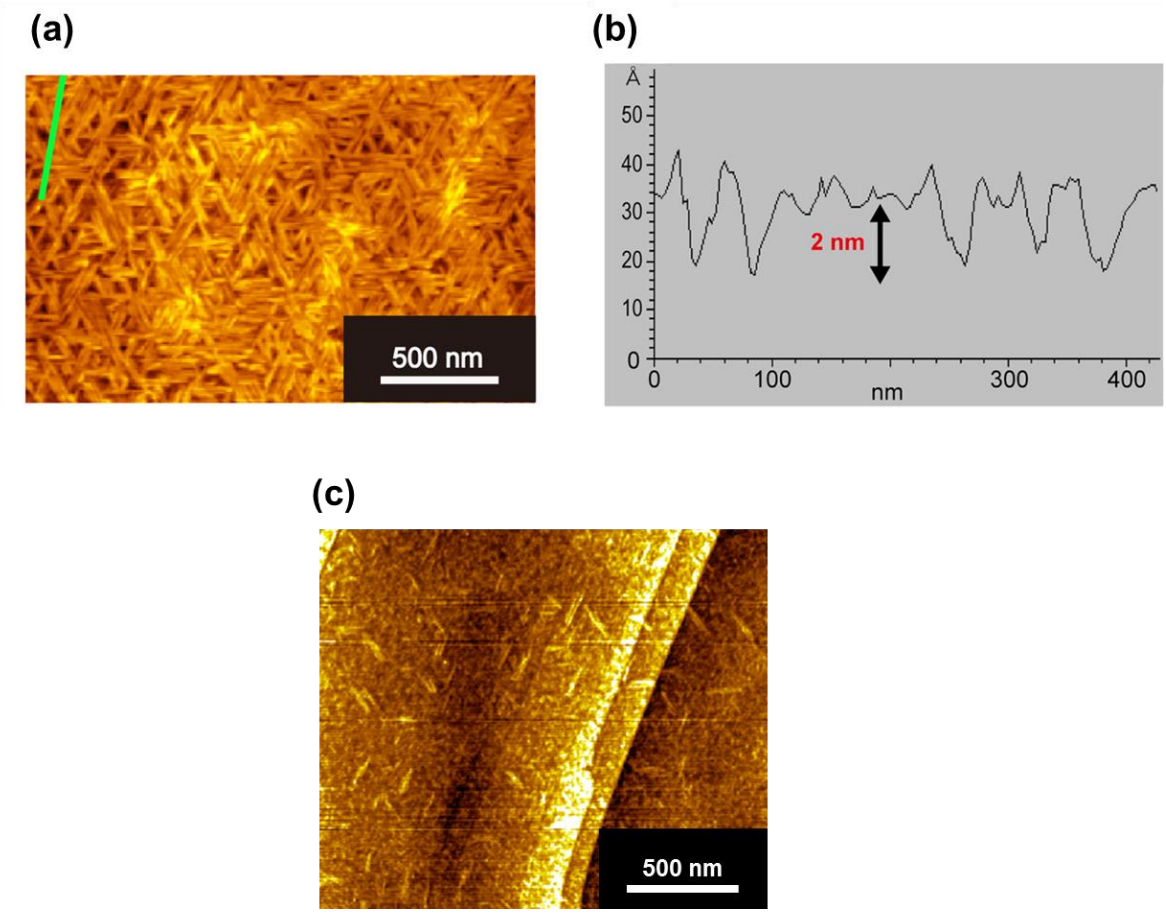

Figure 2-4-3. (a) An AFM image of **A1** drop-cast from 1 mM solution onto the HOPG substrate. (b) A height profile along the green line in (a). (c) An AFM image of **A1** drop-cast from 20 μM solution onto the HOPG substrate.

2-4-2 TTA-UC properties of self-assembly system

The fluorescence of **A1** around 450 nm in chloroform gave a high absolute quantum yield of 88% ([**A1**] = 10 mM), which does not show a large overlap with the absorption band of PtOEP (Fig. 2-4-4). Note that this quantum yield of 88% remained almost similar after diluting the solution for 1000 times (91%, [**A1**] = 10 μM), which indicates the self-quenching of the acceptor singlet is insignificant.

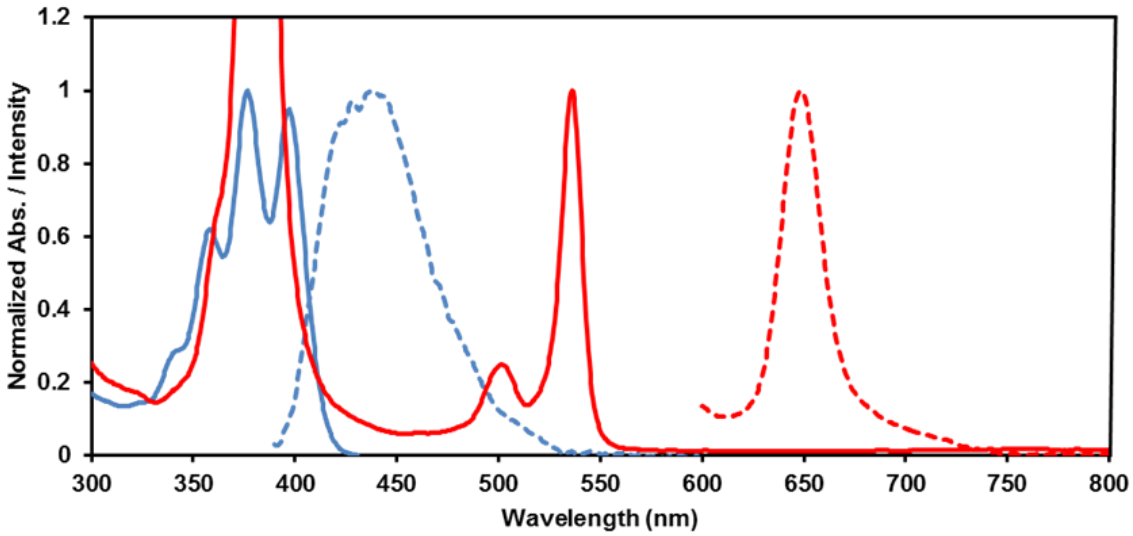

Figure 2-4-4. Normalized absorption (solid lines) and emission (dashed lines) spectra of chloroform solution of **A1** (blue, λ_{ex} = 375 nm, 1 mM) and PtOEP (red, λ_{ex} =510 nm, 10 μM) at the room temperature.

The TTA-UC emission of a chloroform solution containing **A1** and PtOEP ([**A1**] = 10 mM, [PtOEP] = 10 μM) was measured after deaeration by repeated freeze-pump-thaw cycles. Under excitation at 532 nm, upconverted blue emission was clearly observed around 450 nm (Fig. 2-4-5). The donor phosphorescence intensity observed at 650 nm is very weak, indicating that the TET quantum efficiency Φ_{ET} is close to 1.[39] In general, the TET process depends on molecular diffusion and collision, and thus the Φ_{ET} value decreases with the decrease in acceptor concentration.[40] However, in the case of the **A1**-PtOEP pair, the Φ_{ET} value remained unchanged regardless of the degree of dilution (Fig. 2-4-6a). This behavior is explicable only by the unaltered donor-to-acceptor ratio in diluted supramolecular assemblies, clearly demonstrating their high structural integrity which arouse from the strong solvophobic binding of PtOEP molecules to the acceptor self-assemblies.[41] Importantly, the UC emission was clearly observed even at 77 K, well below the melting point of the solvent (Fig. 2-4-6b). A control experiment was carried out by using molecularly dispersed DPA instead of **A1** in the identical conditions (same chromophore concentrations, excitation power, and optical setups). No upconverted emission was detected from the frozen chloroform solution of DPA-PtOEP at 77 K (Fig. 2-4-6b). These results confirm the formation of supramolecular assembly structure, and furthermore, supports that present TTA-UC is based on triplet energy migration and not the classical molecular diffusion mechanism.

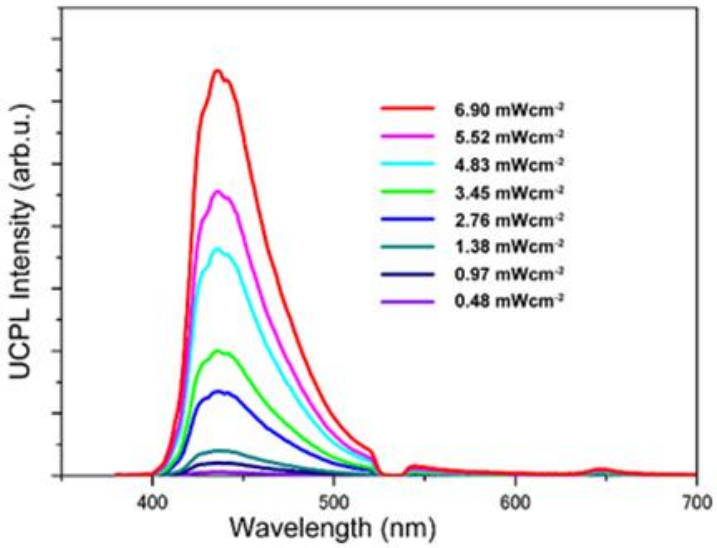

Figure 2-4-5. Photoluminescence spectra of **A1** and PtOEP in deaerated chloroform ([**A1**] = 10 mM, [PtOEP] = 10 μM) with different incident power densities of 532 nm laser at the room temperature.

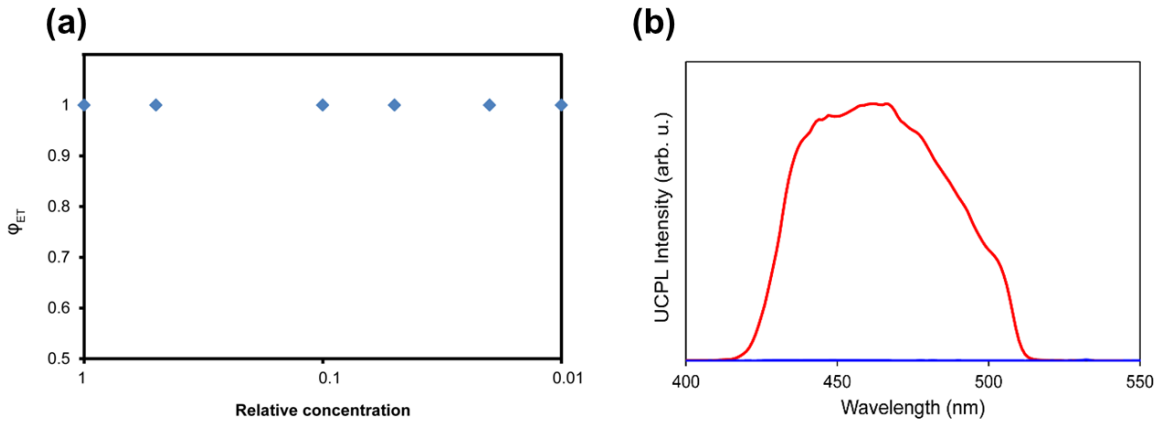

Figure 2-4-6. (a) The donor-to-acceptor TET efficiency Φ_{ET} as a function of relative concentration of **A1** and PtOEP at the room temperature. The initial concentrations were [**A1**] = 10 mM and [PtOEP] = 10 μM, and the solution was diluted up to 100 times. (b) Photoluminescence spectrum of **A1**-PtOEP (red, [**A1**] = 10 mM, [PtOEP] = 10 μM) and of DPA-PtOEP (blue, [DPA] = 10 mM, [PtOEP] = 10 μM) in air-saturated chloroform at 77 K under 532 nm excitation (excitation power density = 982 mW cm^{-2}).

The TTA-UC efficiency, Φ_{UC}, was determined by using a tetrahydrofuran solution of DPA and PtOEP as the standard, having the similar emission spectra to **A1**. This is to reduce the error induced by the optical response of the instrumental setup at different wavelengths (Fig. 2-4-7).[10] Note that we reproduced the standard Φ_{UC} value (26%, [DPA] = 10 mM, [PtOEP] = 100 μM) by using Rhodamine B as a standard with the optical setup used for the current study. Because the TTA-UC process converts two photons to one photon with higher energy, the theoretical maximum of Φ_{UC} is defined as 50%.[12] Significantly, the Φ_{UC} value of our system reached 30%, exceeding the previous highest value of 26% reported for the pair consisting of DPA and PtOEP.[10] To confirm this result, we repeated the same measurements using different batches of **A1** (Fig. 2-4-7). The standard solutions were freshly made for each measurements. The Φ_{UC} of 30±1% with small error was repeatedly observed, which clearly ensures the high accuracy of our measurements and confirms the high TTA-UC efficiency of 30%. The Φ_{UC} is described by the following expression[10]

$$\Phi_{\mathrm{UC}} = \frac{1}{2} f \Phi_{ISC} \Phi_{ET} \Phi_{TTA} \Phi_{A} \qquad (1)$$

where Φ_{ISC}, Φ_{ET}, Φ_{TTA}, and Φ_{A} represent the quantum efficiencies of donor ISC, TET, TTA, and acceptor emission. The parameter f is the statistical probability for obtaining a singlet excited state after the annihilation of two triplet states. In the current system, the Φ_{ISC} and Φ_{ET} are regarded as 1, and Φ_{A} was experimentally determined as 0.88. The fluorescence lifetime of **A1** in the presence of donor (5.3 ns) was identical to that in the absence of donor (5.3 ns). It indicates that the back energy transfer is almost negligible. As discussed later, at the saturation regime where Φ_{UC} is maximum and constant, the Φ_{TTA} can be assumed to be 1.[16] Thus the f value is calculated as 0.68, which is notably larger than the reported f value of 0.52 for DPA.[10] We presume that the high T_2 energy level and/or specific dye arrangement of the self-assembly system result in the observed enhanced f value. The TTA process is mediated by the formation of collisional complexes of singlet, triplet and quintet multiplicities, where the weighted statistical probability of formation of these states is 1 : 3 : 5.[10] Schmidt and coworkers reported that the pure statistical factor f = 1/9 can be enlarged to f = 2/5, because the quintet state of polyaromatic organic compounds is usually energetically inaccessible and the higher energy triplet product T_2 decays back to T_1[42]. This limit can be further broken when the T_2 energy is higher than twice the T_1 energy,[42] as is the case for DPA (f = 0.52).[10] The f value may also be affected by the mutual distance and orientation of adjacent acceptor moieties, since the interchange rate from T_1-T_1 dimer to S_1-S_0 state can be dependent on the intermolecular electronic coupling.[43]

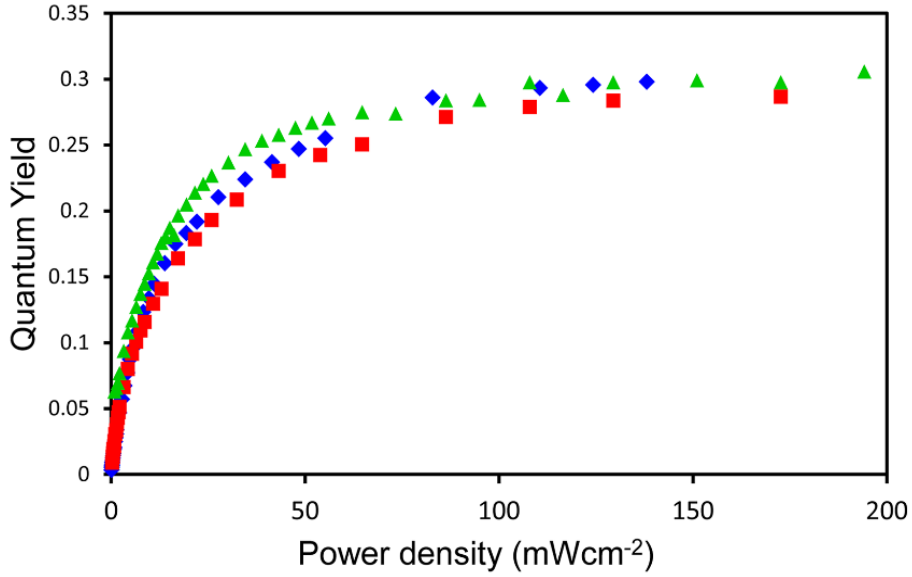

Figure 2-4-7. UC quantum yield of **A1**-PtOEP in deaerated chloroform ([**A1**] = 10 mM, [PtOEP] = 10 μM) with different incident power densities of 532 nm laser. Different colors represent the data obtained for samples under the same condition.

Along with the maximum Φ_{UC}, the TTA-UC threshold excitation intensity I_{th} is another important parameter characterizing the TTA-UC processes because it defines the excitation intensity at which Φ_{TTA} becomes 0.5. The TTA-UC emission intensity generally shows a quadratic and first-order dependence on the incident intensity in the low- and high-excitation intensity ranges, respectively, and the I_{th} value is experimentally determined as the intersection point of these two lines.[42,44,45] Such incident power dependence was observed for **A1**-PtOEP (Fig. 2-4-8a), and it shows a very low I_{th} of 8.9 mW cm^{-2}, which is close to the solar irradiance of 1.6 mW cm^{-2} at 532 ± 5 nm. To explain the observed low I_{th}, we estimated the triplet exciton diffusion constant D in the supramolecular assemblies. The second order annihilation constant γ_{TT} of acceptor triplets was determined as 3.1 × 10^{-11} cm^{3}s^{-1} by using the equation[40]

$$I_{th} = (\alpha(E)\Phi_{ET}\gamma_{TT}\tau_T{}^2)^{-1} \quad (2)$$

where $\alpha(E)$ is the system absorption coefficient in cm^{-1}, and τ_T is the lifetime of the acceptor triplet measured using time-resolved photoluminescence experiments (Fig. 2-4-8b). Given that $\gamma_{TT} = (8\pi D a_0)$, by assigning a_0 the value of 9.1 Å reported for the interaction distance of a DPA triplet pair,[44] we obtained a D value of 1.4 × 10^{-5} cm^2 s^{-1}. Significantly, this triplet energy migration rate in the acceptor assemblies is comparable to the large diffusion constant of DPA in a low-viscosity solvent (1.2 × 10^{-5} cm^2 s^{-1})[40] and to that observed for anthracene crystals.[21] This fast triplet energy migration in the self-assembly allowed the highly efficient TTA-UC process even under low excitation power. It is to note that the higher level of self-assembly achieved in this system lead to superior TTA-UC characteristics beyond the condensed amorphous acceptor system (I_{th} ~ 50 mW cm^{-2}).[29]

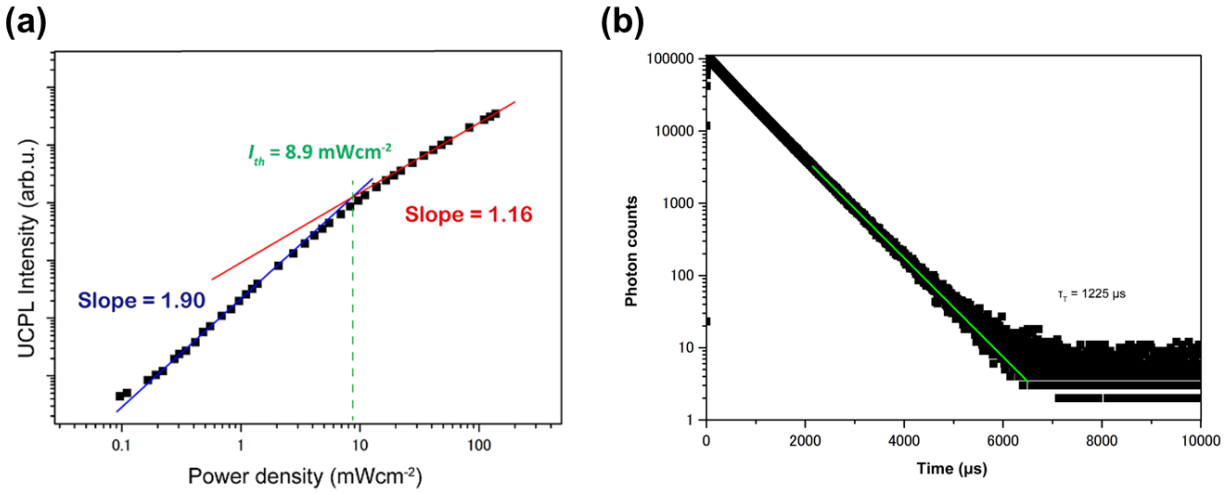

Figure 2-4-8. (a) Dependence of UC emission intensity at 440 nm on the incident power density in the deaerated condition at the room temperature ([**A1**] = 10 mM, [PtOEP] = 10 μM). (b) The UC emission decays at 440 nm of **1**-PtOEP in deaerated chloroform ([**A1**] = 10 mM, [PtOEP] = 10 μM) under 531 nm pulsed excitation at the room temperature. The fitting curves were obtained by considering the relationship of $I_{UC}(t) \propto \exp(-t/\tau_{UC}) = exp(-2t/\tau_T)$, where τ_{UC} and τ_T are the lifetimes of the UC emission and acceptor triplet, respectively.[16]

2-4-3 Oxygen stability of the TTA-UC emission of supramolecular system

We found that the UC emission of the current supramolecular system largely remained even in air-saturated dispersions (Fig. 2-4-9). Before addressing its detail, we first explain results of a control experiment with DPA-PtOEP in chloroform. Prior to the preparation of air-saturated solutions, the solvent chloroform was bubbled with air for 1 h to make sure the complete saturation. Figure 2-4-9a shows time dependences of upconverted emission intensity under continuous excitation of DPA-PtOEP in deaerated and air-saturated chloroform. In the absence of oxygen, the UC emission intensity immediately reached to a certain value and remained almost constant. On the other hand, the UC emission intensity of the air-saturated solution showed a gradual increase for ca. 100 seconds, and then reached a constant. The observed gradual rise for the air-saturated solution suggests the consumption of oxygen molecules by chemical reactions.[46] The saturated UC emission intensity of the aerated solution showed a decrease of about 40% compared with that of the deaerated condition, which is comparable to the recently reported behavior in DMF and DMSO.[47] Note that this quenching ratio would be dependent on solvents having different saturated oxygen concentrations. This observation implies the incomplete oxygen consumption in a cylindrical volume of the laser beam, and the physical/chemical quenching of the excited triplets by remaining oxygen.[46]

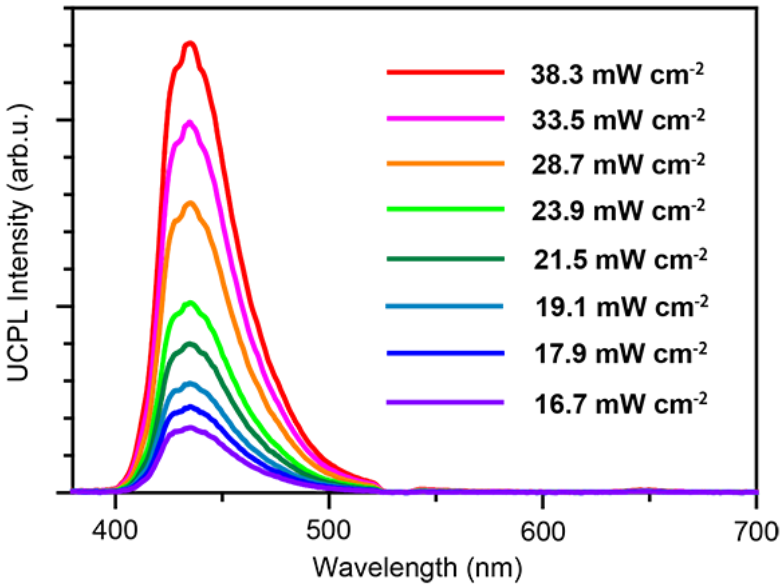

Figure 2-4-8 Photoluminescence spectra of **A1** and PtOEP in air-saturated chloroform ([**A1**] = 10 mM, [PtOEP] = 10 μM) with different incident power densities of 532 nm laser at the room temperature. The shape of UC emission spectra in air is similar to those in the deaerated condition.

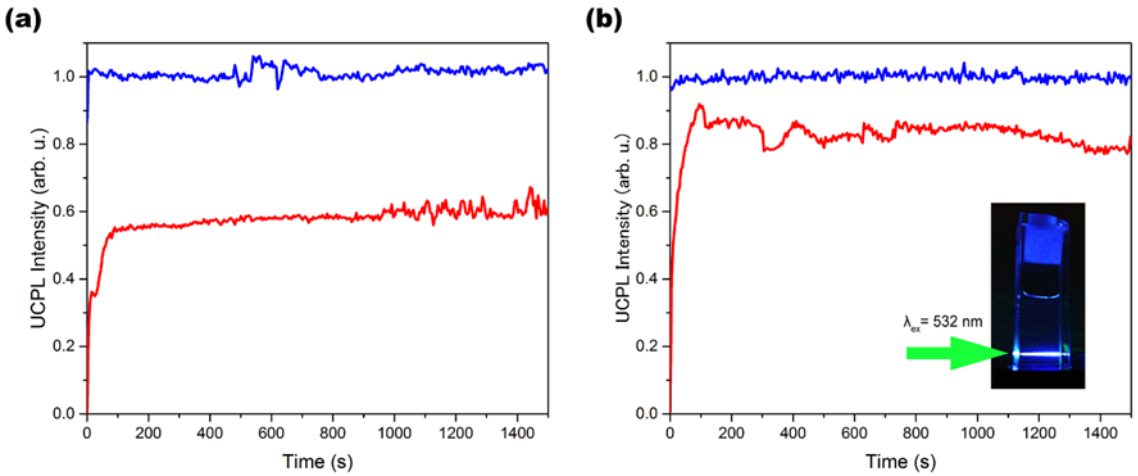

Figure 2-4-9. Time dependence of upconverted emission intensity at 435 nm upon continuous excitation at 532 nm of (a) DPA-PtOEP ([DPA] = 10 mM, [PtOEP] = 10 μM) and (b) **A1**-PtOEP ([**A1**] = 10 mM, [PtOEP] = 10 μM) in deaerated (blue line) and air-saturated (red line) chloroform at the room temperature. Excitation power density was 250 mW cm^{-2}. Inset of (b): a photograph of the blue upconverted emission of the **A1**-PtOEP pair in air-saturated chloroform.

Next, we compare these results of DPA-PtOEP with our supramolecular system. Similar to the case of DPA-PtOEP, the UC intensity of the deaerated **A1**-PtOEP solution was constant from immediately after the light irradiation (Fig. 2-4-9b). In the air-saturated condition, again as is the case in the DPA-PtOEP pair, the time dependence of the **A1**-PtOEP solution exhibited a gradual increase within 100 seconds, suggesting the consumption of surrounding oxygen molecules. To our interest, the **A1**-PtOEP pair showed only ca. 17% of decrease by the presence of oxygen, which is much smaller than 40% quenching observed for DPA-PtOEP. This difference may be explained by the lower concentration of remaining oxygen molecules in the local space around the dye moieties in our supramolecular system than the molecularly dispersed system, and this picture is consistent with the formation of closely-assembled array of chromophores. Further efforts to decrease local oxygen concentration around chromophore moieties based on the optimization of supramolecular architectures will open new opportunities to solve the oxygen-related problems. Our current work offers a critical first step toward the realization of such ideal UC systems based on supramolecular chemistry.

To achieve efficient donor-to-acceptor TET in air-saturated systems, the location of donor molecules in the acceptor assembly is also crucial. To obtain this information, we measured the donor phosphorescence intensity and lifetime for frozen dispersions at 77 K (Fig. 2-4-10).

The frozen PtOEP solution without the acceptor showed a single exponential decay with a lifetime τ_0 of 144 μs. In the presence of acceptor **A1**, a bi-exponential photoluminescence decay was observed with lifetimes τ_{ET} of 20 ns and 120 μs. Importantly, no free PtOEP luminescence was detected, which means that almost all the donor molecules are accommodated in the acceptor nanoassemblies. By using the Perrin approximation for short-range interactions,[39] the donor-to-acceptor Dexter energy transfer efficiency can be written as a function of the center-to-center distance between donor and acceptor $r_{D\text{-}A}$ by the equation

$$\Phi_{ET} = 1 - \exp\left[-\left(\frac{r_0}{r_{D-A}}\right)^3\right] = 1 - \frac{\tau_{ET}}{\tau_0} \qquad (2)$$

where r_0 is an effective interaction distance in the process energy transfer between PtOEP and DPA, being previously estimated as 9.8 Å.[44] The $r_{D\text{-}A}$ values were calculated as 4.8 Å and 17.3 Å for the short (20 ns) and long (120 μs) τ_{ET} components, respectively. This suggests the bimodal spatial distribution of donor in the acceptor assemblies, taking into account the molecular length of the acceptor **A1** is about 60 Å and it self-assembles into the nanotape-like structure with single molecular thickness. Moreover, it demonstrates that, by following Eq. S1, in a frozen system where molecular diffusion is completely avoided, only the first-(or nearest)-neighbors donor population (τ_{ET} = 20 ns) with ($r_0/r_{D\text{-}A}$) > 1 can efficiently transfer the energy to the acceptors (Φ_{ET}= 1).

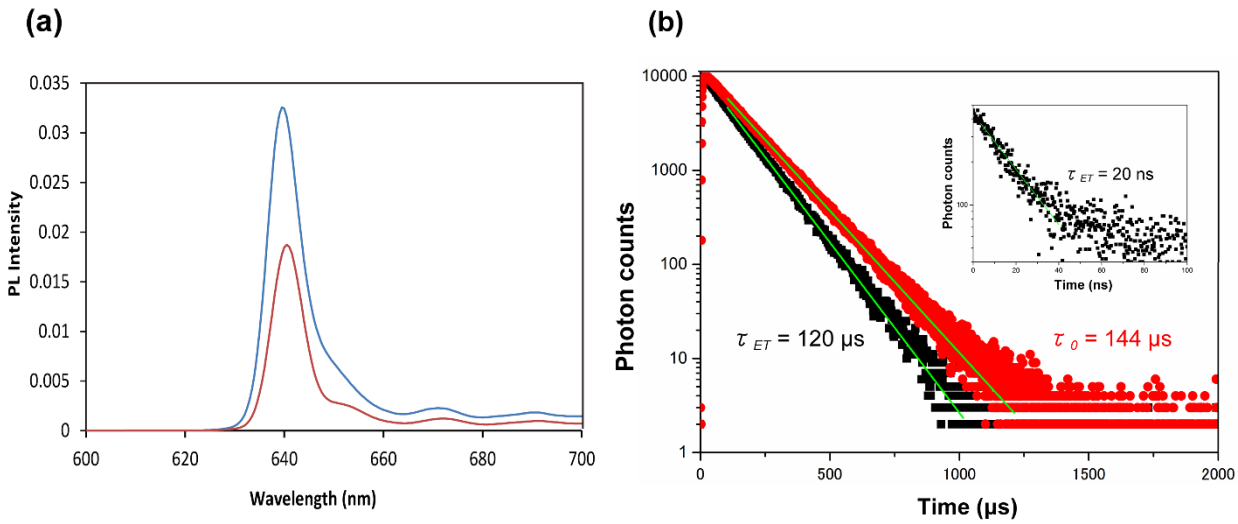

Figure 2-4-10. (a) Phosphorescence spectrum of PtOEP with (red) and without (blue) acceptor **A1** ([**1**] = 10 mM, [PtOEP] = 10 μM) in aerated chloroform at 77K under continuous excitation at 532 nm. (b) Phosphorescence decays of PtOEP with (black) and without (red) acceptor **1A** ([**A1**] = 10 mM, [PtOEP] = 10 μM; black) in aerated chloroform at 77 K under pulsed excitation at 531 nm. Inset: Nanosecond-scale phosphorescence decay at 650 nm of the **1**-PtOEP chloroform solution ([**A1**] = 10 mM, [PtOEP] = 10 μM) at 77 K with excitation of 365 nm.

For the second (or distant)-neighbors donor population (τ_{ET} = 120 μs) with ($r_0/r_{D\text{-}A}$) < 1, the energy transfer yield is low (Φ_{ET} = 0.17). The comparison of donor phosphorescence intensities between with and without acceptor **A1** at 77 K provides the abundance ratio of 35 mol% and 65 mol% for the close and separated population, respectively.

From these considerations, we confirmed that almost all of the donor molecules are bound to the acceptor nanoassemblies, where the donors show a bimodal distribution with shorter (4.8 Å, 35 mol%) and larger (17.3 Å, 65 mol%) average distances from the acceptor. At the ambient temperature, a fast equilibrium could naturally exist between these binding sites that allows efficient TET to DPA units.

2-4-4 TTA-UC of the supramolecular system in condensed media

The potential of the present supramolecular strategy can be extended beyond the dispersion systems. Supramolecular gels have recently received intense attention for designing photofunctional soft-materials including singlet energy harvesting systems.[18,19,48,49] The acceptor **A1** was found to form organogels in 1,2-dichloroethane with a critical gelation concentration of 8 mM. Interestingly, the 1,2-dichloroethane gel of **A1** doped with PtOEP showed a clear UC emission even in air, indicating the stabilization of triplets in the molecular assemblies. These triplet states migrate in supramolecular gel networks, and the light energy is harvested to achieve upconversion in soft-materials (Fig. 2-4-11a). Furthermore, the self-assembly-based UC emission is also observed in the solid cast films prepared by casting the chloroform solution under ambient conditions (Fig. 2-4-11b). This is surprising, since TTA-UC in the crystalline system has long been suffered from the oxygen quenching issue and very limited miscibility of acceptor-donor pairs as well.[10] This is an important step towards the solid-state TTA-UC devices that operate even in air. These observations clearly confirm the potential of the present self-assembly strategy, which would offer a general and powerful means to overcome the outstanding problem in TTA-UC. The integration of self-assembly with TTA-UC thus pushes back the boundaries of the traditional methods and promises wide applicability in many disciplines.

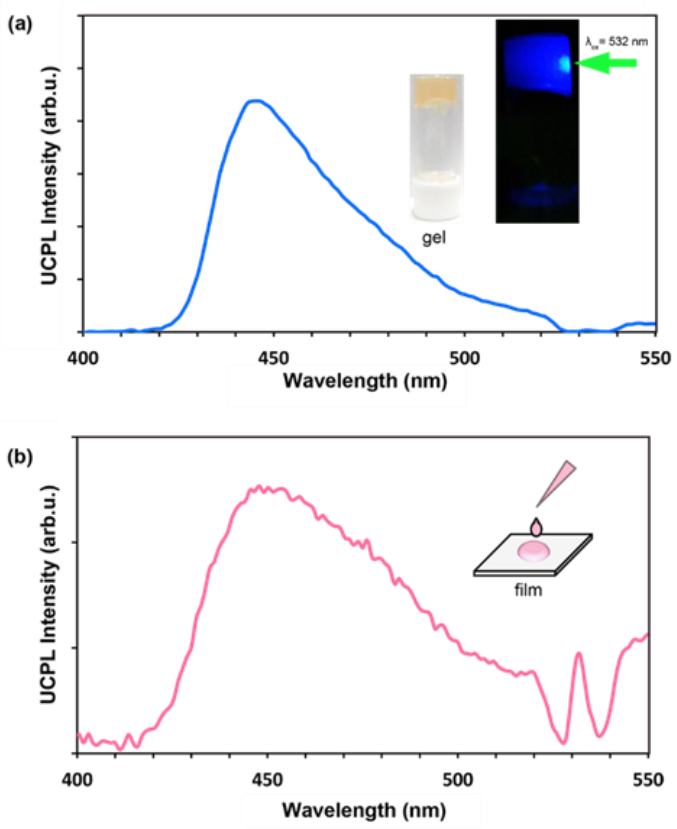

Figure 2-4-11. (a) Photoluminescence spectra of the 1,2-dichloroethane gel of **A1** doped with PtOEP ([**A1**] = 16 mM, [PtOEP] = 16 μM) upon 532 nm laser excitation in the ambient conditions. Inset pictures show the doped gel under white light and 532 nm green laser. (b) Photoluminescence spectra of the cast film of PtOEP-doped **A1** (PtOEP/**A1** = 0.1 mol%) obtained by 532 nm laser excitation in the ambient conditions.

2-5 Conclusions

In this study, the highly efficient, low-power, in-air light-harvesting TTA-UC systems have been developed by introducing the concept of supramolecular self-assembly. The current work offers an important bridge between photon upconversion and supramolecular chemistry. The suitably designed amphiphilic acceptor molecules spontaneously self-assemble in organic media to give developed, nanotape-like monolayer assemblies. They efficiently uptake donor molecules that lead to the highly efficient UC emission both in deaerated and aerated conditions. A number of applications of the current light-harvesting system is conceivable, which would open new avenues to self-assembly-based molecular technology in many disciplines. The rational extension of light-harvesting self-assemblies to the other combination of chromophores will lead to novel near IR-to-visible or visible-to-UV upconversion systems for improving photovoltaic and photocatalytic devices. The design of amphiphilic light harvesting systems in water would find many biological applications. Beyond TTA-UC, we envisage the formation and migration of triplet excitons in various self-assemblies and their aerobic stability would exert great impacts on materials science.

References

(1) S. Baluschev, T. Miteva, V. Yakutkin, G. Nelles, A. Yasuda and G. Wegner, *Phys. Rev. Lett.*, 2006, **97**, 143903.

(2) Y. Y. Cheng, B. Fuckel, T. Khoury, R. G. C. R. Clady, M. J. Y. Tayebjee, N. J. Ekins-Daukes, M. J. Crossley and T. W. Schmidt, *J. Phys. Chem. Lett.*, 2010, **1**, 1795-1799.

(3) T. N. Singh-Rachford and F. N. Castellano, *Coordin. Chem. Rev.*, 2010, **254**, 2560-2573.

(4) W. H. Wu, H. M. Guo, W. T. Wu, S. M. Ji and J. Z. Zhao, *J. Org. Chem.*, 2011, **76**, 7056-7064.

(5) M. Haring, R. Perez-Ruiz, A. Jacobi von Wangelin and D. D. Diaz, *Chem. Commun.*, 2015, **51**, 16848-16851.

(6) Z. Y. Huang and M. L. Tang, *J. Am. Chem. Soc.*, 2017, **139**, 9412-9418.

(7) Y. C. Simon and C. Weder, *J. Mater. Chem.*, 2012, **22**, 20817-20830.

(8) J. H. Kim, F. Deng, F. N. Castellano and J. H. Kim, *Chem. Mater.*, 2012, **24**, 2250-2252.

(9) Q. Liu, T. S. Yang, W. Feng and F. Y. Li, *J. Am. Chem. Soc.*, 2012, **134**, 5390-5397.

(10) A. Monguzzi, R. Tubino, S. Hoseinkhani, M. Campione and F. Meinardi, *Phys. Chem. Chem. Phys.*, 2012, **14**, 4322-4332.

(11) H. Ono, T. Hosokawa, K. Ichii, S. Matsuo, H. Nasu and M. Yamada, *Opt. Express*, 2015, **23**, 27405-27418.

(12) V. Gray, D. Dzebo, M. Abrahamsson, B. Albinsson and K. Moth-Poulsen, *Phys. Chem. Chem. Phys.*, 2014, **16**, 10345-10352.

(13) H. Ono, T. Hosokawa, K. Ichii, S. Matsuo and M. Yamada, *Electron. Lett*, 2015, **51**, 172-U152.

(14) J. H. Kim and J. H. Kim, *J. Am. Chem. Soc.*, 2012, **134**, 17478-17481.

(15) K. Shibahara, T. Mizuno, H. Takara, A. Sano, H. Kawakami, D. Lee, Y. Miyamoto, H. Ono, M. Oguma, Y. Abe, T. Kobayashi, T. Matsui, R. Fukumoto, Y. Amma, T. Hosokawa, S. Matsuo, K. Saito, H. Nasu and T. Morioka, *2015 Optical Fiber Communications Conference and Exhibition (Ofc)*, 2015.

(16) A. Monguzzi, F. Bianchi, A. Bianchi, M. Mauri, R. Simonutti, R. Ruffo, R. Tubino and F. Meinardi, *Adv. Energy Mater.*, 2013, **3**, 680-686.

(17) D. Botha and F. Cronje, *Sa J Hum Resour Mana*, 2015, **13**.

(18) A. Ajayaghosh, V. K. Praveen and C. Vijayakumar, *Chem. Soc. Rev.*, 2008, **37**, 109-122.

(19) T. Nakashima and N. Kimizuka, *Adv. Mater.*, 2002, **14**, 1113-1116.

(20) R. M. Hochstrasser, *J. Chem. Phys.*, 1964, **40**, 1038-&.

(21) B. B. Song, B. Liu, W. Lin, Y. P. Miao, H. Zhang, J. X. Wu, H. F. Liu and D. L. Yan, *24th International Conference on Optical Fibre Sensors*, 2015, **9634**.

(22) A. Kohler and H. Bassler, *Mater. Sci. Eng. R Rep.*, 2009, **66**, 71-109.

(23) W. Klöpffer, N. J. Turro, M. F. Chow and Y. Noguchi, *Chem. Phys. Lett.*, 1978, **54**, 457-460.

(24) M. Wohlgenannt, K. Tandon, S. Mazumdar, S. Ramasesha and Z. V. Vardeny, *Nature*, 2001, **409**, 494-497.

(25) Y. Tamai, H. Ohkita, H. Benten and S. Ito, *Chem. Mater.*, 2014, **26**, 2733-2742.

(26) P. E. Keivanidis, S. Baluschev, T. Miteva, G. Nelles, U. Scherf, A. Yasuda and G. Wegner, *Adv. Mater.*, 2003, **15**, 2095-2098.

(27) S. Baluschev, P. E. Keivanidis, G. Wegner, J. Jacob, A. C. Grimsdale, K. Müllen, T. Miteva, A. Yasuda and G. Nelles, *Appl. Phys. Lett.*, 2005, **86**.

(28) S. Baluschev, V. Yakutkin, G. Wegner, B. Minch, T. Miteva, G. Nelles and A. Yasuda, *J. Appl. Phys.*, 2007, **101**, 023101.

(29) P. F. Duan, N. Yanai and N. Kimizuka, *J. Am. Chem. Soc.*, 2013, **135**, 19056-19059.

(30) J. S. Lissau, D. Nauroozi, M. P. Santoni, S. Ott, J. M. Gardner and A. Morandeira, *J. Phys. Chem. C*, 2013, **117**, 14493-14501.

(31) T. Kunitake, *Angew. Chem. Int. Ed.*, 1992, **31**, 709-726.

(32) H. Ihara, H. Hachisako, C. Hirayama and K. Yamada, *J. Chem. Soc. Chem. Comm.*, 1992, 1244-1245.

(33) Y. Ishikawa, H. Kuwahara and T. Kunitake, *J. Am. Chem. Soc.*, 1994, **116**, 5579-5591.

(34) N. Kimizuka, T. Kawasaki, K. Hirata and T. Kunitake, *J. Am. Chem. Soc.*, 1995, **117**, 6360-6361.

(35) K. Okumura, K. Mase, N. Yanai and N. Kimizuka, *Chem. -Eur. J.*, 2016, **22**, 7721-7726.

(36) H. Jintoku and H. Ihara, *Chem. Commun.*, 2012, **48**, 1144-1146.

(37) S. Q. Ma, D. F. Sun, P. M. Forster, D. Q. Yuan, W. J. Zhuang, Y. S. Chen, J. B. Parise and H. C. Zhou, *Inorg. Chem.*, 2009, **48**, 4616-4618.

(38) I. M. Hauptvogel, R. Biedermann, N. Klein, I. Senkovska, A. Cadiau, D. Wallacher, R. Feyerherm and S. Kaskel, *Inorg. Chem.*, 2011, **50**, 8367-8374.

(39) M. Brandalero and A. C. S. Beck, *Des. Autom. Embed. Syst.*, 2016, **20**, 155-169.

(40) A. Monguzzi, R. Tubino and F. Meinardi, *Phys. Rev. B*, 2008, **77**, 155122.

(41) P. F. Duan, N. Yanai, H. Nagatomi and N. Kimizuka, *J. Am. Chem. Soc.*, 2015, **137**, 1887-1894.

(42) Y. Y. Cheng, T. Khoury, R. G. C. R. Clady, M. J. Y. Tayebjee, N. J. Ekins-Daukes, M. J. Crossley and T. W. Schmidt, *Phys. Chem. Chem. Phys.*, 2010, **12**, 66-71.

(43) C. L. Chung, C. Y. Chen, H. W. Kang, H. W. Lin, W. L. Tsai, C. C. Hsu and K. T. Wong, *Org. Electron.*, 2016, **28**, 229-238.

(44) A. Monguzzi, J. Mezyk, F. Scotognella, R. Tubino and F. Meinardi, *Phys. Rev. B*, 2008, **78**, 195112.

(45) A. Haefele, J. Blumhoff, R. S. Khnayzer and F. N. Castellano, *J. Phys. Chem. Lett.*, 2012, **3**, 299-303.

(46) Y. M. Tang, J. X. Xu, W. W. Liu, L. J. Xu and H. M. Li, *Int. J. Polym. Mater. Po.*, 2016, **65**, 143-150.

(47) R. Vadrucci, C. Weder and Y. C. Simon, *Mater. Horiz.*, 2015, **2**, 120-124.

(48) H. N. Schwerdt, H. Shimazu, K. Amemori, S. Amemori, P. L. Tierney, D. J. Gibson, S. Hong, T. Yoshida, R. Langer, M. J. Cima and A. M. Graybiel, *Proc. Natl. Acad. Sci. U. S. A.*, 2017, **114**, 13260-13265.

(49) Y. Sasaki, S. Amemori, H. Kouno, N. Yanai and N. Kimizuka, *J. Mater. Chem. C*, 2017, **5**, 5063-5067.

Chapter 3 Kinetically-Controlled Crystal Growth Approach to Enhance Triplet Energy Migration-based Photon Upconversion

Abstract

Improving efficiency of triplet-triplet annihilation-based photon upconversion (TTA-UC) in crystalline media is challenging because it usually suffers from the severe aggregation of donor (sensitizer) molecules in acceptor (emitter) crystals. In this study, we show a kinetically-controlled crystal growth approach to improve donor dispersibility in acceptor crystals. As the donor-acceptor combination, a benchmark pair of platinum (II) octaethylporphyrin (PtOEP) and 9,10-diphenylanthracence (DPA) is employed. A surfactant-assisted reprecipitation technique is employed, where the concentration of the injected PtOEP-DPA solution holds the key to control dispersibility; at a higher PtOEP-DPA concentration, a rapid crystal growth results in better dispersibility of PtOEP molecules in DPA crystals. The improvement of donor dispersibility significantly enhances the TTA-UC quantum yield. Thus the inherent function of donor-doped acceptor crystals can be maximized by controlling the crystallization kinetics.

3-1 Introduction

Photon upconversion based on triplet-triplet annihilation (TTA-UC) has attracted much attention for its potential applications in renewable energy production technologies.[1-10] In the typical TTA-UC process, (1) a triplet excited state of donor is formed by intersystem crossing (ISC) from a photo-excited singlet state, (2) acceptor triplet excited states are populated by triplet energy transfer (TET) from the donor triplets, and (3) annihilation between two acceptor triplets (TTA) generates an acceptor singlet excited state, from which upconverted delayed fluorescence is emitted. One of the advantages of TTA-UC is its occurrence at lower excitation intensity compared with the other UC mechanisms thanks to the large absorption coefficient of the donor chromophores and the long triplet lifetime of acceptor molecules.

To achieve efficient TTA-UC under weak incident light sources, diffusion of triplet species should be high enough to enable annihilation within their lifetimes. Consequently, the majority of TTA-UC systems have been studied in solution[8,11-15] or soft polymer matrices[16-20] in which the TET and TTA processes are mediated by molecular diffusion and collision. Meanwhile, it is desirable for device applications that TTA-UC processes occur in the solid state without molecular diffusion. In this perspective, it is natural to develop triplet energy migration-based photon upconversion (TEM-UC)[10], in which triplet excitons effectively diffuse in dense molecular assemblies and the molecular diffusion is not required.[13,21-31] Among various assembly systems, molecular crystals with ordered chromophore arrangements should be promising for achieving fast TEM. However, the crystalline systems have suffered from the aggregation of donor molecules and their segregation in acceptor crystals, which caused poor TET efficiency.[4] Despite efforts to solve this problem[28,29,31-33], the development of a simple and rational strategy to molecularly accommodate donor molecules in acceptor crystals is still anticipated.

Here, we describe a kinetically-controlled crystal growth approach which improves the dispersibility of donors in acceptor crystals and consequently increased the efficiency of TEM-UC. We employed the donor-acceptor pair of Pt(II) octaethylporphyrin (PtOEP) and 9,10-diphenylanthracene (DPA), which has been widely used as a benchmark. Due to their inherent structural mismatch, PtOEP and DPA do not mix homogeneously in crystals and tend to phase-segregate.[4] Meanwhile, miscibility of molecules coexisting in multicomponent assemblies has been kinetically controlled for organic molecular crystals[34] and peptide assemblies.[35,36] We apply this kinetic control concept to improve the miscibility of donor PtOEP and acceptor DPA in nanocrystals. For this, we adopted a colloid chemistry approach; tetrahydrofuran (THF) solutions of DPA-PtOEP were injected into aqueous cetyltrimethylammonium bromide (CTAB).[37-39] Upon the diffusion of injected THF into the aqueous phase, the nucleation of water-insoluble aromatic crystals occurs. Absorption of CTAB molecules on the growing crystal surfaces would reduce their interfacial energy, thus enhancing the dispersion stability of these crystals.[37-39] It was found that increase in the concentration of DPA-PtOEP caused faster crystallization

of DPA, which allowed PtOEP molecules to be kinetically trapped with improved dispersibility in DPA crystals (Fig. 3-1-1).

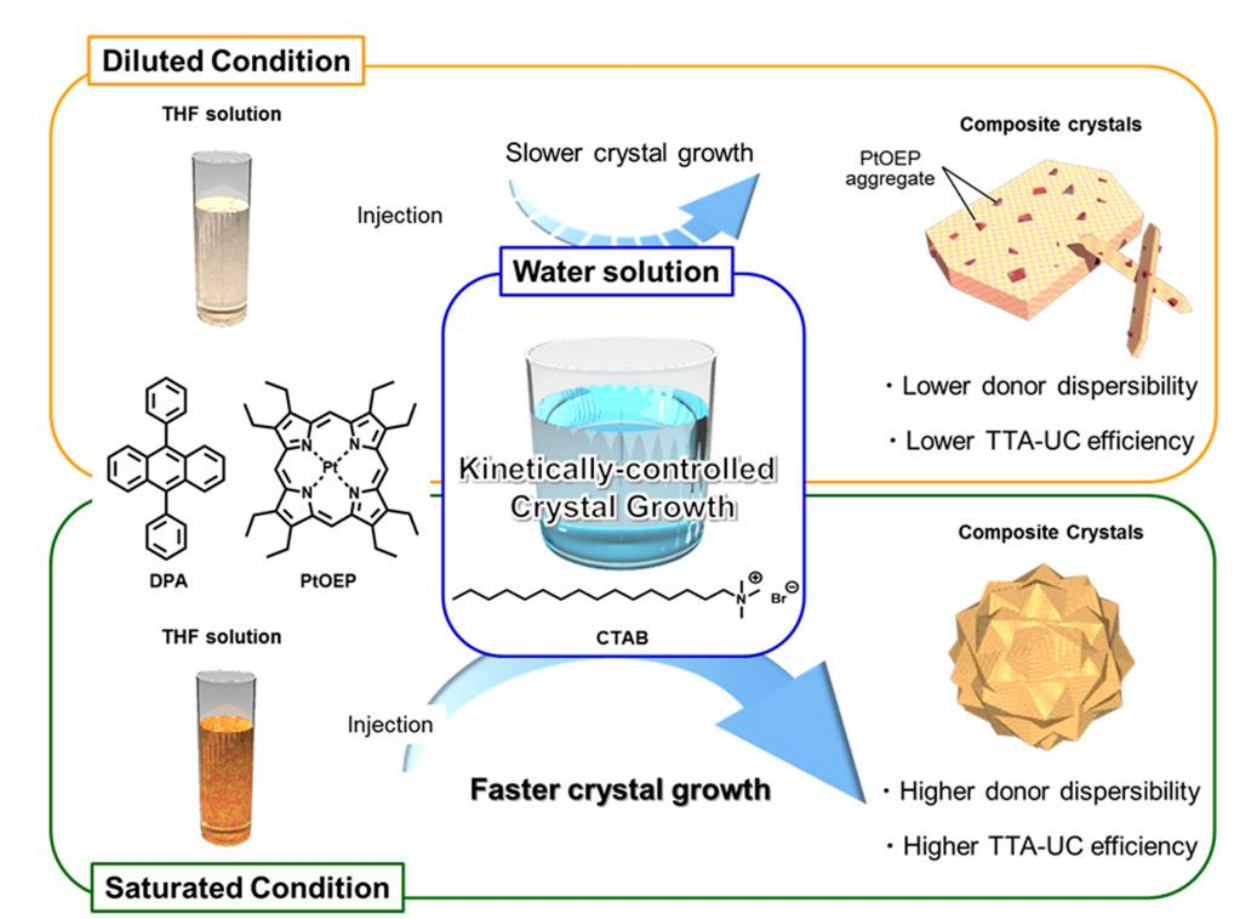

Figure 3-1-1. Schematic illustration of the concept of this study. DPA-PtOEP composite crystals are formed by reprecipitation in the presence of CTAB. A diluted THF solution of DPA-PtOEP provides slower crystal growth, resulting in lower donor dispersibility and lower TTA-UC efficiency. On the other hand, a saturated THF solution of DPA-PtOEP induces a faster crystal growth, resulting in higher donor dispersibility and higher TTA-UC efficiency.

3-2. Experimental section

3-2-1 Materials and Methods

All the solvents were used as received without further purification. DPA was purchased from Aldrich and purified by sublimation in order to minimize the amount of impurities which may act as quenchers in the solid system. PtOEP and CTAB were purchased from Aldrich and Wako chemical and used as received.

UV-visible absorption spectra were recorded on a JASCO V-670 spectrophotometer. Fluorescence spectra were measured by using a PerkinElmer LS 55 fluorescence spectrometer. Powder X-ray diffraction (PXRD) analyses were conducted on a BRUKER D2 PHASER with a Cu Kα source (λ_{ex} = 1.5418 Å). Scanning electron microscope (SEM) images were obtained by using a Hitachi S-5000. For SEM measurements, samples were collected by suction filtration using membrane filters with pore size of 0.2 μm. These filters were directly used for SEM measurements after platinum sputtering with the thickness of ca. 2 nm. Time-resolved photoluminescence lifetime measurements were carried out by using a time-correlated single photon counting lifetime spectroscopy system, HAMAMATSU Quantaurus-Tau C11567-01.

For TTA-UC measurements, the samples were sealed between quartz plates by using hot-melt adhesive in an Ar-filled glove box ([O_2] < 0.1 ppm). For TTA-UC emission spectra, a diode laser (532 nm, 200 mW, RGB Photonics) was used as an excitation source. The laser power was controlled by combining a software (Ltune) and a variable neutral density filter and measured using a PD300-UV photodiode sensor (OPHIR Photonics). The laser beam was focused on a sample using a lens. The diameter of the laser beam ($1/e^2$) was measured at the sample position using a CCD beam profiler SP620 (OPHIR Photonics). Typical area of laser irradiation spot estimated from the diameter was 2.9×10^{-4} cm^2. The emitted light was collimated by an achromatic lens, the excitation light was removed using a notch filter (532 nm), and the emitted light was again focused by an achromatic lens to an optical fiber connected to a multichannel detector MCPD-9800 which was supplied and calibrated by Otsuka Electronics and equipped with a CCD sensor for the detection of whole visible range with high sensitivity.

TTA-UC and donor phosphorescence quantum yields were measured by using an absolute quantum yield measurement system. The sample was held in an integration sphere and excited by the laser excitation source (532 nm, 200 mW, RGB Photonics). The scattered excitation light was removed using a 532 nm notch filter and emitted light was monitored with a multichannel detector C10027-01 (Hamamatsu Photonics). The spectrometer was calibrated including the integration sphere and notch filter by Hamamatsu Photonics.[22]

3-2-2 Sample preparation

DPA and PtOEP were dissolved in THF at three different concentrations. As a moderately diluted condition, DPA (2 mM)–PtOEP (2 μM) in THF was employed (Condition 1). Separately, saturated solutions of DPA (140 mM) with two different PtOEP concentrations (140 μM and 14 μM) were prepared for the rapid crystallization (Condition 2A and 2B). All the experiments of crystal growth and collection were carried out at room temperature (around 20 °C). No pre-formed crystals in the 140 mM DPA solution were detected by dynamic light scattering (DLS) measurements. 0.5 mL of DPA–PtOEP mixed THF solutions were rapidly injected into the aqueous CTAB (0.5 mM, 5 mL) at room temperature under 1000 rpm stirring. These mixtures were kept stirring for 3 minutes and then left to stand for 2 hrs. After the incubation for 2 hrs, the crystals were collected by centrifugation at 10000 rpm for 5 minutes, washed with water for three times, and dried under vacuum at room temperature.

3-3 Results and discussion

3-3-1 Characterization of the crystals

When the THF solution of DPA (2 mM)–PtOEP (2 μM) was injected into the aqueous CTAB (Condition 1) under stirring, the immediately formed suspension turned into a uniform dispersion within 3 minutes of stirring. This specimen was then incubated for 2 hrs, during which crystalline particles were gradually formed. On the other hand, precipitates were immediately formed upon injection of the saturated DPA solutions into aqueous CTAB ([DPA] = 140 mM, [PtOEP] = 140 μM and 14 μM, Condition 2A and 2B), which showed almost no changes during the standing for 2 hrs.

The composition of the obtained crystals was determined by dissolving the crystals in THF and measuring their absorption spectra. The DPA-PtOEP molar ratio were 2100:1, 700:1, and 7300:1 for those obtained under the Condition 1, 2A, and 2B, respectively. The content of PtOEP in the obtained crystals was lower than the initial mixing ratio in THF for Condition 1 (1000:1), while it was higher than those for Condition 2A (1000:1) and 2B (10000:1). The enhanced accumulation of PtOEP in DPA crystals under Conditions 2A and 2B suggests that the rapid growth of DPA microcrystals facilitate kinetic entrapment of PtOEP molecules in the interior.

The crystallinity of obtained samples was confirmed by using powder X-ray diffraction (PXRD) measurements (Fig. 3-3-1). The crystals formed under these conditions showed diffractions which showed good agreements with the PXRD pattern of bulk DPA. On the other hand, the diffraction peaks of bulk PtOEP, for example the peak around at $2\theta = 9.5$, were hardly observed from those of the composite crystals, which may be due to the high dispersibility of the donor molecules or the too small amount of PtOEP for detection. It is confirmed that the basic arrangement of DPA molecules is almost independent of the crystallization conditions.

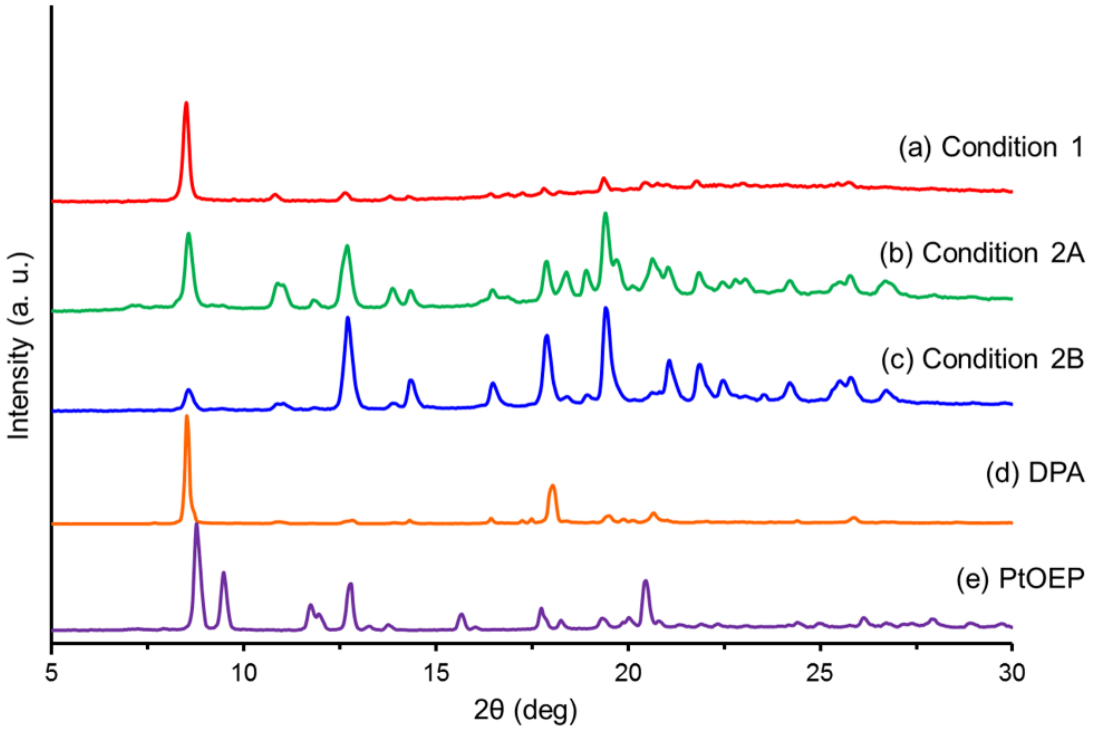

Figure 3-3-1. PXRD patterns of samples prepared by using (a) Condition 1, (b) Condition 2A, and (c) Condition 2B. (d), (e) show the PXRD patterns of bulk DPA (d) and PtOEP (e). All measurements were conducted at room temperature.

To get insights into the crystal growth processes, the crystals were collected by suction filtration before and after the 2 hrs of incubation, and their morphology was observed by scanning electron microscopy (SEM). In the case of the Condition 1 sample, partly aggregated irregular nanorods were observed before incubation. After standing for 2 hrs, a few μm-sized rods and a few tens of μm-sized sheets appeared (Fig. 3-3-2a). The observed morphological changes suggest that the ordered crystals gradually grew in the course of incubation. On the other hand, samples obtained under the Condition 2A and 2B gave larger spherical microstructures with the similar size before and after the incubation process (Fig. 3-3-2b and 3-3-2c). It is to note that the morphology of crystals differs considerably depending on the preparative conditions, i.e., kinetic parameters determine both of the nucleation and growth processes. When the same preparation procedure was carried out without DPA, only a few tens of nm-sized nanocrystals were observed, and thus the above-mentioned μm-sized objects cannot be the pure PtOEP crystals.

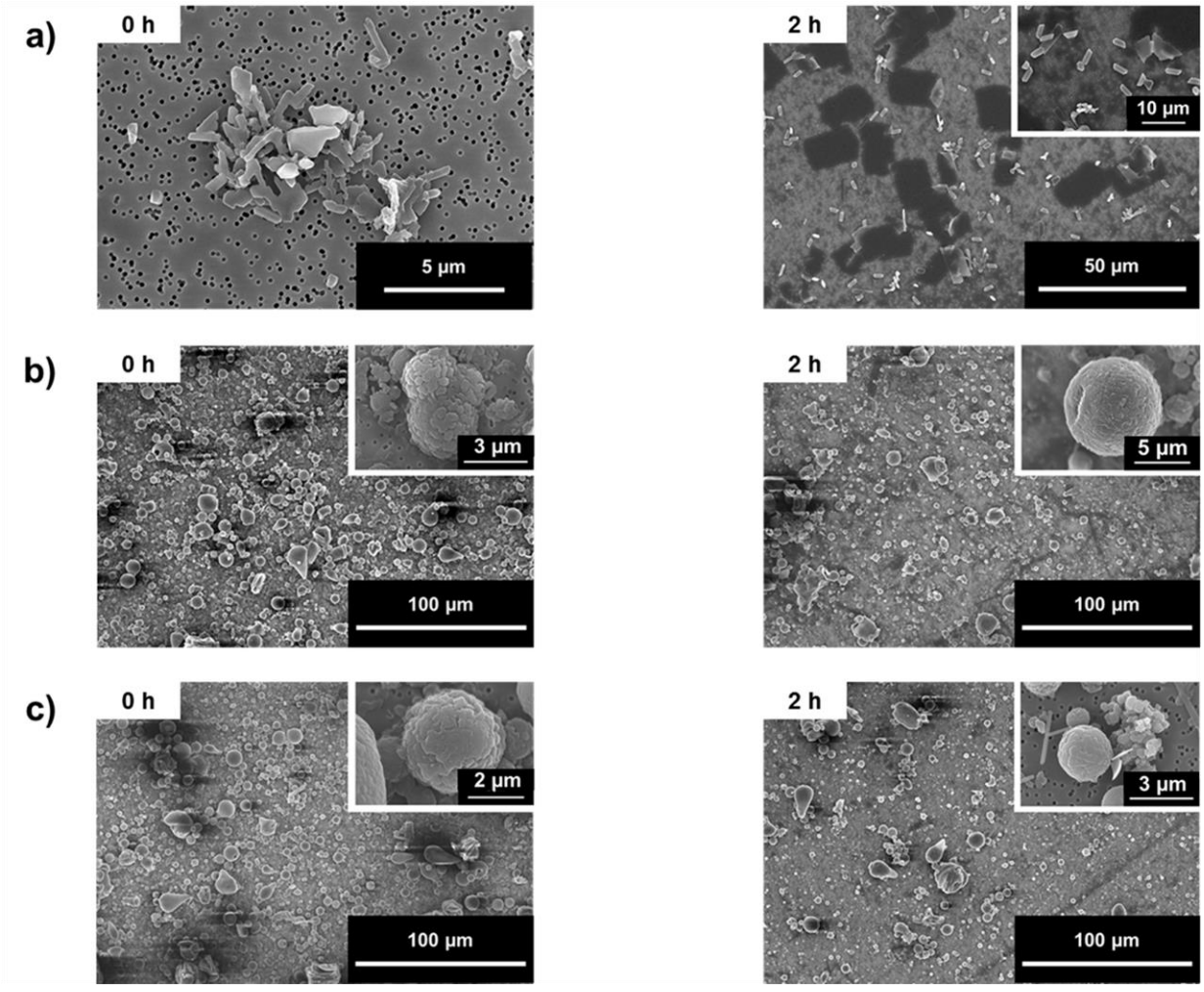

Figure 3-3-2. SEM images of crystals prepared by using (a) Condition 1, (b) Condition 2A, and (c) Condition 2B before (left) and after (right) 2 hrs incubation.

3-3-2 Photophysical Properties of the Crystals

To investigate the dispersed state of PtOEP molecules in acceptor DPA crystals, absorption spectra of PtOEP were measured (Fig. 3-3-3). A THF solution of PtOEP ([PtOEP] = 10 μM) showed a Q(0,0) band at 534 nm, whereas this band is red-shifted to 552 nm in the cast solid sample due to aggregation.[40] Interestingly, absorption spectra obtained for PtOEP in DPA-PtOEP composite crystals showed blue shifts compared to that of the neat cast solid. Notably, the peaks of the Condition 2A (537 nm) and 2B (536 nm) samples are more blue shifted compared to that of the rod-like crystals obtained under Condition 1 (541 nm). It is to note that the main peak of the Condition 2B sample is close to that observed for the diluted THF solution, with a suppressed shoulder component at around 547 nm. This shoulder component reflects the presence of interchromophore interactions among PtOEP molecules. Apparently, the sample prepared under the Condition 2B showed the spectrum revealing the most isolated PtOEP chromophores, showing the highest dispersibility of PtOEP is achieved under the rapid crystal growth condition with the high DPA:PtOEP molar ratio. We confirmed that the DPA-PtOEP crystals prepared in the absence of CTAB showed a pronounced aggregate-shoulder peak, indicating that CTAB significantly influenced the crystallization kinetics in the aqueous mixtures.

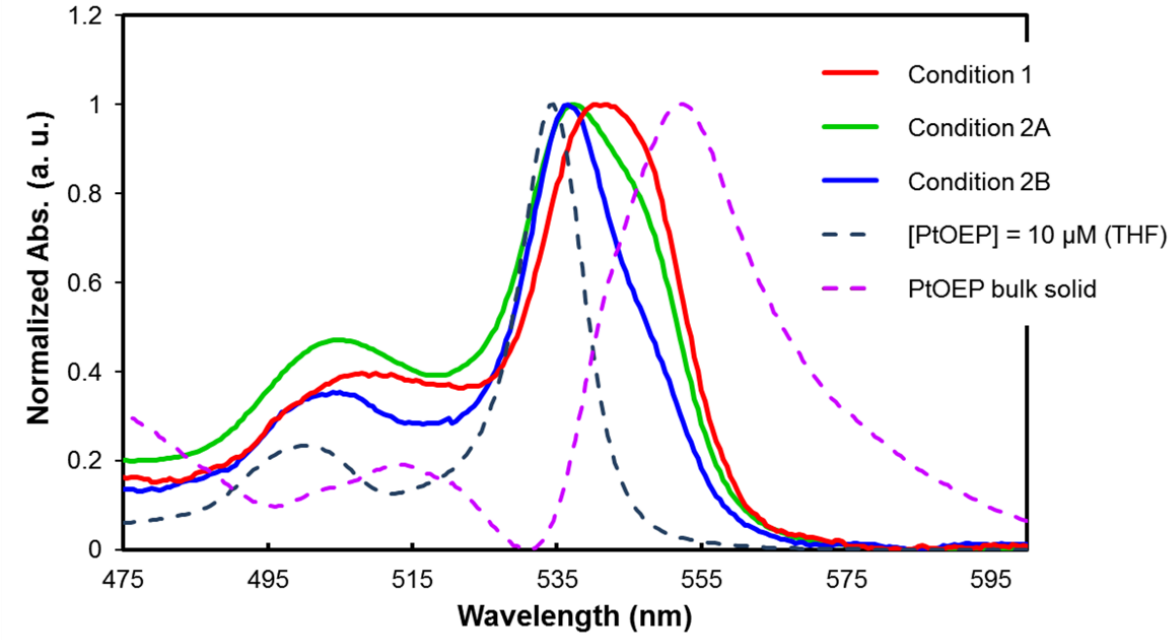

Figure 3-3-3. UV-vis absorption spectra of PtOEP in several conditions. Solid lines represent the absorption of the DPA-PtOEP composite crystals. Dashed lines show the absorption spectra of a diluted THF solution of PtOEP (10 μM) and a bulk PtOEP solid.

The fluorescence quantum yields with direct excitation of DPA (Φ_A, λ_{ex} = 365 nm) were 42%, 28%, and 54% for powdery samples obtained under Condition 1, 2A, and 2B (= Samples 1, 2A and 2B), respectively. Since the higher Φ_A values were observed for crystals with lower PtOEP contents, it is possible that the DPA-to-PtOEP singlet-singlet energy transfer and/or the re-absorption of the DPA fluorescence by the donor molecules takes place.

3-3-3 TTA-UC of DPA-based composite crystals

The TTA-UC characteristics of each composite crystals were then evaluated. Under excitation with a 532 nm laser, upconverted emission was clearly observed for each sample with the maximum intensity around at 440 nm (Fig. 3-3-4). It is to note that these TTA-UC behaviors observed for the present DPA-PtOEP crystals prepared by the CTAB-assisted colloid technique are significantly improved as compared to that previously reported for the DPA single crystal doped with PtOEP.[4]

The donor phosphorescence at 650 nm was much weaker than the UC emission, and the phosphorescence quantum yields of all the three samples were less than 0.1%. These results suggest that the triplet energy of the donor molecules is efficiently transferred to the surrounding acceptor molecules or thermally dissipated in the donor aggregates.[40]

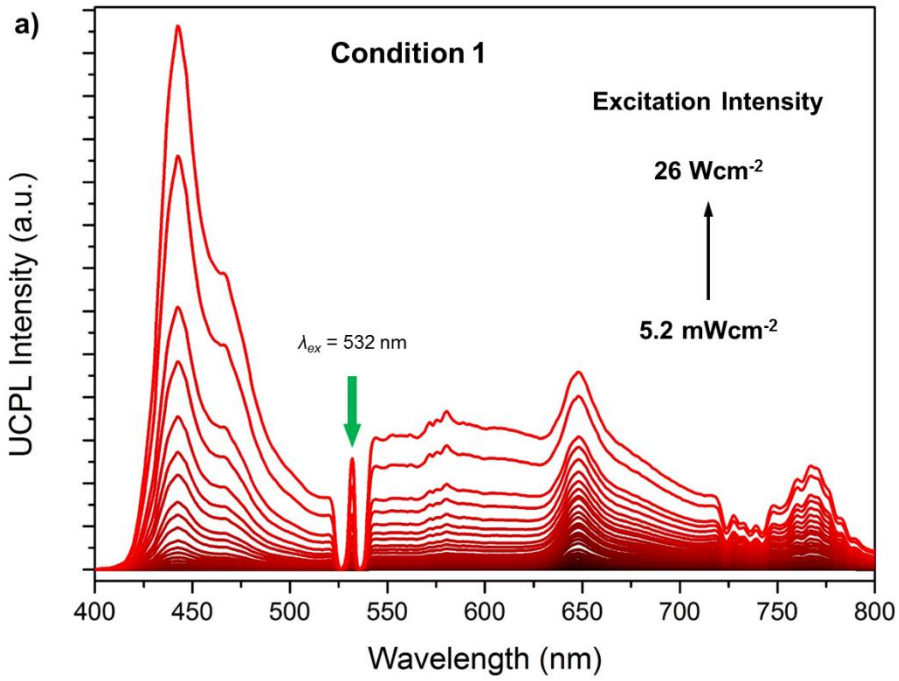

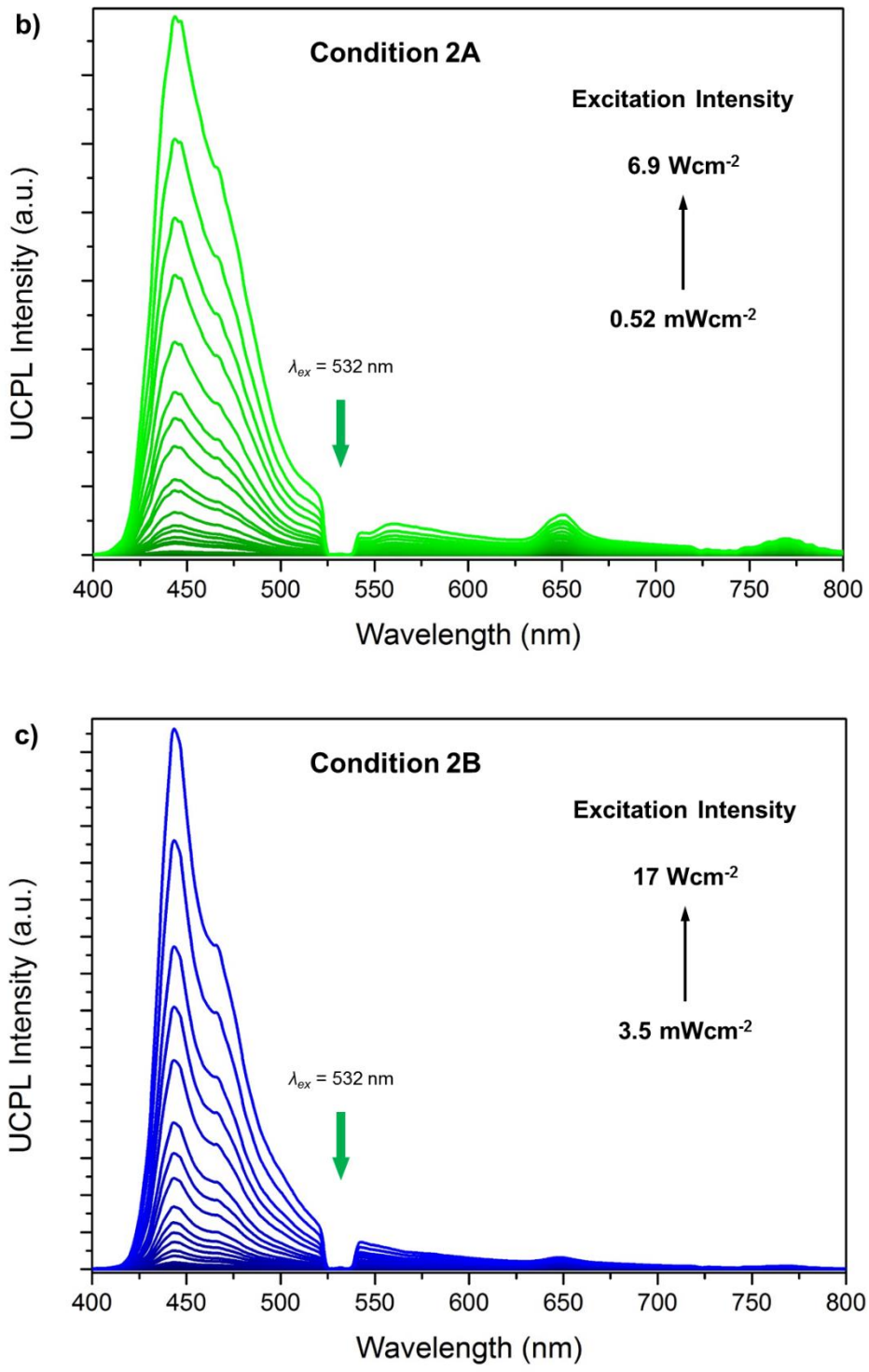

Figure 3-3-4. Photoluminescence spectra of DPA-based crystals prepared under (a) Condition 1, (b) Condition 2A, and (c) Condition 2B under Ar atmosphere with various excitation intensities (λ_{ex} = 532 nm). Scattered incident light was removed by using a 532 nm notch filter.

TTA-UC quantum yields for samples obtained under each condition were determined by the absolute method using the integrating sphere and the laser excitation source, to avoid inaccuracy that could arise from the strong light scattering of the crystals. In general, the quantum yield is defined as the ratio of absorbed photons to emitted photons, and thus the maximum yield (Φ_{UC}) of the bimolecular TTA-UC process is 50%. However, many reports multiply this value by 2 to set the maximum quantum yield at 100%. To avoid the confusion between these different definitions, the UC quantum yield is written as Φ_{UC}' (= $2\Phi_{UC}$) when the maximum efficiency is normalized to 100%. The Φ_{UC}' value detemined for the Condition 1 sample was as low as 0.044±0.011% (Fig. 3-3-5). On the other hand, much higher Φ_{UC}' values were observed for crystals prepared under the Conditions 2A (0.44±0.022%) and 2B (2.0±0.17%).

To understand the observed difference, factors affecting to the Φ_{UC}' value need to be considered. Φ_{UC}' is represented by the following equation,

$$\Phi_{uc}' = f\,\Phi_{ISC}\,\Phi_{ET}\,\Phi_{TTA}\,\Phi_{A} \qquad (1)$$

where Φ_{ISC}, Φ_{ET}, Φ_{TTA}, and Φ_{A} represent the quantum efficiencies of donor ISC, donor-to-acceptor TET, TTA, and acceptor emission[4,8]. The parameter *f* is the statistical probability for obtaining a singlet excited state after the annihilation of two triplet states. Considering that Φ_{A} of Condition 2A sample was smaller (28%) than that of the Condition 1 sample (42%), the higher Φ_{UC}' value of Condition 2A sample as compared to Condition 1 sample should be originated from the other parameters. The *f* value and Φ_{ISC} can be assumed to be the same for the identical donor-acceptor pair with the similar crystal structure as confirmed by PXRD. It is then suggested that the better dispersibility of donor molecules in Condition 2A sample, as evidenced by the absorption spectra (Fig. 3-3-3), improved the net Φ_{ET} value and consequently afforded the better Φ_{UC}'. As described above, the Condition 2B sample showed the highest donor dispersibility among all the samples prepared in this study (Fig. 3-3-3). It is reasonable that the Condition 2B sample showed higher Φ_{UC}' than the Condition 2A sample which was also benefitted from the smaller content of donor which allowed to maintain higher Φ_{A} (54%). The UC quantum yields Φ_{UC}' remain low (< 0.1%) at the solar irradiance (1.6 mW cm^{-2} at 532±5 nm, AM 1.5), requiring future efforts to decrease the needed excitation intensity.

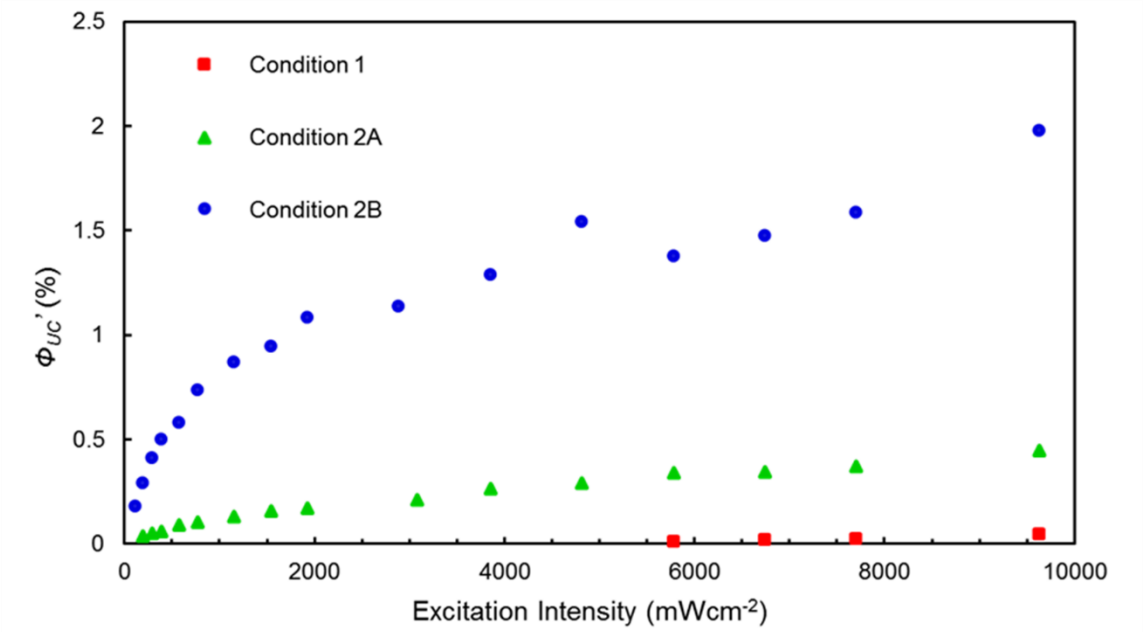

Figure 3-3-5. TTA-UC quantum yield as a function of the excitation intensity of 532 nm laser for DPA-PtOEP composite crystals prepared with three different conditions. A series of Φ_{UC}' data for each sample were obtained from the same specimen, and each points show average values of measurements conducted for more than five times. Error bars are smaller than the dot sizes for most points.

In the condensed systems, inhomogeneous distribution of donor molecules in acceptor crystals needs to be considered. Generally, TTA-UC emission intensity shows a quadratic dependence with the incident light intensity at low excitation intensity, where the thermal deactivation of the triplet states is governed by the main deactivation pathway. The quadratic-to-linear transition occurs by increasing the excitation intensity, and the transition point gives a threshold excitation intensity (I_{th}) [41-43]. Above I_{th}, the TTA becomes the main deactivation channel for the acceptor triplets. The quadratic-to-linear transitions were observed for all the three conditions (Fig. 3-3-6). In spite of the considerable difference in the UC quantum yield (Fig. 3-3-5), these three samples showed rather similar I_{th} values in the range of 326-531 mWcm^{-2}.

This discrepancy might be explained by the following hypothesis. In the Condition 1 sample, not all donor molecules form aggregates and some donor molecules well dispersed in acceptor crystals contribute to the excitation intensity dependence with an I_{th} value similar to the Condition 2B sample. However, as we described above, most of the donor molecules are present as aggregates in the Condition 1 sample, which hinder the donor-to-acceptor triplet energy transfer and resulted in the observed low UC quantum yield. It is therefore essential to characterize the UC characteristics in a comprehensive manner, and the determination of UC quantum yields is prerequisite for the evaluation of solid upconverters.

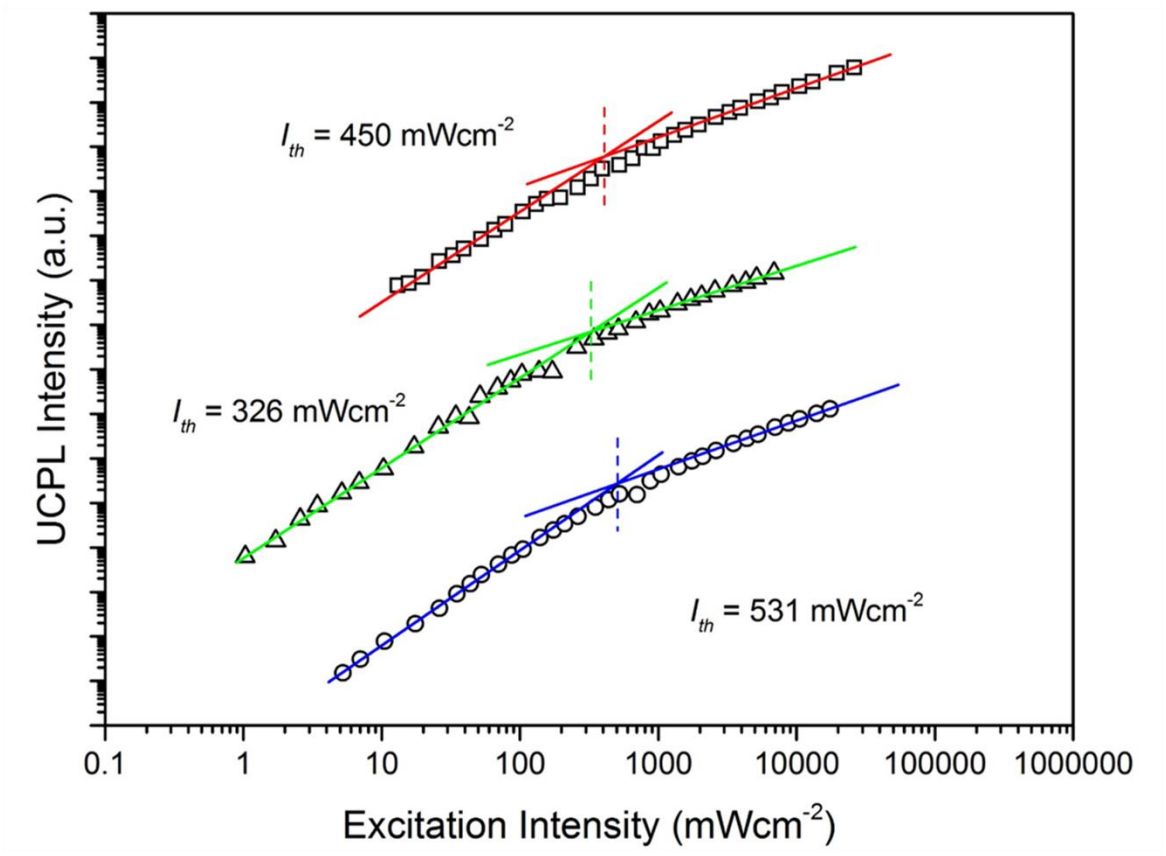

Figure 3-3-6. Double logarithmic plots of the UC photoluminescence (PL) intensity as a function of the excitation intensity for DPA-PtOEP composite crystals prepared with three different conditions. The linear fits with slope 2 and 1 in the lower and higher excitation intensity regimes are shown.

3-4 Conclusions

In this chapter, the promising potentials of the kinetically-controlled crystal growth is shown to improve the dispersibility of donor molecules in acceptor crystals and to achieve efficient TEM-UC in the solid state. By simply increasing the concentration of donor and acceptor in the surfactant-assisted reprecipitation process, the kinetic entrapment of the donor in acceptor crystals is facilitated with the enhanced dispersibility. Consequently, the UC quantum yield was dramatically enhanced. The concept of kinetically-controlled crystal growth is successfully demonstrated for the benchmark TTA-UC pair, DPA and PtOEP, which has been known to undergo severe phase segregation. The present kinetically-controlled crystallization concept for improving donor dispersibility in acceptor crystals would be widely applicable to a variety of chromophore combinations, including the recently-developed precious metal-free systems[25,44,45] and NIR-to-visible UC systems[12-15,46,47]. For further improvement of the current method, we consider that the key is to suppress the formation of defect sites that deactivate the triplet excitons.[28] The development of a new approach to circumvent this issue is under way in our laboratory.

Referances

(1) S. Baluschev, T. Miteva, V. Yakutkin, G. Nelles, A. Yasuda and G. Wegner, *Phys. Rev. Lett.*, 2006, **97**, 143903.

(2) T. N. Singh-Rachford and F. N. Castellano, *Coord. Chem. Rev.*, 2010, **254**, 2560-2573.

(3) J. Z. Zhao, S. M. Ji and H. M. Guo, *RSC Adv.*, 2011, **1**, 937-950.

(4) A. Monguzzi, R. Tubino, S. Hoseinkhani, M. Campione and F. Meinardi, *Phys. Chem. Chem. Phys.*, 2012, **14**, 4322-4332.

(5) Y. C. Simon and C. Weder, *J. Mater. Chem.*, 2012, **22**, 20817-20830.

(6) J. H. Kim and J. H. Kim, *J. Am. Chem. Soc.*, 2012, **134**, 17478-17481.

(7) V. Gray, D. Dzebo, M. Abrahamsson, B. Albinsson and K. Moth-Poulsen, *Phys. Chem. Chem. Phys.*, 2014, **16**, 10345-10352.

(8) T. W. Schmidt and F. N. Castellano, *J. Phys. Chem. Lett.*, 2014, **5**, 4062-4072.

(9) J. Zhou, Q. Liu, W. Feng, Y. Sun and F. Y. Li, *Chem. Rev.*, 2015, **115**, 395-465.

(10) N. Yanai and N. Kimizuka, *Chem. Commun.*, 2017, **53**, 655-655.

(11) M. A. Filatov, E. Heinrich, D. Busko, I. Z. Ilieva, K. Landfester and S. Baluschev, *Phys. Chem. Chem. Phys.*, 2015, **17**, 6501-6510.

(12) Z. Y. Huang, X. Li, M. Mahboub, K. M. Hanson, V. M. Nichols, H. Le, M. L. Tang and C. J. Bardeen, *Nano Lett.*, 2015, **15**, 5552-5557.

(13) K. Okumura, K. Mase, N. Yanai and N. Kimizuka, *Chem. Eur. J.*, 2016, **22**, 7721-7726.

(14) C. Mongin, S. Garakyaraghi, N. Razgoniaeva, M. Zamkov and F. N. Castellano, *Science*, 2016, **351**, 369-372.

(15) Y. Sasaki, S. Amemori, H. Kouno, N. Yanai and N. Kimizuka, *J. Mater. Chem. C*, 2017, **5**, 5063-5067.

(16) R. R. Islangulov, J. Lott, C. Weder and F. N. Castellano, *J. Am. Chem. Soc.*, 2007, **129**, 12652-12653.

(17) J. H. Kim, F. Deng, F. N. Castellano and J. H. Kim, *Chem. Mater.*, 2012, **24**, 2250-2252.

(18) F. Marsico, A. Turshatov, R. Pekoz, Y. Avlasevich, M. Wagner, K. Weber, D. Donadio, K. Landfester, S. Baluschev and F. R. Wurm, *J. Am. Chem. Soc.*, 2014, **136**, 11057-11064.

(19) S. H. Lee, D. C. Thevenaz, C. Weder and Y. C. Simon, *J. Polym. Sci. A Polym. Chem.*, 2015, **53**, 1629-1639.

(20) A. Monguzzi, M. Mauri, A. Bianchi, M. K. Dibbanti, R. Simonutti and F. Meinardi, *J. Phys. Chem. C*, 2016, **120**, 2609-2614.

(21) R. Vadrucci, C. Weder and Y. C. Simon, *J. Mater. Chem. C*, 2014, **2**, 2837-2841.

(22) P. F. Duan, N. Yanai, H. Nagatomi and N. Kimizuka, *J. Am. Chem. Soc.*, 2015, **137**, 1887-1894.

(23) T. Ogawa, N. Yanai, A. Monguzzi and N. Kimizuka, *Sci. Rep.*, 2015, **5**, 10882.

(24) P. F. Duan, N. Yanai, Y. Kurashige and N. Kimizuka, *Angew. Chem. Int. Ed.*, 2015, **54**, 7544-7549.

(25) T. C. Wu, D. N. Congreve and M. A. Baldo, *Appl. Phys. Lett.*, 2015, **107**, 031103.

(26) S. Hisamitsu, N. Yanai and N. Kimizuka, *Angew. Chem. Int. Ed.*, 2015, **54**, 11550-11554.

(27) J. S. Lissau, D. Nauroozi, M. P. Santoni, S. Ott, J. M. Gardner and A. Morandeira, *J. Phys. Chem. C*, 2015, **119**, 25792-25806.

(28) M. Hosoyamada, N. Yanai, T. Ogawa and N. Kimizuka, *Chem.-Eur. J.*, 2016, **22**, 2060-2067.
(29) M. Oldenburg, A. Turshatov, D. Busko, S. Wollgarten, M. Adams, N. Baroni, A. Welle, E. Redel, C. Woll, B. S. Richards and I. A. Howard, *Adv. Mater.*, 2016, **28**, 8477-8482.
(30) A. Monguzzi, M. Mauri, M. Frigoli, J. Pedrini, R. Simonutti, C. Larpent, G. Vaccaro, M. Sassi and F. Meinardi, *J. Phys. Chem. Lett.*, 2016, **7**, 2779-2785.
(31) K. Kamada, Y. Sakagami, T. Mizokuro, Y. Fujiwara, K. Kobayashi, K. Narushima, S. Hirata and M. Vacha, *Mater. Horiz.*, 2017, **4**, 83-87.
(32) S. Baluschev, V. Yakutkin, G. Wegner, B. Minch, T. Miteva, G. Nelles and A. Yasuda, *J. Appl. Phys.*, 2007, **101**, 023101.
(33) H. Goudarzi and P. E. Keivanidis, *J. Phys. Chem. C*, 2014, **118**, 14256-14265.
(34) Q. H. Cui, Y. S. Zhao and J. N. Yao, *Adv. Mater.*, 2014, **26**, 6852-6870.
(35) B. Li, S. S. Li, Y. C. Zhou, H. A. M. Ardona, L. R. Valverde, W. L. Wilson, J. D. Tovar and C. M. Schroeder, *ACS Appl. Mater. Inter.*, 2017, **9**, 3977-3984.
(36) H. A. M. Ardona, E. R. Draper, F. Citossi, M. Wallace, L. C. Serpell, D. J. Adams and J. D. Tovar, *J. Am. Chem. Soc.*, 2017, **139**, 8685-8692.
(37) X. J. Zhang, G. D. Yuan, Q. S. Li, B. Wang, X. H. Zhang, R. Q. Zhang, J. C. Chang, C. S. Lee and S. T. Lee, *Chem. Mater.*, 2008, **20**, 6945-6950.
(38) B. Yang, J. C. Xiao, J. I. Wong, J. Guo, Y. C. Wu, L. Ong, L. L. Lao, F. Boey, H. Zhang, H. Y. Yang and Q. C. Zhang, *J. Phys. Chem. C*, 2011, **115**, 7924-7927.
(39) C. Zhang, J. Y. Zheng, Y. S. Zhao and J. N. Yao, *Adv. Mater.*, 2011, **23**, 1380-1384.
(40) M. Campione, E. Fumagalli, L. Raimondo, A. Monguzzi, F. Meinardi and A. Sassella, *Chem. Mater.*, 2011, **23**, 832-840.
(41) A. Monguzzi, J. Mezyk, F. Scotognella, R. Tubino and F. Meinardi, *Phys. Rev. B*, 2008, **78**, 195112.
(42) Y. Y. Cheng, T. Khoury, R. G. C. R. Clady, M. J. Y. Tayebjee, N. J. Ekins-Daukes, M. J. Crossley and T. W. Schmidt, *Phys. Chem. Chem. Phys.*, 2010, **12**, 66-71.
(43) A. Haefele, J. Blumhoff, R. S. Khnayzer and F. N. Castellano, *J. Phys. Chem. Lett.*, 2012, **3**, 299-303.
(44) N. Yanai, M. Kozue, S. Amemori, R. Kabe, C. Adachi and N. Kimizuka, *J. Mater. Chem. C*, 2016, **4**.
(45) V. Gray, A. Dreos, P. Erhart, B. Albinsson, K. Moth-Poulsen and M. Abrahamsson, *Phys. Chem. Chem. Phys.*, 2017, **19**, 10931-10939.
(46) S. Amemori, Y. Sasaki, N. Yanai and N. Kimizuka, *J. Am. Chem. Soc.*, 2016, **138**, 8702-8705.
(47) M. F. Wu, D. N. Congreve, M. W. B. Wilson, J. Jean, N. Geva, M. Welborn, T. Van Voorhis, V. Bulovic, M. G. Bawendi and M. A. Baldo, *Nat. Photon.*, 2016, **10**, 31-34.

Chapter 4 Rational Strategy for Photon Upconversion Crystals: Aggregation-free Sensitizer Accommodation in Ionic Crystals with Less Defects

Abstract

There are two major long-standing questions for triplet-triplet annihilation-based photon upconversion (TTA-UC) in solid crystals. Why is the UC efficiency often low in crystalline systems? What is the rational strategy to construct efficient upconverting crystals? In this work, we addressed these issues by employing a simple model system where ionic interactions play a key role. When crystals of an anthracene-based ionic acceptor (emitter) were grown in the presence of anionic donor (sensitizer) molecules, the donor molecules were spontaneously taken up and dispersed homogenously in acceptor crystals without aggregation. Highly efficient UC was achieved as a consequence of quantitative triplet energy transfer (TET) from the incorporated donor to the surrounding acceptor. We also found that the mechanical grinding of the donor-doped single crystals lead to a significant decrease in UC efficiency, suggesting that trap sites formed in the crystals have a significant negative impact on the UC performance. The fundamental knowledge obtained from the current ionic crystal system offers rational design guidelines towards the development of efficient TTA-UC systems in the solid-state.

4-1 Introduction

Although high UC efficiencies have been achieved in solution because of the ease of molecular diffusion and collision processes, it is indispensable to develop solid upconversion materials for the real-world application of TTA-UC towards solar energy utilization devices such as photovoltaic cells. Several approaches have been proposed such as droplets in rigid matrices,[1,2] molecular diffusion in rubbery polymers,[3-7] and triplet energy migration (TEM) in dense chromophore assemblies.[8-15] Among them, TEM-based UC in crystalline materials has the potential to attain an ultimate UC system with high UC efficiency at low excitation intensity thanks to fast TEM in ordered chromophore arrays. However, most of the crystalline TEM-UC systems have suffered from the phase separation of donor molecules in acceptor crystals, resulting in low TET efficiency.[9,16] In recent years, a few strategies have been reported to overcome this problem. For example, the modification of acceptor units with flexible alkyl chains can create the room for donor molecules to be accommodated in acceptor crystals.[12] As another approach, fast and kinetically-controlled crystal growth enables to trap donor molecules in rigid acceptor crystals during the crystallization process.[15] In these approaches, the interactions operating among donor and acceptor molecules are weak van der Waals dispersion forces. However, these dispersion-force based strategies unfortunately sacrificed the advantages of crystalline systems; they reduced crystal regularity in exchange for the homogeneous donor accommodation, which inhibited the fast and efficient energy diffusion. In addition, while defects caused by disordered structures were suspected to act as quenching sites for excitons that reduce the efficiency of UC, there have been no reports to directly prove such situation. Thus, it remains a grand challenge to solve these issues and to develop highly efficient solid UC systems. To unveil the relationship between the crystal quality and photophysical properties involved in UC, it is desired to introduce specific interactions to improve structural integrity of the mixed crystals and to develop a rational strategy that simultaneously fulfills the controlled molecular dispersion of donors in acceptor crystals and the maintenance of regularity in the whole crystalline systems.

Here we show that an introduction of ionic interactions as additional cohesive interaction can realize the aggregation-free dispersion of donor molecules in acceptor ionic crystals without losing the high crystal regularity. The ionic interactions can compensate the inherent structural mismatch between the donor and acceptor molecules since they exert the major interaction in the crystal formation process. As a proof-of-concept, one of the simplest anionic acceptors 9,10-anthracenedicarboxylate (ADC) was employed as a model system, and it was combined with dicyclohexyl ammonium (DCA) cations to form ionic crystals $(DCA)_2ADC$ (Fig. 4-1-1a). When the ionic crystals were prepared in the presence of an anionic donor, palladium mesoporphyrin (PdMesoP), the donor molecules were successfully introduced into the crystals. Remarkably, the accommodated donor molecules were found to be molecularly dispersed, resulting in quantitative donor-to-acceptor TET (Fig. 4-1-1b). The ionic interactions play a key role in this excellent donor dispersion as evidenced by the segregation of commonly-used nonionic donor Pt(II) octaethylporphyrin (PtOEP) formed aggregation in the ionic crystals (Fig. 4-1-1b). The impact of crystal defects upon TTA-UC properties was proved for the first time by comparing UC efficiency and emission decay profiles for single crystals and mechanically-ground powder samples. This work offers an unequivocal answer to the long-standing questions; what makes the UC efficiency in crystalline systems low, and how to rationally achieve efficient UC in solid crystals. While the main objective of this work is to prove the concept in the simple model system, the generalization of obtained basic knowledge would open a path towards the realization of ultimate solid-state upconverters.

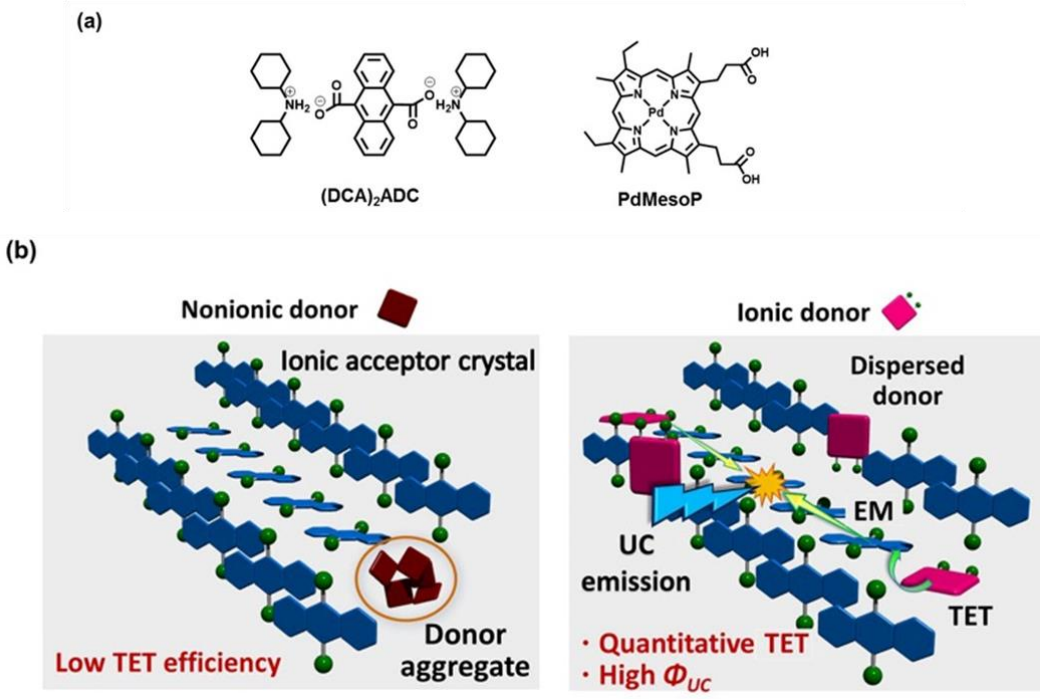

Figure 4-1-1. (a) Chemical structures of $(DCA)_2ADC$ and PdMesoP. (b) Schematic illustration of the concept of this study. Nonionic donor molecules aggregate in the acceptor ionic crystals, which ends up with poor TET efficiency (left). On the other hand, ionic donor molecules are molecularly dispersed in the acceptor ionic crystals, resulting in quantitative TET and high UC efficiency (right).

4-2 Experimental section

4-2-1 General methods

All the chemicals were used as received otherwise noted. H_2ADC, dicyclohexylamine, and PtOEP were purchased from Aldrich. PdMesoP was purchased from Frontier Scientific. 9,10-diphenylanthracene (DPA) was purchased from TCI and purified by sublimation.

UV-visible absorption spectra were recorded on a JASCO V-670 spectrophotometer. Fluorescence spectra were measured by using a PerkinElmer LS 55 fluorescence spectrometer. Single crystal X-ray data were collected on a CCD diffractometer (Rigaku Saturn VariMax) with graphite-monochromated Mo Kα radiation (λ_{ex} = 0.71070 Å). Powder X-ray diffraction (PXRD) analyses were conducted on a BRUKER D2 PHASER with a Cu Kα source (λ_{ex} = 1.5418 Å).

For TTA-UC measurements, the samples were sealed between quartz plates by using hot-melt adhesive in an Ar-filled glove box ([O_2] < 0.1 ppm). For TTA-UC emission spectra, a diode laser (532 nm, 200 mW, RGB Photonics) was used as an excitation source. The laser power was controlled by combining a software (Ltune) and a variable neutral density filter and measured using a PD300-UV photodiode sensor (OPHIR Photonics). The laser beam was focused on a sample using a lens. The diameter of the laser beam ($1/e^2$) was measured at the sample position using a CCD beam profiler SP620 (OPHIR Photonics). A typical area of laser irradiation spot estimated from the diameter was 2.9×10^{-4} cm^2. The emitted light was collimated by an achromatic lens, the excitation light was removed using a notch filter (532 nm), and the emitted light was again focused by an achromatic lens to an optical fiber connected to a multichannel detector MCPD-9800 (Otsuka Electronics). Time-resolved photoluminescence lifetime measurements were carried out by using a time-correlated single photon counting lifetime spectroscopy system, HAMAMATSU Quantaurus-Tau C11567-01.

TTA-UC and donor phosphorescence quantum yields were measured by using an absolute quantum yield measurement system.[17] The sample was held in an integrating sphere and excited by the laser excitation source (532 nm, 200 mW, RGB Photonics). The scattered excitation light was removed using a 532 nm notch filter and emitted light was monitored with a multichannel detector C10027-01 (Hamamatsu Photonics). The spectrometer was calibrated including the integration sphere and notch filter by Hamamatsu Photonics. In general, a quantum yield is defined as the ratio of absorbed photons to emitted photons, and thus the maximum quantum yield (Φ_{UC}) of the bimolecular TTA-UC process is 50%. However, many reports multiply this value by 2 to set the maximum efficiency at 100%. To avoid the confusion between these different definitions, the UC efficiency is written as Φ_{UC}' (= $2\Phi_{UC}$) when its maximum is normalized to be 100%.

4-2-2 Sample preparation

To prepare ionic crystals $(DCA)_2ADC$, 50 μmol (13.3 mg) of H_2ADC was dissolved in 5.0 mL of methanol, to which 0.1 mmol (20 μL) of dicyclohexylamine was added. Colourless precipitates were immediately formed, and this suspension was left for 3 days at room temperature. The precipitates gradually changed to colorless crystals of $(DCA)_2ADC$ during the incubation. Donor-doped ionic crystals referred as PdMesoP-$(DCA)_2ADC$, were prepared by the similar way of $(DCA)_2ADC$, except for the presence of 0.1 μmol (67.1 μg) of PdMesoP in the methanol solution of H_2ADC before adding dicyclohexylamine. Pale-pink crystals of PdMesoP-$(DCA)_2ADC$ were formed during incubation. As control experiments, crystals with two other compositions were prepared. Nonionic donor PtOEP was used instead of PdMesoP, and the similar crystallization procedure gave PtOEP-$(DCA)_2ADC$. Nonionic crystals of DPA was doped with PdMesoP by recrystallization of 50 μmol (16.5 mg) of DPA from a hot methanol (30 mL) in the presence of 0.1 μmol (67.1 μg) of PdMesoP. All the prepared crystals were collected by suction filtration and washed with methanol, and dried under vacuum at room temperature before measurements. For upconversion measurements, the crystals were placed between two glass plates and sealed in an Ar-filled glove box ($[O_2] < 0.1$ ppm) by using a hot-melt adhesive.

4-3 Results and discussion

4-3-1 Characterization of the ionic crystals

When a quantitative amount of dicyclohexylamine (2.0 mM) was added to the 1.0 mM methanol solution of 9,10-anthracenedicarboxylic acid H_2ADC, the luminescence color of the solution immediately changed from cyan to deep-blue. The sharpening and blue-shift of fluorescence spectra after adding the dicyclohexylamine to an H_2ADC solution would reflect a conformational change of the carboxylic group, suggesting a formation of the ionic pair (Fig. 4-3-1a).[18,19] FT-IR spectra also indicate the formation of the ionic pairs. The C=O vibration band (1676 cm^{-1}) of carboxylic acid group disappeared, and replaced by new peaks at 1518 cm^{-1} and 1398 cm^{-1} assignable to C=O vibration of COO^- moiety (Fig. 4-3-1b).[20]

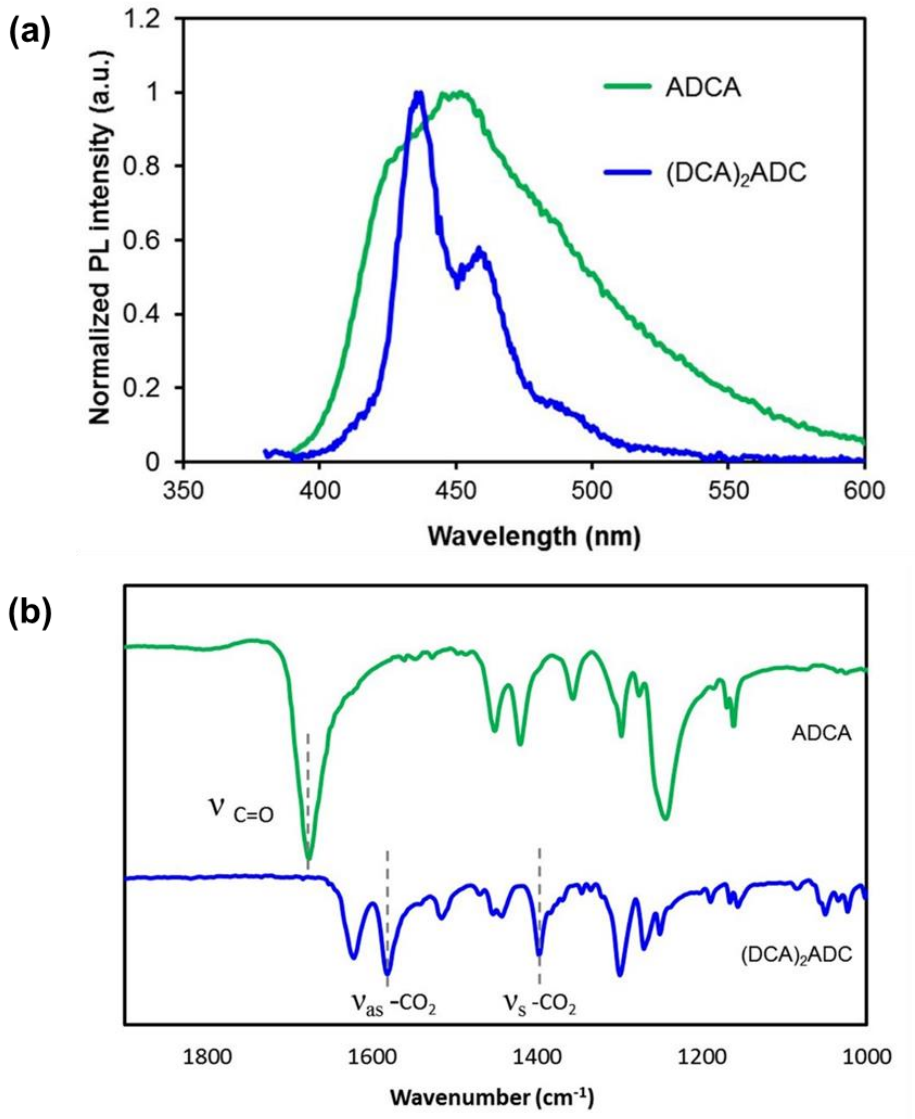

Figure 4-3-1. (a) Emission spectra of ADCA (blue) and $(DCA)_2ADC$ (green) in 1.0 mM methanol solution. Excitation wavelength was selected as λ_{ex} =365 nm. (b) FT-IR spectra of ADCA (blue) and DCA_2ADC (green) powder samples.

When the concentration of H_2ADC was increased from 1.0 mM to 10 mM, colorless precipitates were formed immediately after mixing with 20 mM dicyclohexylamine. Incubation of this mixture for 3 days at room temperature produced sub-mm sized crystals. Single crystal structural analysis was conducted for this ionic crystal $(DCA)_2$ADC. The space group was assigned to the $P2_1/c$ monoclinic system. A lamellar structure separated by ionic and nonionic domains was observed (Fig. 4-3-2a). In the *b*-*c* plane, continuous ionic networks are constructed by carboxylate and ammonium moieties. The edges of anthracene rings are overlapped along the *a*-axis with the nearest C-C distance of 3.6 Å, indicating the existence of a weak π-π interaction (Fig. 4-32b). In benchmark acceptor 9,10-diphenylanthracene (DPA), phenyl rings provide steric hinderance to avoid the concentration quenching and it shows large Stokes shift associated with the strong π-π interaction. In this work, we employed ADC without phenyl groups as the simplest model, but cyclohexyl moieties effectively serve as the spacers to tune the inter-chromophore interactions. The weak inter-chromophore interactions between anthracene moieties are reflected to the optical properties as mentioned below.

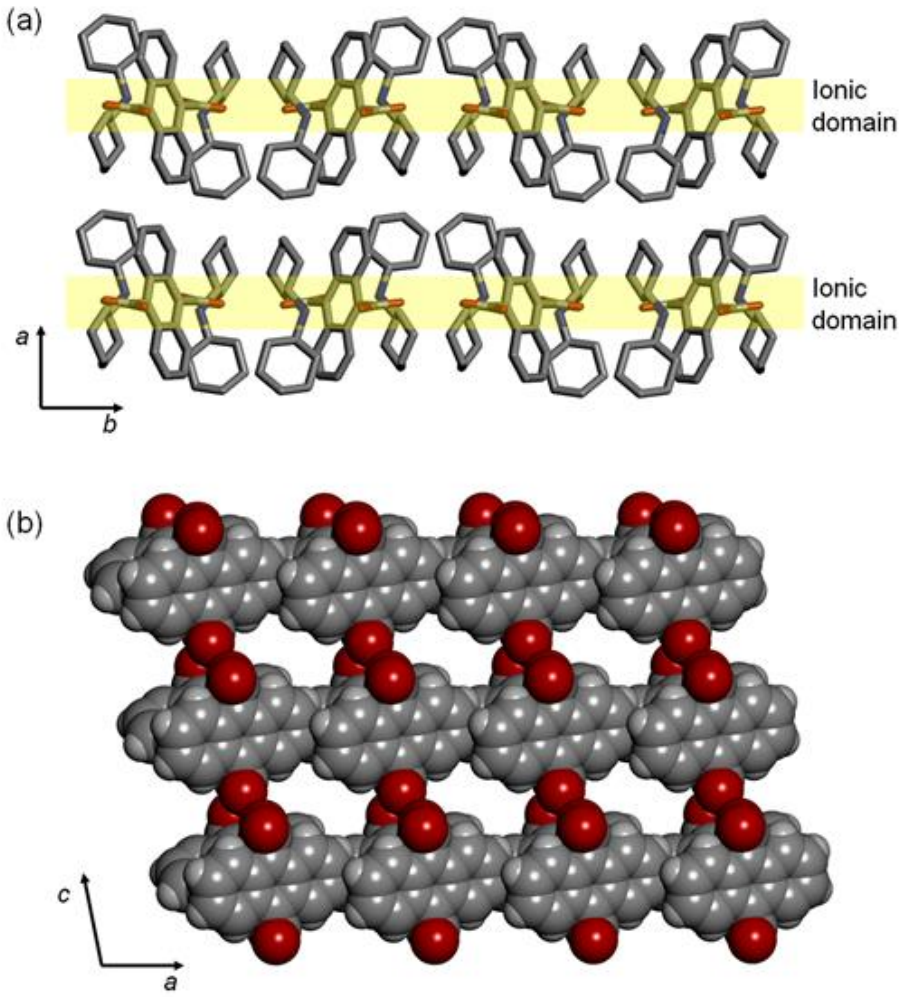

Figure 4-3-2. (a) Crystal structure of $(DCA)_2$ADC viewed along the c-axis, showing a lamellar structure consisting of ionic and non-ionic domains. N, blue; O, red; C, grey. Hydrogen atoms are omitted for clarity. (b) Packing structure of ADC. DCA moieties are omitted for clarity. N, blue; O, red; C, grey; H, light gray.

UV-vis absorption spectrum of a diluted methanol solution of $(DCA)_2ADC$ (10 μM) showed π-π* transition bands with vibronic structures at 337 (0-3), 353 (0-2), 371 (0-1) and 392 nm (0-0) which are characteristic to anthracene-based compounds (Fig. 4-3-3). The emission spectrum in methanol shows a vibronic progression mirroring that of the absorption spectra starting with the 0-0 band near 400 nm. In the crystals of $(DCA)_2ADC$, absorption peaks were moderately broadened and red-shifted to 342, 363, 381 and 402 nm. This change reflects an existence of weak dipole-dipole interactions between the transition dipole moments of anthracene moieties. Emission bands of the $(DCA)_2ADC$ crystals showed disappearance of the 0-0 vibrational band, indicating the internal filter effect widely observed for the condensed solid sample (Fig. 4-3-3). It however showed small red shifts compared to those of the diluted methanol solution of $(DCA)_2ADC$. The width of the observed red shift was as small as 75 meV in energy, and such small energy loss is advantageous as emitting materials in sensitized TTA-UC. Interestingly, the ionic crystal $(DCA)_2ADC$ showed a higher fluorescence quantum yield Φ_{FL} of 74% compared to that of $(DCA)_2ADC$ in solution (49%), suggesting the restriction of vibrational deactivation in the rigid crystalline environment.

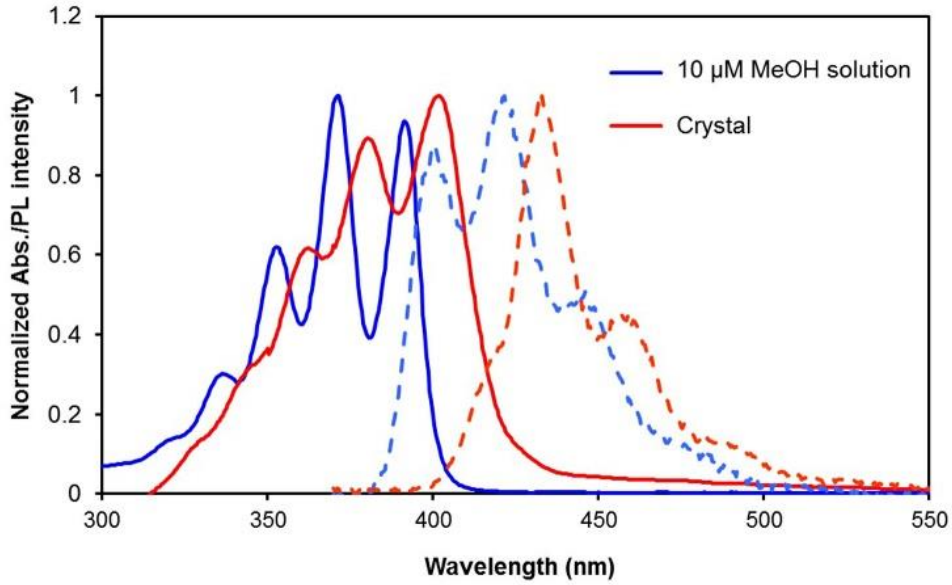

Figure 4-3-3. UV-vis absorption spectra (solid lines) and emission spectra (broken lines) of (DCA)2ADC in a 10 μM methanol solution (blue) and ionic crystals (red). The excitation wavelength was selected as λex =365 nm.

4-3-2 Incorporation of the donor into the ionic crystals

The donor PdMesoP molecules weretaken up from the solution to acceptor ionic crystals $(DCA)_2ADC$ during the crystallization process. Pale-pink crystals were obtained after 3 days by incubating the ternary mixture of H_2ADC, dicyclohexylamine and PdMesoP in methanol, suggesting the formation of composite crystals PdMesoP-$(DCA)_2ADC$ (see Experimental section for details). The amount of accommodated donor was estimated by dissolving the composite crystals in methanol and measuring UV-vis absorption spectra. The donor-acceptor molar ratio in PdMesoP-$(DCA)_2ADC$ was estimated as ca. 10000 to 1. Interestingly, the single-crystal X-ray analysis of PdMesoP-$(DCA)_2ADC$ showed that the inclusion of such small amount of donor did not affect the basic acceptor crystal structure. To investigate the dispersed state of PdMesoP molecules in the ionic crystal, absorption spectra were measured (Fig. 4-3-4). A 10 μM DMF solution of PdMesoP showed a Q(0,0) band at 545 nm, whereas this band is broadened and red-shifted to 558 nm in bulk PdMesoP solid due to aggregation. Significantly, absorption spectra of PdMesoP-$(DCA)_2ADC$ showed almost similar peaks compared to that in DMF. This result clearly indicates that PdMesoP molecules are molecularly dispersed without aggregation in the ionic crystals. The inclusion of PdMesoP in $(DCA)_2ADC$ ionic crystals was also evident from the slight decrease of fluorescence quantum yield Φ_{FL} from 74% to 56% which is ascribable to reabsorption and/or back energy transfer to in-crystal PdMesoP molecules.

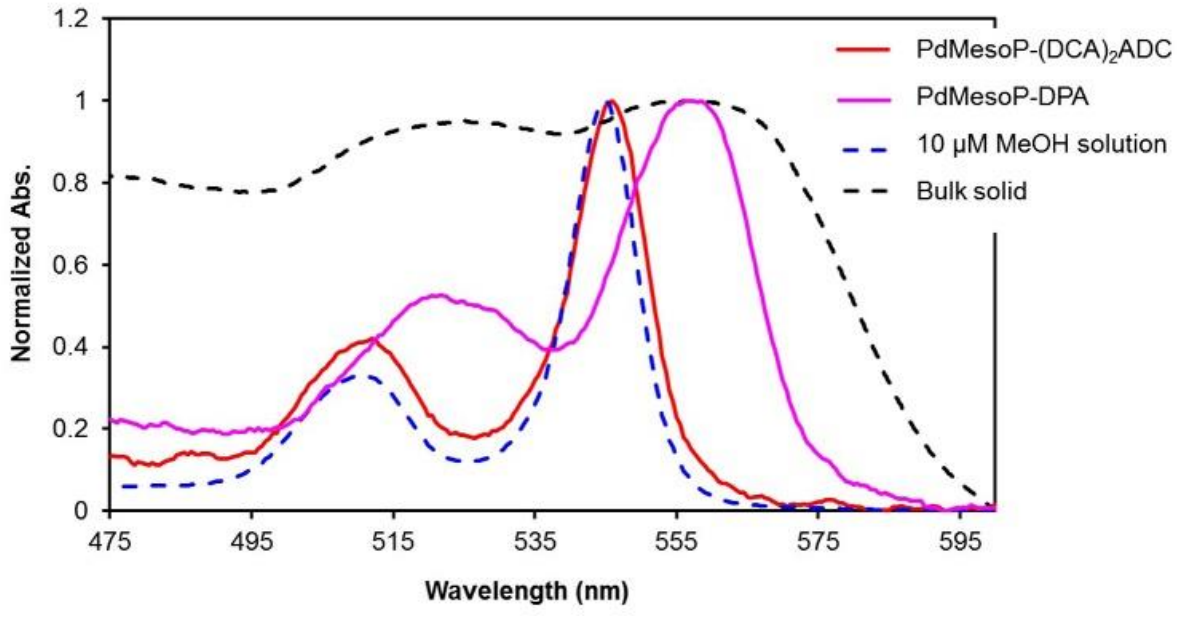

Figure 4-3-4. UV-vis absorption spectra of PdMesoP-$(DCA)_2ADC$ crystals (red), PdMesoP-DPA crystals (pink), 10 μM DMF solution of PdMesoP (blue) and bulk PdMesoP (black).

To confirm the role of ionic interactions for molecularly dispersing PdMesoP in $(DCA)_2ADC$ crystals, control experiments were carried out by using nonionic donor PtOEP or non-ionic acceptor DPA (see Experimental Section for the sample preparation). A certain amount of nonionic PtOEP molecules was incorporated into the ionic crystals of $(DCA)_2ADC$, but the absorption peaks of PtOEP in the crystals exhibited broadening and red-shift compared to that in molecularly dispersed solution, indicating the aggregation of PtOEP (Fig. 4-3-5). Likewise, PdMesoP in DPA crystals showed broadened, red-shifted spectrum and ionic PdMesoP formed aggregates when nonionic acceptor DPA was used as host crystals (Fig. 4-3-4). That is, the linear ionic networks formed in ionic crystals (DCA)2ADC show adaptive ability which can alleviate structural mismatch of the incorporated ionic PdMesoP molecules. That is, the linear ionic networks formed in ionic crystals (DCA)2ADC show adaptive ability which can alleviate structural mismatch of the incorporated ionic PdMesoP molecules.

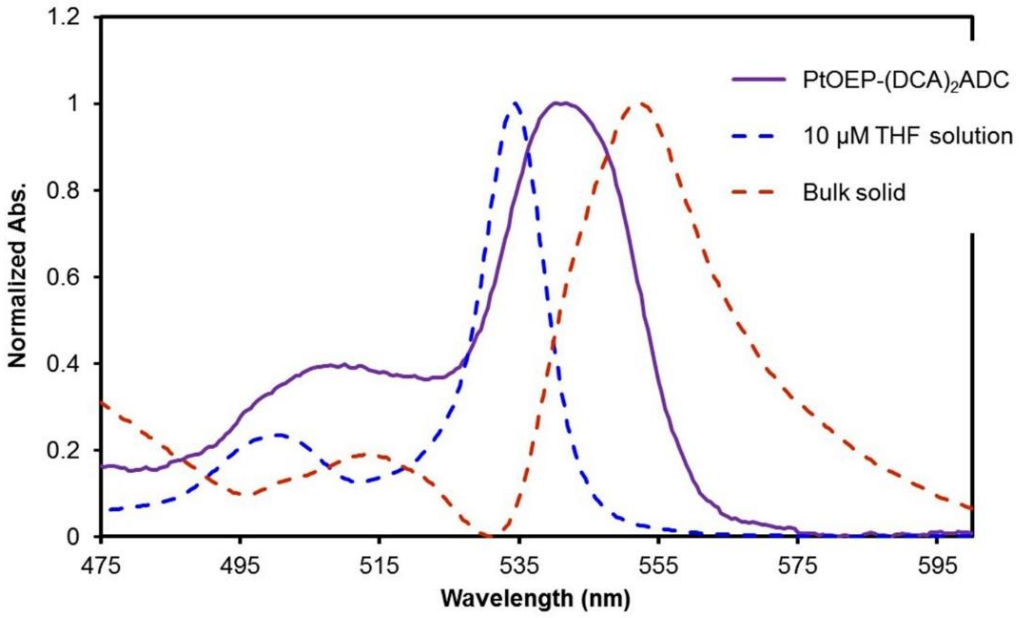

Figure 4-3-5. UV-vis absorption spectra of PtOEP-$(DCA)_2ADC$ crystals (purple), diluted THF solution of PtOEP (10 μM, blue) and bulk PtOEP solid (red).

4-3-3 TTA-UC of the ionic crystals

The TTA-UC characteristics were evaluated by using sub-mm-sized single crystals of PdMesoP-$(DCA)_2ADC$. The crystals were collected and sealed in an Ar-filled glove box. Under excitation with a 532 nm laser, upconverted emission was clearly observed with the maximum intensity at around 435 nm (Fig. 4-3-6). Interestingly, a negligible phosphorescence emission from PdMesoP was observed from PdMesoP-$(DCA)_2ADC$, where the phosphorescence quantum yield (Φ_P) was estimated as less than 0.1%. Taking into account the fact that PdMesoP molecules are molecularly dispersed in the crystals, a quantitative TET from the donor to the surrounding acceptor is strongly suggested. The excitation intensity dependence of UC emission intensity showed a quadratic-to-linear transition by increasing the excitation intensity, characteristic to TTA-based UC mechanism (Fig. 4-3-7).[21-23] The crossing point of these two regimes is called as threshold excitation intensity I_{th}, and it represents a useful figure-of-merit of TTA-UC. A relatively low I_{th} value of 49 mW cm^{-2} was observed in PdMesoP-$(DCA)_2ADC$, reflecting the efficient TET and effective triplet diffusion in ionic crystals.

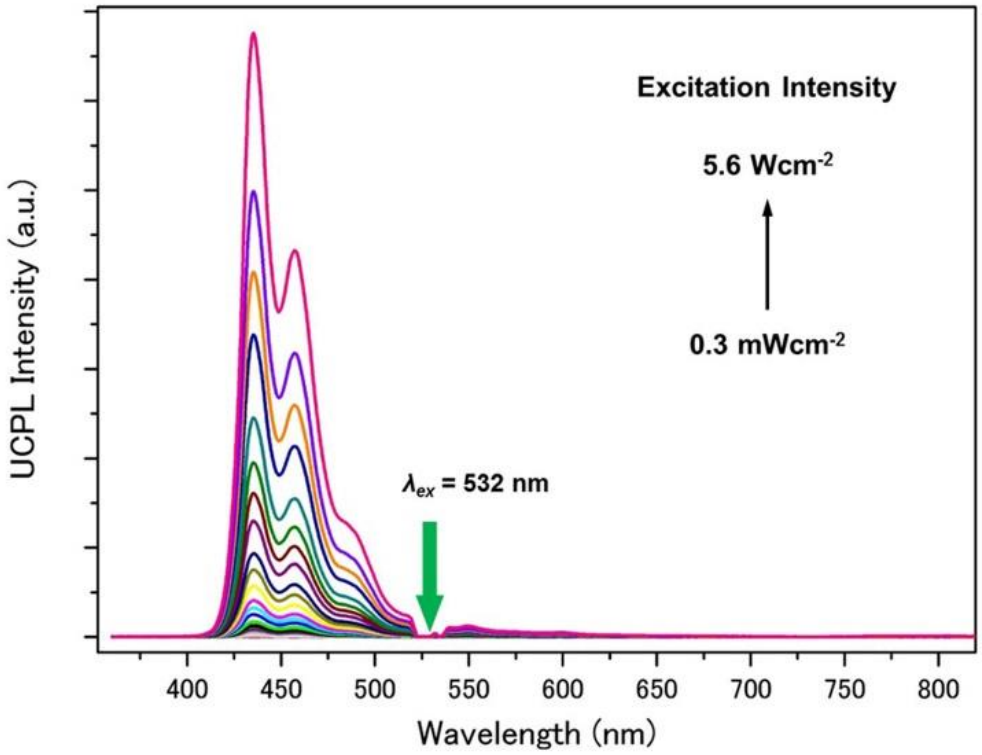

Figure 4-3-6. Photoluminescence spectra of PdMesoP-$(DCA)_2ADC$ crystals at various excitation intensities (λ_{ex} = 532 nm). The scattered incident light was removed by a 532 nm notch filter.

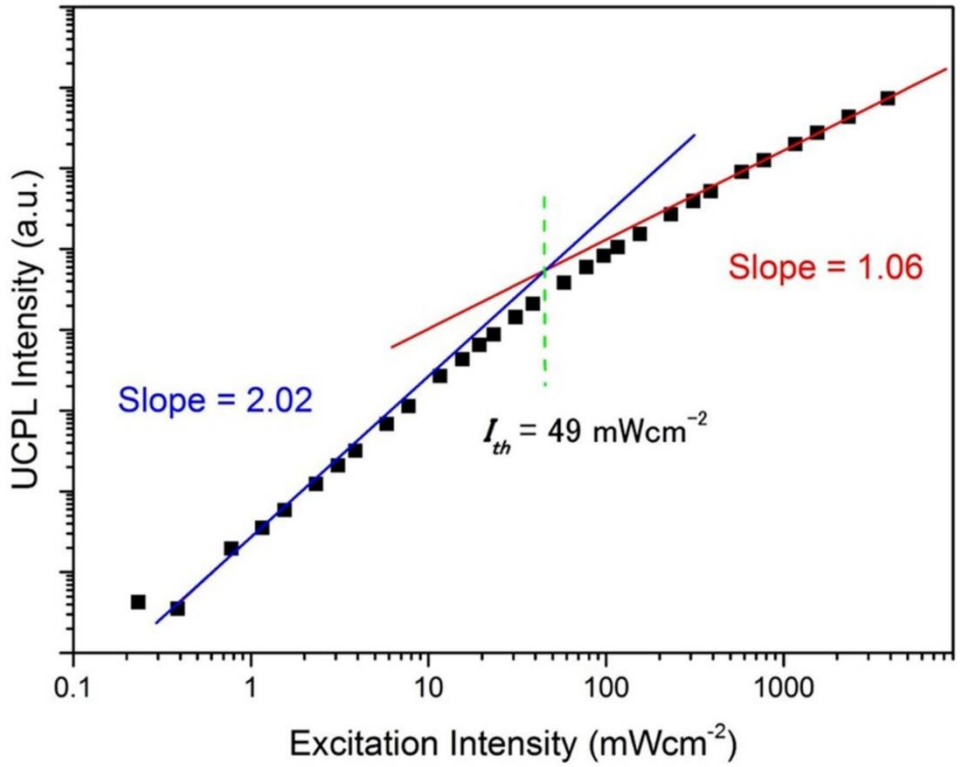

Figure 4-3-7. Double logarithmic plots of the UC PL intensity of PdMesoP-$(DCA)_2$ADC crystals as a function of the excitation intensity. Linear fits with slope 2 and 1 in the lower and higher excitation intensity regimes are shown.

The TTA-UC efficiency Φ_{UC}' of PdMesoP-$(DCA)_2$ADC was determined by the absolute method using an integrating sphere and the laser excitation source to avoid inaccuracy that could arise from the strong light scattering of the crystals. While the main objective of the current work is to prove the concept using the model ionic crystals, the composite ionic crystals PdMesoP-$(DCA)_2$ADC already showed a high Φ_{UC}' value of about 6% (Fig. 4-3-8). This relatively high Φ_{UC}' value originates from not only the aggregation-free donor accommodation but the less structural defects as discussed below.

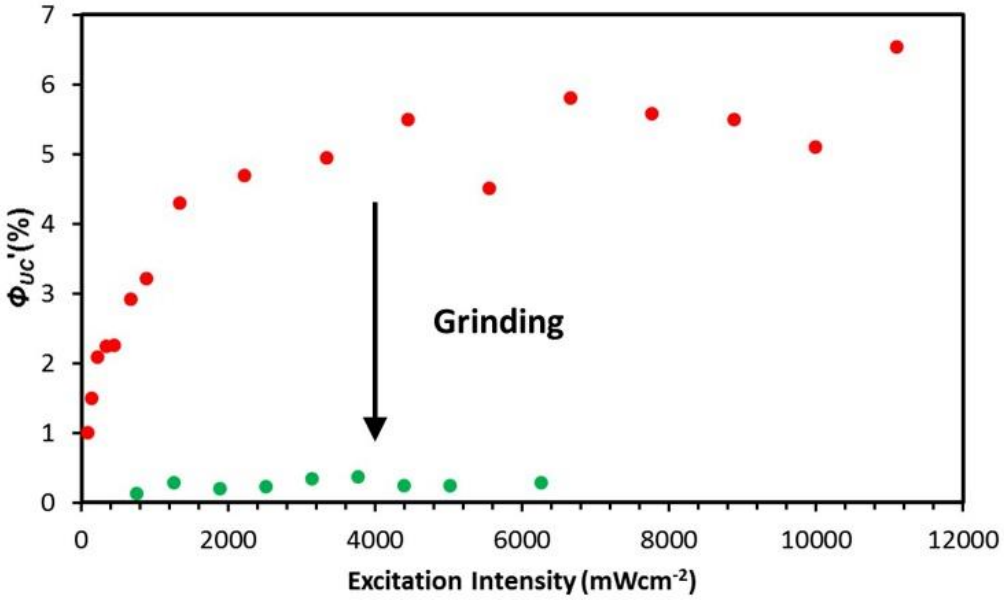

Figure 4-3-8. TTA-UC efficeincy as a function of the excitation intensity of 532 nm laser for single crystals (red) and ground powders (green) of PdMesoP-$(DCA)_2$ADC.

To unveil the relationship between the UC efficiency and defects, we compared the basic photophysical properties of samples with different degree of the structural disorder while keeping the identical composition and structure. To introduce defects on purpose, single crystals of PdMesoP-$(DCA)_2$ADC were mechanically ground using a mortar for 10 min in the Ar-filled glove box. PXRD measurements confirmed that this ground powder keeps the crystal structure of $(DCA)_2$ADC (Fig. 4-3-9) The absorption and emission spectral features are mostly maintained after the grinding, supporting the intact crystal structure (Fig. 4-3-10).

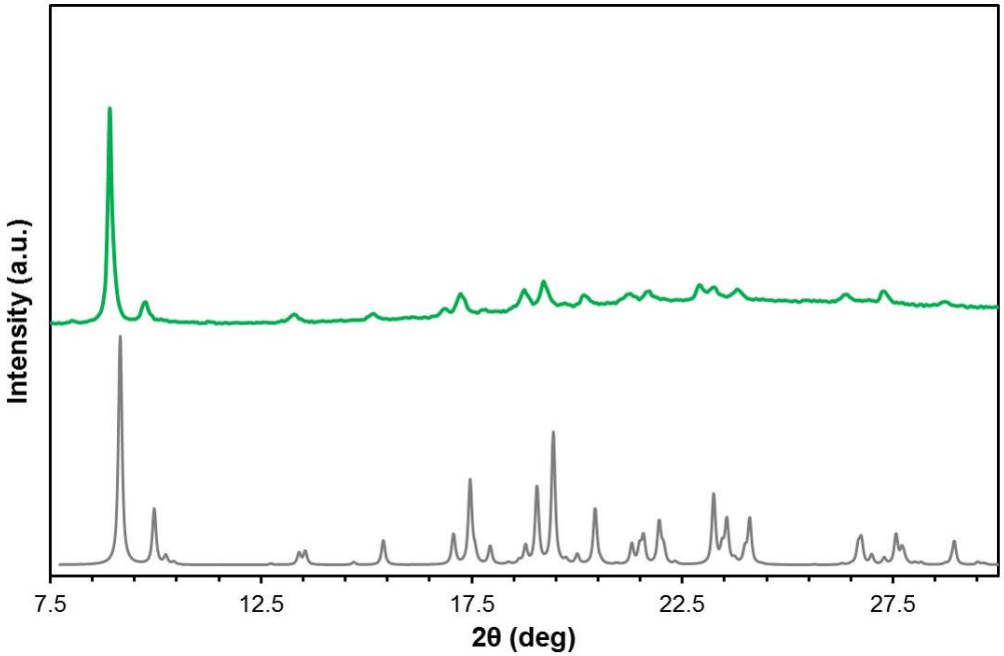

Figure 4-3-9. A PXRD pattern of PdMesoP-$(DCA)_2$ADC powder (green) and a simulated pattern of $(DCA)_2$ADC from its single crystal structure measured (gray).

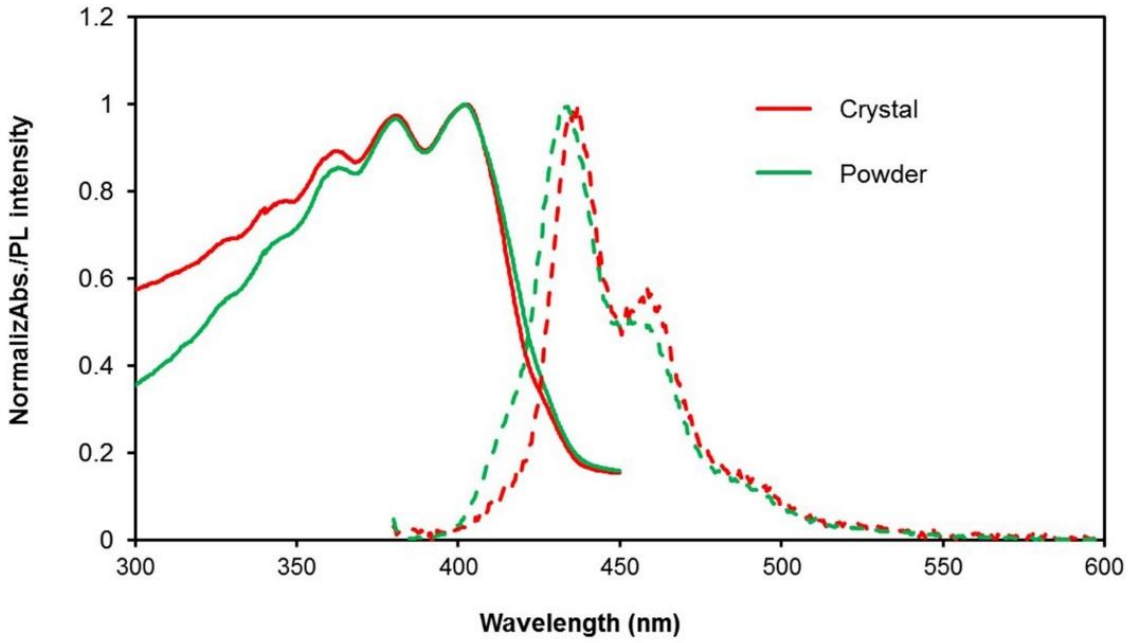

Figure 4-3-10. UV-vis absorption spectra (solid lines) and emission spectra (broken lines) of single crystals (red) and ground powder (green) of PdMesoP-$(DCA)_2$ADC. Excitation wavelength was selected as λ_{ex} =365 nm.

Interestingly, the ground powder of PdMesoP-$(DCA)_2$ADC showed about 20 times lower UC efficiency Φ_{UC}' (0.3%) than that of original crystals (6%) (Fig. 4-3-8). To get insight into this drastic difference in UC efficiency, related parameters were examined. The Φ_{UC}' can be described by the following expression,

$$\Phi_{UC}' = f\Phi_{ISC}\Phi_{ET}\Phi_{TTA}\Phi_{FL} \quad (1)$$

where Φ_{ISC}, Φ_{ET}, and Φ_{TTA} represent the quantum efficiencies of donor ISC, donor-to-acceptor TET, acceptor-acceptor TTA. The parameter f is the statistical probability for obtaining a singlet excited state after the annihilation of two triplet states. In both systems of single crystals and powder, the Φ_{ISC} can be regarded as same. The Φ_{ET} are quantitative in both systems because of no detectable donor phosphorescence peak at 660 nm (Fig. 4-3-6 and 4-3-11). In general, the parameter f is controlled by a relationship between an energy level of S_1 state and other triplet states.[22,24] Considering that the crystal structure and absorption/emission spectra were identical between the single crystals and powder, these samples can be assumed to have the similar f value. From these considerations, the differences between the two samples are limited to Φ_{FL} and Φ_{TTA}. We observed a lower Φ_{FL} value for the powder sample (44%) compared with that of single crystals (56%). However, this difference cannot explain the 20 times difference in Φ_{UC}'. These results suggest that a lower Φ_{TTA} value in the powder sample significantly reduces Φ_{UC}'.

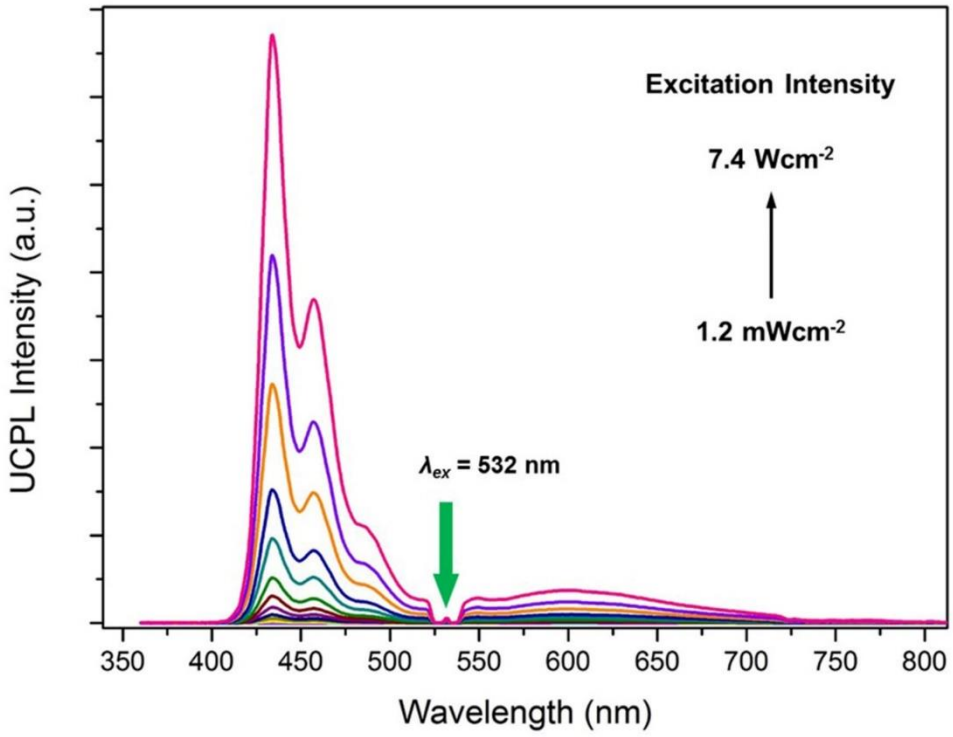

Figure 4-3-11. Photoluminescence spectra of PdMesoP-$(DCA)_2$ADC ground powder prepared under Ar atmosphere with various excitation intensities (λ_{ex} = 532 nm). Scattered incident light was removed by using a 532 nm notch filter.

In typical in-solution TTA-UC, Φ_{TTA} value can be estimated by fitting UC emission decays with the following equation,[24,25]

$$I_{UC}(t) \propto [T_A] = [T_A]_0 \left(\frac{1-\Phi_{TTA}}{exp[k_A t]-\Phi_{TTA}}\right)^2 \qquad (2)$$

where $I_{UC}(t)$ is the time-dependent UC emission intensity and $[T_A]$ is the population density of acceptor triplets. However, this equation did not fit well the decay curves of the delayed fluorescence from the both of our single crystals and powder, especially at a shorter time range (Fig. 4-3-12), implying the presence of deactivation channels not observed in solution. While it is difficult to quantitatively estimate the Φ_{TTA} value, from the tail part of UC emission decays, we observed a shorter triplet lifetime τ_T for the powder sample (1.7 ms) than that for the single-crystal sample (2.9 ms). This comparison gives another support of more prevailing quenching sites in the ground powder. The effect of trap sites upon exciton behaviors have been reported for various crystalline systems.[26-28] However, to the best of our knowledge, there have been no reports on the direct evaluation of defect influence in sensitized TTA-UC. This gives the better understanding of the reported poor UC efficiencies in crystalline TTA-UC systems and offers important design guidelines to develop solid-state photon upconverters.

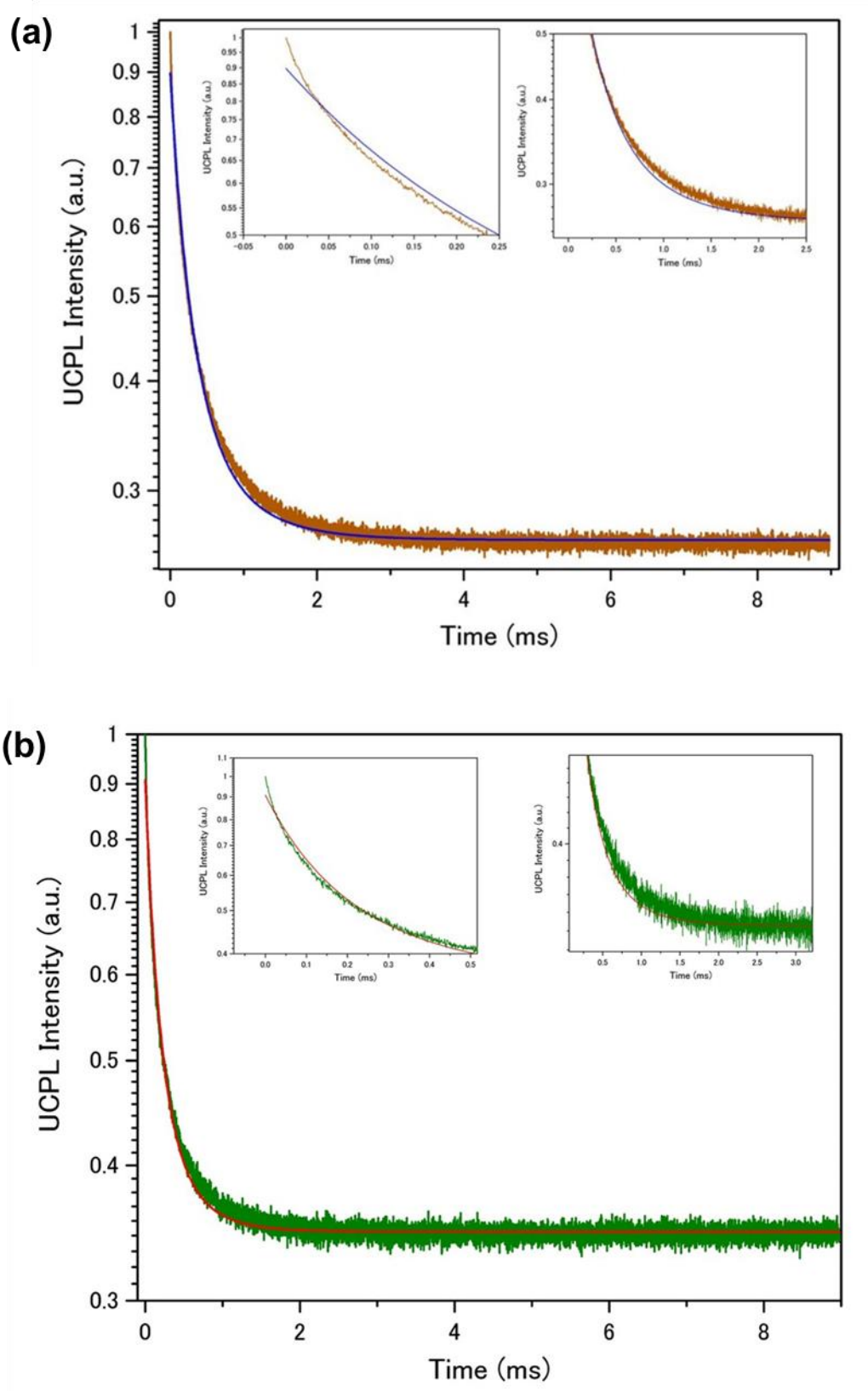

Figure 4-3-12. Photoluminescence decays at 435 nm for (a) single crystals and (b) ground powder of PdMesoP-$(DCA)_2$ADC. The blue fitting curves were obtained by considering the equation (2) in the main text. Insets show magnifications at faster decay range.

4-4 Conclusion

In this chapter, it is shown that the use of ionic interactions serves as a be the rational strategy to achieve homogeneous dispersion of ionic donor molecules in acceptor ionic crystals with maintenance of highly-ordered rigid structure. In the simple anthracene-based model ionic crystal system, the accommodated anionic donor quantitatively transfers the triplet energy to the anionic acceptor, resulting in the relatively high UC efficiency. Besides, we unveiled the effect of defects upon TTA-UC properties for the first time by evaluating TTA-UC properties between two samples, single crystals and mechanically-ground powder. The basic knowledge obtained in the current simple model system offers important guidelines for designing upconverting crystals; the formation of ionic networks that adaptively alleviate the structural mismatches of donor molecules and the consequent suppression of disorder. The rational extension of this concept to other chromophore systems with higher fluorescence quantum yield and larger orbital overlaps between neighbouring chromophores would lead to the realization of ultimate solid upconverters exhibiting a close-unity UC efficiency at the solar irradiance.

References

(1) J. H. Kim and J. H. Kim, *J. Am. Chem. Soc.*, 2012, **134**, 17478-17481.

(2) R. Vadrucci, A. Monguzzi, F. Saenz, B. D. Wilts, Y. C. Simon and C. Weder, *Adv. Mater.*, 2017, **29**.

(3) R. R. Islangulov, J. Lott, C. Weder and F. N. Castellano, *J. Am. Chem. Soc.*, 2007, **129**, 12652-12653.

(4) J. H. Kim, F. Deng, F. N. Castellano and J. H. Kim, *Chem. Mater.*, 2012, **24**, 2250-2252.

(5) F. Marsico, A. Turshatov, R. Pekoz, Y. Avlasevich, M. Wagner, K. Weber, D. Donadio, K. Landfester, S. Baluschev and F. R. Wurm, *J. Am. Chem. Soc.*, 2014, **136**, 11057-11064.

(6) S. H. Lee, D. C. Thevenaz, C. Weder and Y. C. Simon, *J. Polym. Sci. A Polym. Chem.*, 2015, **53**, 1629-1639.

(7) A. Monguzzi, M. Mauri, A. Bianchi, M. K. Dibbanti, R. Simonutti and F. Meinardi, *J. Phys. Chem. C*, 2016, **120**, 2609-2614.

(8) S. Baluschev, V. Yakutkin, G. Wegner, B. Minch, T. Miteva, G. Nelles and A. Yasuda, *J. Appl. Phys.*, 2007, **101**, 023101.

(9) R. Vadrucci, C. Weder and Y. C. Simon, *J. Mater. Chem. C*, 2014, **2**, 2837-2841.

(10) H. Goudarzi and P. E. Keivanidis, *J. Phys. Chem. C*, 2014, **118**, 14256-14265.

(11) R. Andemach, H. Utzat, S. D. Dimitrov, I. McCulloch, M. Heeney, J. R. Durrant and H. Bronstein, *J. Am. Chem. Soc.*, 2015, **137**, 10383-10390.

(12) M. Hosoyamada, N. Yanai, T. Ogawa and N. Kimizuka, *Chem.-Eur. J.*, 2016, **22**, 2060-2067.

(13) N. Yanai and N. Kimizuka, *Chem. Commun.*, 2017, **53**, 655-655.

(14) K. Kamada, Y. Sakagami, T. Mizokuro, Y. Fujiwara, K. Kobayashi, K. Narushima, S. Hirata and M. Vacha, *Mater. Horiz.*, 2017, **4**, 83-87.

(15) T. Ogawa, N. Yanai, H. Kouno and N. Kimizuka, *J. Photon. Energy*, 2017, **8**, 022003.

(16) A. Monguzzi, R. Tubino, S. Hoseinkhani, M. Campione and F. Meinardi, *Phys. Chem. Chem. Phys.*, 2012, **14**, 4322-4332.

(17) P. F. Duan, N. Yanai, H. Nagatomi and N. Kimizuka, *J. Am. Chem. Soc.*, 2015, **137**, 1887-1894.

(18) J. Dey, J. L. Haynes, I. M. Warner and A. K. Chandra, *J. Phys. Chem. A*, 1997, **101**, 2271-2278.

(19) W. Rodriguez-Cordoba, R. Noria-Moreno, P. Navarro and J. Peon, *J. Lumin.*, 2014, **145**, 697-707.

(20) A. Dawn, N. Fujita, S. Haraguchi, K. Sada and S. Shinkai, *Chem. Commun.*, 2009, **0**, 2100-2102.

(21) A. Monguzzi, J. Mezyk, F. Scotognella, R. Tubino and F. Meinardi, *Phys. Rev. B*, 2008, **78**, 195112.

(22) Y. Y. Cheng, T. Khoury, R. G. C. R. Clady, M. J. Y. Tayebjee, N. J. Ekins-Daukes, M. J. Crossley and T. W. Schmidt, *Phys. Chem. Chem. Phys.*, 2010, **12**, 66-71.

(23) A. Haefele, J. Blumhoff, R. S. Khnayzer and F. N. Castellano, *J. Phys. Chem. Lett.*, 2012, **3**, 299-303.

(24) Y. Y. Cheng, B. Fuckel, T. Khoury, R. G. C. R. Clady, M. J. Y. Tayebjee, N. J. Ekins-Daukes, M. J. Crossley and T. W. Schmidt, *J. Phys. Chem. Lett.*, 2010, **1**, 1795-1799.

(25) A. Monguzzi, F. Bianchi, A. Bianchi, M. Mauri, R. Simonutti, R. Ruffo, R. Tubino and F. Meinardi, *Adv. Energy Mater.*, 2013, **3**, 680-686.

(26) K. Yokoi and Y. Ohba, *Chem. Phys. Lett.*, 1986, **129**, 240-243.

(27) B. Manna, R. Ghosh and D. K. Palit, *J. Phys. Chem. C*, 2015, **119**, 10641-10652.

(28) C. Grieco, G. S. Doucette, R. D. Pensack, M. M. Payne, A. Rimshaw, G. D. Scholes, J. E. Anthony and J. B. Asbury, *J. Am. Chem. Soc.*, 2016, **138**, 16069-16080.

Chapter 5 Donor-Acceptor-Collector Ternary Crystalline Films for Efficient Solid-State Photon Upconversion

Abstract

It is pivotal to achieve efficient triplet-triplet annihilation based photon upconversion (TTA-UC) in the solid-state for enhancing potentials of renewable energy production devices. However, the UC efficiency of solid materials is largely limited by low fluorescence quantum yield due to the chromophore aggregation as well as severe back energy transfer from the acceptor singlet state to the triplet donor in the condensed state. In this work, to overcome these issues, we introduce a highly fluorescent singlet energy collector as the third component of donor-doped acceptor crystalline films. Anthracene-based acceptor containing alkyl chains and a carboxylic moiety is mixed with the triplet donor Pt(II) octaethylporphyrin (PtOEP) and the energy collector 2,5,8,11-tetra-*tert*-butylperylene (TTBP) in solution, and spin-coating of the mixed solution gives crystalline acceptor films homogeneously doped with PtOEP and TTBP. Interestingly, delocalized singlet excitons in acceptor crystals are found to diffuse effectively over the distance of ~20 nm. Thanks to this high diffusivity, only 0.5 mol% of doped TTBP can harvest the most of singlet excitons, which successfully doubles the solid-state fluorescent quantum yield to 76%. Furthermore, since donor PtOEP and the collector TTBP are separately fixed in acceptor crystals, the singlet back energy transfer from collector to the donor is effectively avoided. Such efficient singlet energy collection and prohibited back energy transfer result in a large increase of UC efficiency up to 9.0%, offering the rational design principles towards ultimately efficient solid-state upconverters.

5-1 Introduction

On the demands for utilization of solar energy, photon upconversion (UC) has the great potential to go beyond Shockley-Quiesser limit by recovering sub-bandgap photons. Among various UC mechanisms, triplet-triplet annihilation based photon upconversion (TTA-UC) has attracted much attention because of its inherent ability to utilize weak excitation power sources like sunlight.[1-13] In the common TTA-UC scheme, photo-excited triplet donor molecules undergo intersystem crossing (ISC) from S_1 to T_1 and triplet energy transfer (TET) to acceptor molecules, followed by acceptor-acceptor TTA and UC emission from the acceptor S_1 state.

For applications of TTA-UC to real-world devices, solid-state systems are highly preferred since they are free from volatile and toxic organic solvents. To achieve solid-state TTA-UC, mainly two different approaches have been proposed; molecular diffusion in rubbery polymer matrices and energy migration in chromophore assemblies. Castellano, Weder, Kim and coworkers have reported highly efficient TTA-UC by dispersing donor and acceptor dyes in soft rubbery polymers,[14-17] but the inevitably slow molecular diffusion in the solid-state remains as an essential challenge for further improvement. On the other hand, a few groups including us have pursued the development of solid-state upconverters by doping donor molecules in acceptor assemblies, and utilizing TET from donor to adjacent acceptors and triplet energy migration in the regularly self-assembled acceptor arrays.[18-24] While this energy migration-based UC has the potential to attain ultimate solid upconverters with high efficiency at low excitation intensity, the TTA-UC efficiency is often quite limited. The reasons for this low UC efficiency are closely associated with the condensed material structures. First, donor molecules tend to aggregate, which results in the inefficient TET. Second, although the large orbital overlap between acceptor moieties is required for fast triplet energy migration, it often decreases the acceptor fluorescence efficiency through various deactivation pathways in the assembled state. Third, since the donor and acceptor molecules are highly condensed, a certain part of upconverted singlet energy is consumed by undesirable back energy transfer from acceptor to the donor. The third issue should become more serious with new triplet donors such as semiconductor nanocrystals and singlet-to-triplet (S-T) absorption metal complexes, recently developed for the near-infrared (NIR)-to-visible TTA-UC, due to the severe overlap between donor absorption and acceptor emission.[11,25-30] Therefore, the development of a rational strategy is strongly desired to solve these issues based on the understanding of exciton behaviors in the complex condensed state.

In this chapter, the UC efficiency is shown to be largely improved by the introduction of the third component, highly fluorescent singlet energy collector, for improving the fluorescence quantum yield and avoiding the back energy transfer to the donor (Figure 5-1-1a). As previously discussed, the modification of acceptor anthracene with carboxylic acid and multiple alkyl chains (**A2**, Figure 5-1-1b) satisfies both the good crystallinity and the good dispersibility of donor platinum octaethylporphyrin (PtOEP). In this work, an energy collector, 2,5,8,11-tetra-*tert*-butylperylene (TTBP) was further added to the system, whose absorption has a larger spectral overlap with the acceptor fluorescence compared with donor's absorption. By simple spin-coating of a mixed solution of **A2**, PtOEP, and TTBP, PtOEP and TTBP could be molecularly dispersed in crystalline **A2** thin films. By the addition of TTBP, the UC efficiency was successfully improved from 4.2% to 9.0%. To understand this observation, various experiments were conducted to study the basic exciton behavior in the condensed films. By analyzing the dynamics of acceptor singlet state with the aid of Monte Carlo simulation, it was found that delocalized singlet excitons with a long lifetime of 29.7 ns give a significantly long singlet diffusion length of 26.1 nm. Thanks to this excellent singlet diffusivity, only 0.5 mol% of doped TTBP could harvest most of the acceptor singlet energy. Furthermore, since the donor PtOEP and the collector TTBP are fixed in a spatially separated manner in the **A2** film, the singlet back energy transfer from TTBP to PtOEP was completely suppressed, which has been difficult to achieve with donor-acceptor two-component systems. The current UC efficiency enhancement based on the detailed understanding of exciton behaviors would provide an important research direction toward processable solid-state upconverters with ultimate efficiency.

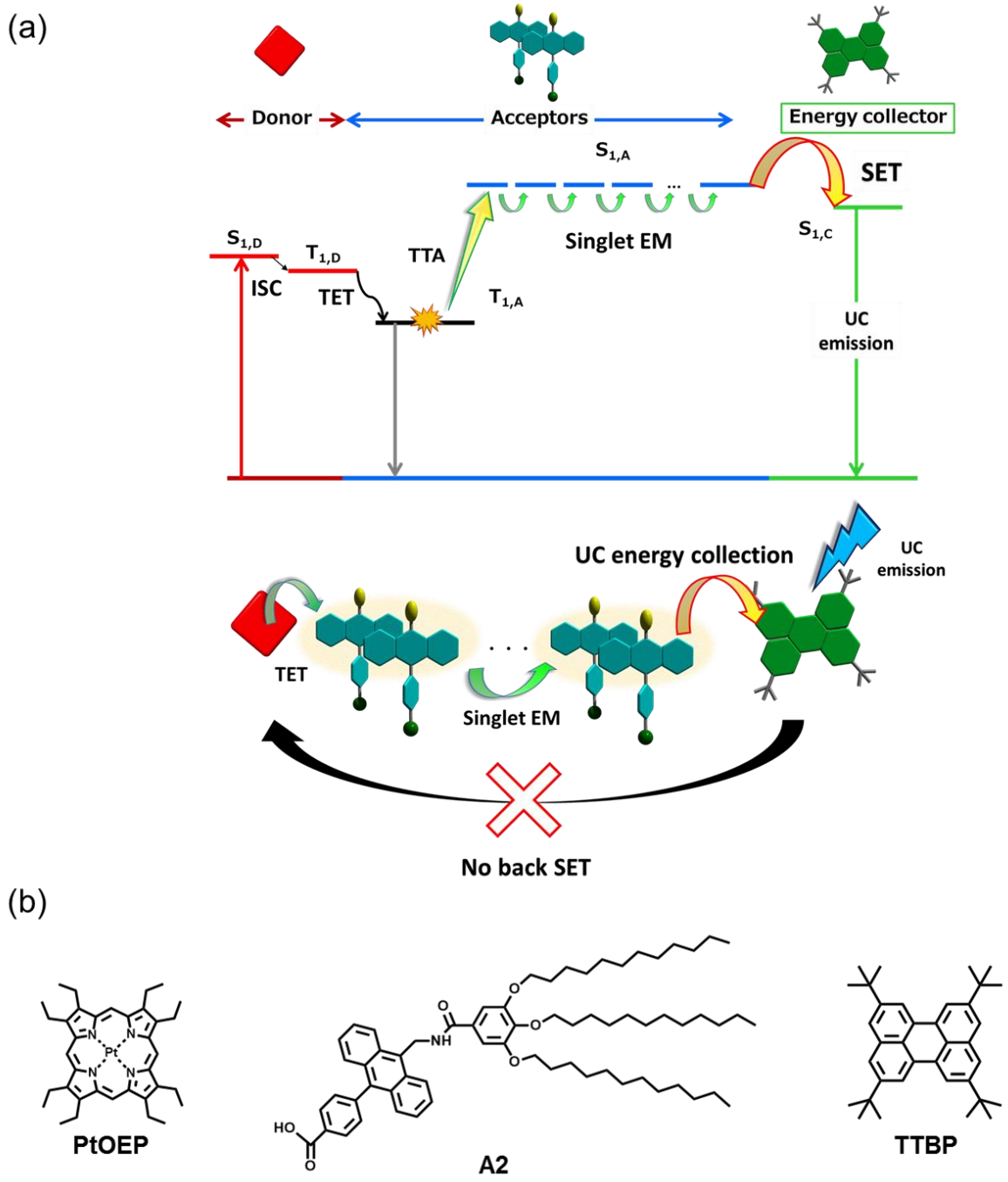

Figure 5-1-1. (a) Energy diagram for TTA-UC, followed by singlet energy migration and collection. A triplet state of donor $T_{1,D}$, formed by intersystem crossing (ISC) from the photo-excited singlet state $S_{1,D}$, experiences triplet energy transfer (TET) to an acceptor. Two acceptor triplets $T_{1,A}$ annihilate to form a higher singlet energy level $S_{1,A}$. Singlet energy migration among acceptor arrays and singlet energy transfer (SET) to the collector, which consequently produces upconverted delayed fluorescence. Back SET from collector to donor is effectively suppressed since they are spatially fixed in the separated geometry. (b) Chemical structures of donor PtOEP, acceptor **A2** and energy collector TTBP.

5-2 Experimental section

5-2-1 Materials

All the solvents were used as received without further purification. Acceptor **A2** was synthesized by following our previous report.[21] TTBP was purchased from TCI and purified by sublimation. PtOEP was purchased from Aldrich and used as received. Nile Red was purchased from TCI and used as received.

5-2-2 General methods

UV-visible absorption spectra were recorded on a JASCO V-670 spectrophotometer. Fluorescence spectra were measured by using a PerkinElmer LS 55 fluorescence spectrometer. Time-resolved photoluminescence lifetime measurements were carried out by using a time-correlated single photon counting lifetime spectroscopy system, HAMAMATSU Quantaurus-Tau C11367-02 (for fluorescence lifetime) and C11567-01 (for delayed luminescence lifetime).

Photophysical measurements. For TTA-UC measurements, the films were prepared by spin-coating of 0.1 mL of $CHCl_3$ solution containing PtOEP (20 μM), **A2** (20 mM) and TTBP (100 μM) in an Ar-filled glove box ($[O_2] < 0.1$ ppm). Spin-coated films were sealed between glass plates by using epoxy resin.

For TTA-UC emission spectra, a diode laser (532 nm, 200 mW, RGB Photonics) was used as an excitation source. The laser power was controlled by combining a software (Ltune) and a variable neutral density filter and measured using a PD300-UV photodiode sensor (OPHIR Photonics). The laser beam was focused on a sample using a lens. The diameter of the laser beam ($1/e^2$) was measured at the sample position using a CCD beam profiler SP620 (OPHIR Photonics). A typical area of laser irradiation spot estimated from the diameter was 1.0×10^{-3} cm^2. The emitted light was collimated by an achromatic lens, the excitation light was removed using a notch filter (532 nm), and the emitted light was again focused by an achromatic lens to an optical fiber connected to a multichannel detector MCPD-9800 which was supplied and calibrated by Otsuka Electronics and equipped with a CCD sensor for the detection of whole visible range with high sensitivity.

The UC efficiency was determined relative to a standard (Nile red in the **A2** films) according to the following equation:[2]

$$\Phi'_{UC} = 2\Phi_{std}\left(\frac{A_{std}}{A_{UC}}\right)\left(\frac{F_{UC}}{F_{std}}\right)\left(\frac{I_{std}}{I_{UC}}\right)\left(\frac{\eta_{UC}}{\eta_{std}}\right)^2$$

where Φ, A, F, I, and η represent quantum yield, absorbance at the excitation wavelength, integrated photoluminescence spectral profile, excitation intensity, and the refractive index, respectively. The absolute fluorescence quantum yield of the standard, Nile red in the **A2** film (Nile red/**A2** = 0.2 mol%), was determined as 0.36.

5-3 Results and discussion

5-3-1 Preparation and photophysical properties of A2 films.

The preparation of the film of lipophilic acceptor **A2** was conducted by spin-coating chloroform solution of **A2** (see experimental section for detail). The film thickness and density was about 100 nm and 1.02 g cm^{-3}, respectively. The presence of inter-chromophore interactions in **A2** films were investigated by absorption and fluorescence measurements. Figure 5-3-1a shows UV-visible absorption and emission spectra of **A2** in a diluted (50 μM) $CHCl_3$ solution and a spin-coated film. The solution spectrum showed π-π* transition bands with peaks at 342, 359, 376 and 397 nm characteristic to anthracene-based compounds. These peaks showed small redshifts of ca. 5 nm to 347, 364, 382 and 403 nm in the film. Larger redshifts of ca. 32 nm from 426 nm to 458 nm were observed for the fluorescence spectra. These spectral shifts in absorption and emission spectra suggest the existence of inter-chromophore interactions both in the ground and excited states. These imply the formation of energetically-stabilized delocalized excitons in the assembled state, which was also supported by the fluorescence lifetime measurements (Figure 5-3-1b). The $CHCl_3$ solution of **A2** showed a single-exponential decay with a lifetime of 5.9 ns. On the other hand, the **A2** film showed a much longer fluorescence lifetime of 29.7 ns with two components (1.50 ns, 3% and 30.5 ns, 97%). This long lifetime in the assembled state enables a long-range diffusion of the delocalized excitons as shown below.

(a)

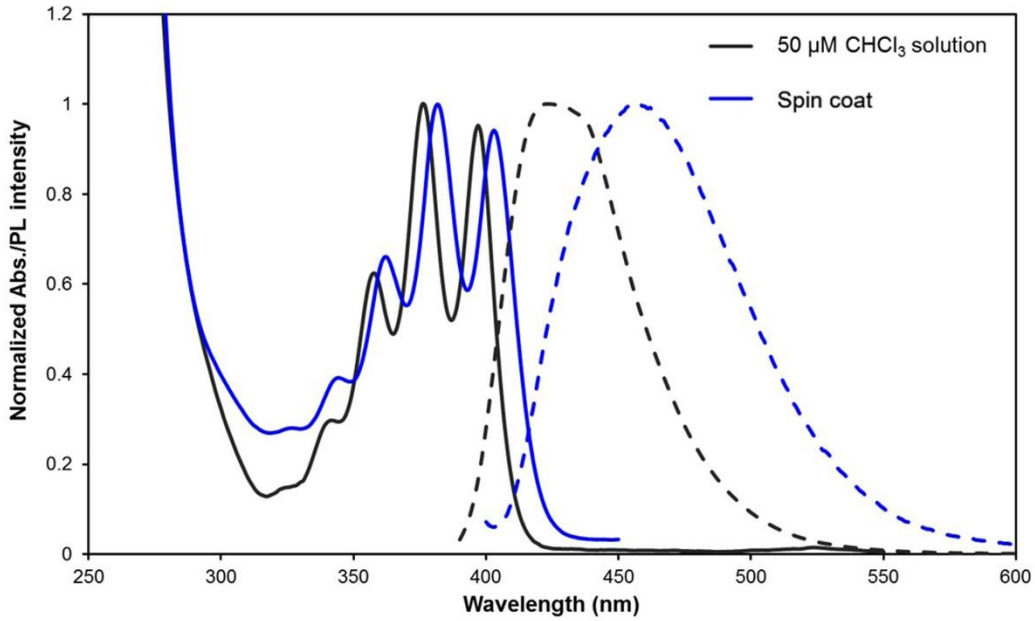

(b)

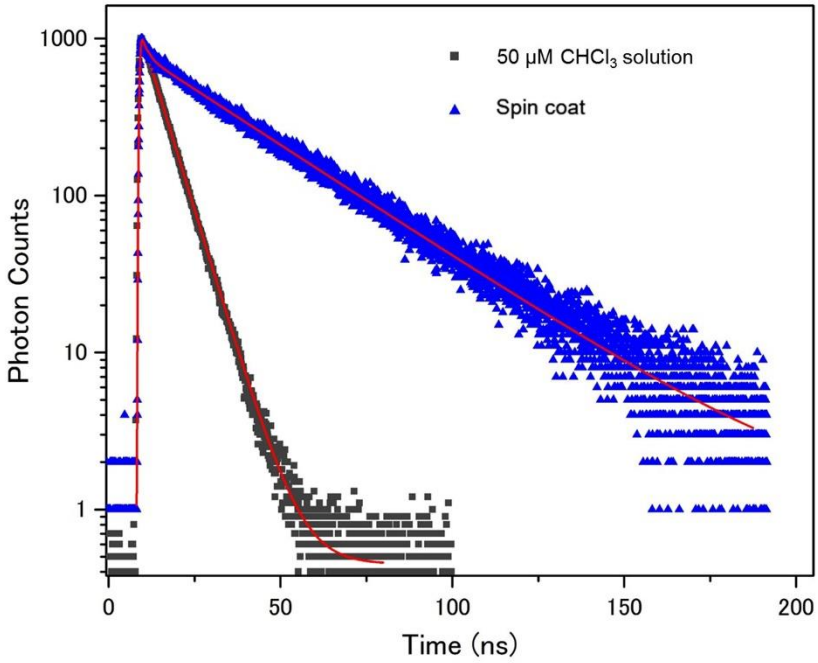

Figure 5-3-1. (a) UV-vis absorption spectra (solid lines) and emission spectra (dashed lines) of **A2** in 50 μM $CHCl_3$ solution (black) and spin-coated film (blue). The excitation wavelength was selected as λ_{ex} = 350 nm. (b) Photoluminescence decays of **A2** in 50 μM $CHCl_3$ solution (black) and spin-coated film (blue). The excitation wavelength was selected as λ_{ex} = 365 nm. Fitting lines are indicated by red lines.

5-3-2 Singlet exciton diffusion in A2 films

The detailed understanding of singlet exciton dynamics gives a foundation to achieve an efficient upconverted singlet energy collection. For this purpose, we evaluated the singlet diffusion coefficient and length in **A2** films by modeling the PL decays of **A2**/quencher blends with different quencher concentrations using Monte Carlo simulation. This method has been developed by Mikhnenko and Loi et al., and it has been shown that this method can be applied to polymers and small molecules.[31,32] [6,6]-phenyl-C_{61}-butyric acid methyl ester (PCBM) was employed as an exciton quencher molecule, and it was dispersed in the **A2** films during the spin-coating. Figure 5-3-2 shows PL decays of **A2**/PCBM blend films with various PCBM volume fractions. The PL decays could be fitted as bi-exponential decays. These two components were recognized as the emission from a monomeric (shorter lifetime) and assembled state (longer lifetime), respectively. The averaged decay time decreased with increasing the PCBM content, which is consistent with the assumption of non-radiative quenching. It is to note that the assembled state in the **A2** films was maintained in the presence of PCBM, as indicated by the maintenance of similar PL spectral shape (Figure 5-3-3).

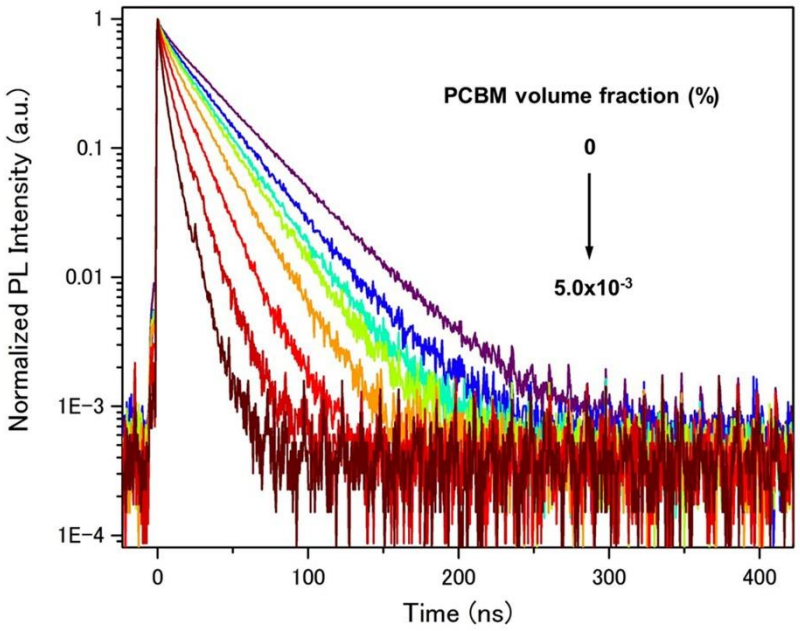

Figure 5-3-2. PL decays of **A2**/PCBM films with various volume fractions (0 to 5.0×10^{-3}%) of PCBM. the excitation wavelength was selected as λ_{ex} = 400 nm.

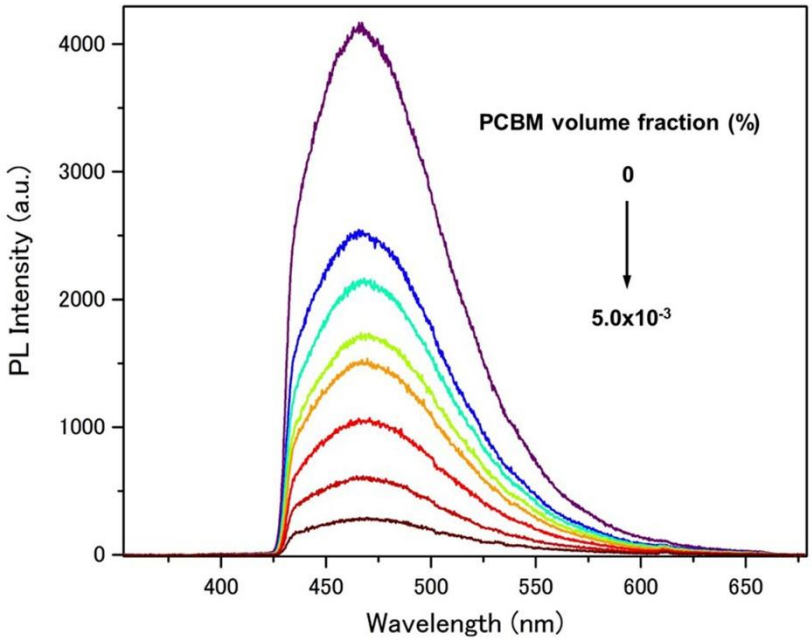

Figure 5-3-3. PL spectra of **A2**/PCBM films with various volume fractions (0 to 5.0×10^{-3}%) of PCBM. The excitation wavelength was selected as λ_{ex} =400 nm, and a 430 nm long-pass filter was used to remove the excitation light scattering.

We applied the Monte Carlo simulation of 3D exciton diffusion in a medium with a morphology of arbitrary complexity. This simulation assumes that non-interacting excitons undergo a random walk in the medium and decay non-radiatively when they reach a quenching site during their lifetime. The relationship between the volume fraction of quencher and quenching efficiency provides the information about the exciton diffusion. This simulation is done with the volume fraction of PCBM molecules, the morphology of the blend (details are mentioned later), and the parameters of the PL decay in the **A2** film as inputs and, a fixed hopping distance δs during each iteration time is obtained δt as an output. According to the Einstein theory of random walks the exciton diffusion coefficient D is related to δs and δt as:[31]

$$D = \frac{\delta s^2}{6\delta t} \qquad (1)$$

From this value, the 3D exciton diffusion length L_D is calculated using the following equation:[33]

$$L_D = \sqrt{3D\tau_0} \qquad (2)$$

where τ_0 represents average PL lifetime in pristine **A2** film. The value L_D is approximately equal to the average displacement of an exciton from its initial position. The fitting results in an exciton diffusion coefficient of $(1.29\pm0.3) \times 10^{-5}$ cm^2s^{-1}, which corresponds to an exciton diffusion length of 26.1±3 nm. This obtained diffusion length is considerably longer than those for typical singlet exciton diffusion in films consisting of small-molecules. Consistency between the experimental and simulated results was confirmed by plotting the relative quenching efficiency Q with various volume fraction of PCBM, which is defined as:[31]

$$Q = 1 - \frac{\int PL_{blend}dt}{\int PL_{pristine}dt} \qquad (3)$$

where PL_{blend} and $PL_{pristine}$ are normalized to the value at time zero PL decays of an **A2**/PCBM blend and **A2** pristine film, respectively. Figure 5-3-4 shows the measured relative quenching efficiency versus PCBM volume fraction in **A2**-PCBM blends. The solid lines were modeled using the Monte Carlo simulation by setting previously extracted exciton diffusion length for each film and assuming the blend morphologies of homogeneous mixture (orange line) and clustering of two PCBM molecules (green line). The measured data for **A2** films is well described by the contribution of these two simulated curves in all the studied range of PCBM volume fractions. It is reasonable to assume that the formation of PCBM clusters easily occurs in blends of higher PCBM fractions during the solvent evaporation. Similar behavior was observed in the original paper of Mikhnenko and Loi et al.[31]

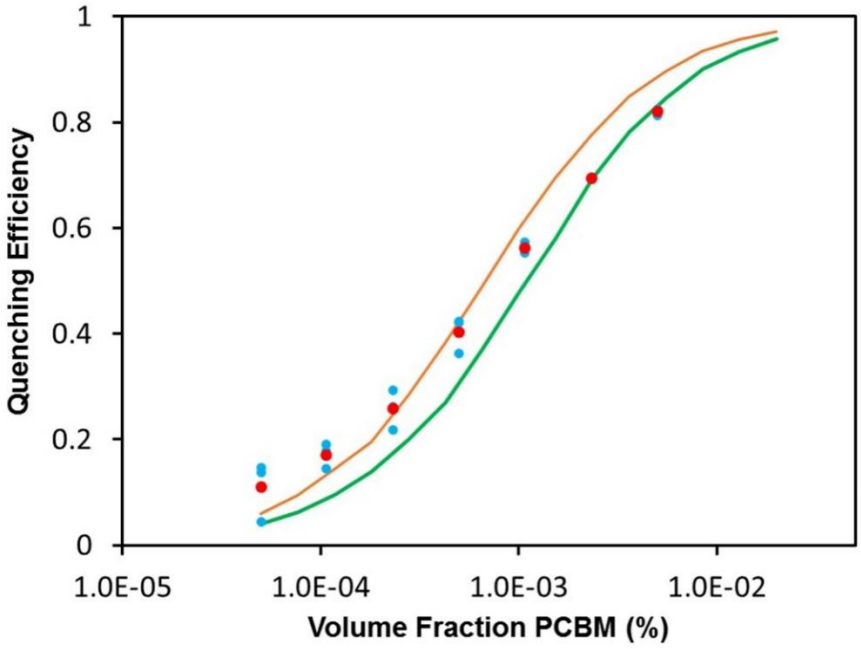

Figure 5-3-4. Measured (circles) and modeled (lines) dependencies of relative quenching efficiency versus volume fraction of **A2**/PCBM blend films. Blue dots represent raw results of three sets of measurements and red dots shows their average. Orange and green lines represent the fittings of the experimental data with Monte Carlo simulation by setting the blend morphology of intimate mixture and two PCBM molecules per cluster, respectively.

To understand the nature of the long singlet exciton diffusion length in **A2** film, we applied a modified Stern-Volmer equation to the measured decay datum, which equation is described as:

$$\frac{1}{\tau} = k[Q] + \frac{1}{\tau_0} \qquad (4)$$

where τ, k and $[Q]$ represent a measured PL decay time of **A2** including a certain amount of PCBM, quenching rate constant, and concentration of quencher molecules, respectively. Each PL decays could be fitted using two components. The origin of the longer component can be attributed to the energetically-stabilized assembled state, and the shorter component is presumably ascribed to monomeric species or defect sites. Figure 5-3-5 shows the fitting results for each component. The component with longer lifetime well follows the linear fitting line ($R^2 = 0.98$), whereas the shorter component does not fulfill the linear relationship ($R^2 = 0.57$). This result strongly suggests that the delocalized excitons in the assembled state with long lifetime mainly contributes to the long-range diffusion.

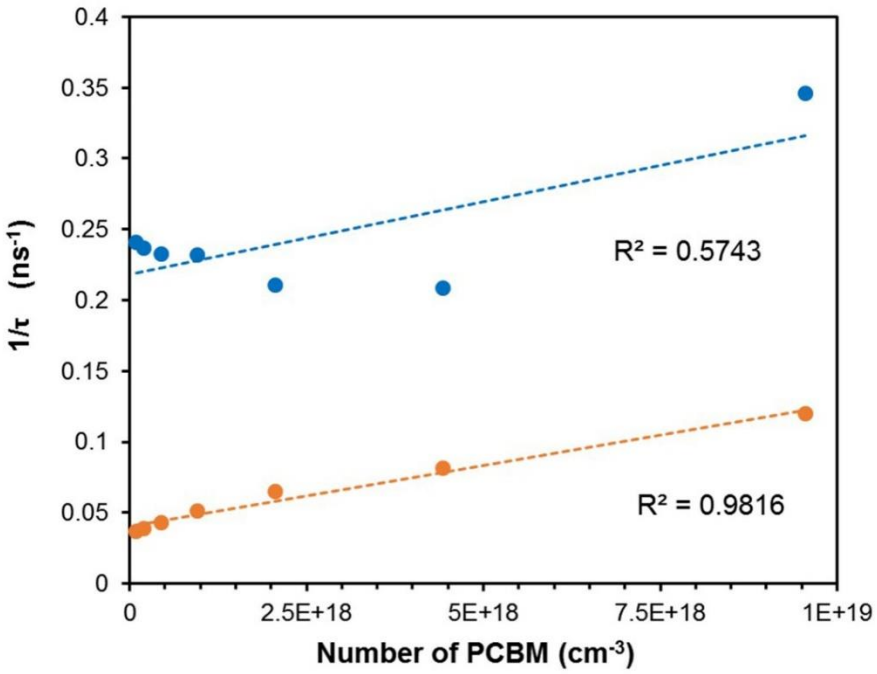

Figure 5-3-5. Modified Stern-Volmer plots for components with shorter lifetime (blue) and longer lifetime (orange) of PL decays of A2/PCBM blend films as a function of PCBM concentration in **A2**.

5-3-3 Singlet energy collection to TTBP in A2 films

The above-mentioned long singlet diffusion length in **A2** films motivated us to introduce singlet energy collector TTBP for the improvement of fluorescence quantum yield. The excited singlet energy levels of **A2** and TTBP were appropriate for energy collection as confirmed by a large spectral overlap between the emission of **A2** films and the absorption of TTBP in solution (Figure 5-3-6). An effective energy harvesting was actually observed in the PL spectra and decays of **A2**/TTBP blend films with different TTBP contents (Figure 5-3-7). By increasing the TTBP content in the **A2** films, the fluorescence spectral shape largely changed from that of **A2** films to TTBP even at 0.1 mol% of TTBP, and the TTBP emission became dominant at as low as 0.5 mol% of TTBP. At the same time, the decay of **A2** emission at λ = 425 nm showed an intense drop by the addition of TTBP. Considering the fact that the absorption spectra of **A2** films are unchanged even with increasing the amount of TTBP (Figure 5-3-8a), the reduction in decay time of **A2** emission was originated from an energy transfer from **A2** to TTBP, and not due to a degradation of **A2** assembly structure. Since the emission at λ = 425 nm exclusively originates from **A2**, we can estimate the energy transfer efficiency, Φ_{ET}, by the following equation:

$$\Phi_{ET} = 1 - \frac{\tau}{\tau_0} \qquad (5)$$

where τ represents average PL lifetime in **A2**/TTBP blend films. Estimated energy transfer efficiency at various TTBP contents are summarized in Figure 5-3-8b and Table 5-3-1. The Φ_{ET} value drastically increases when the TTBP content is increased from 0.01% to 10% and it reaches to about 50% at 0.2 mol% of TTBP. This tendency is consistent with the changes in the emission spectra mentioned above.

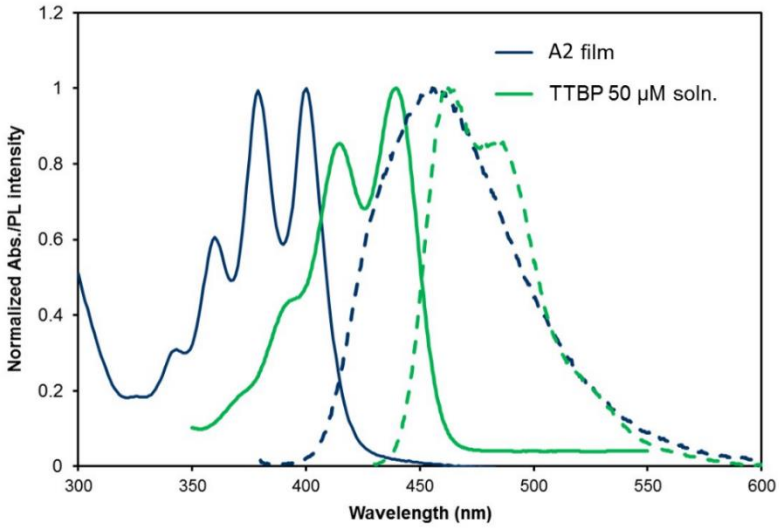

Figure 5-3-6. UV-vis absorption spectra (solid lines) and emission spectra (dashed lines) of **A2** films (blue) and TTBP in 50 μM Chloroform solution (green). The excitation wavelength was selected as λ_{ex} =350 nm for **A2** films and λ_{ex} =360 nm for TTBP solution.

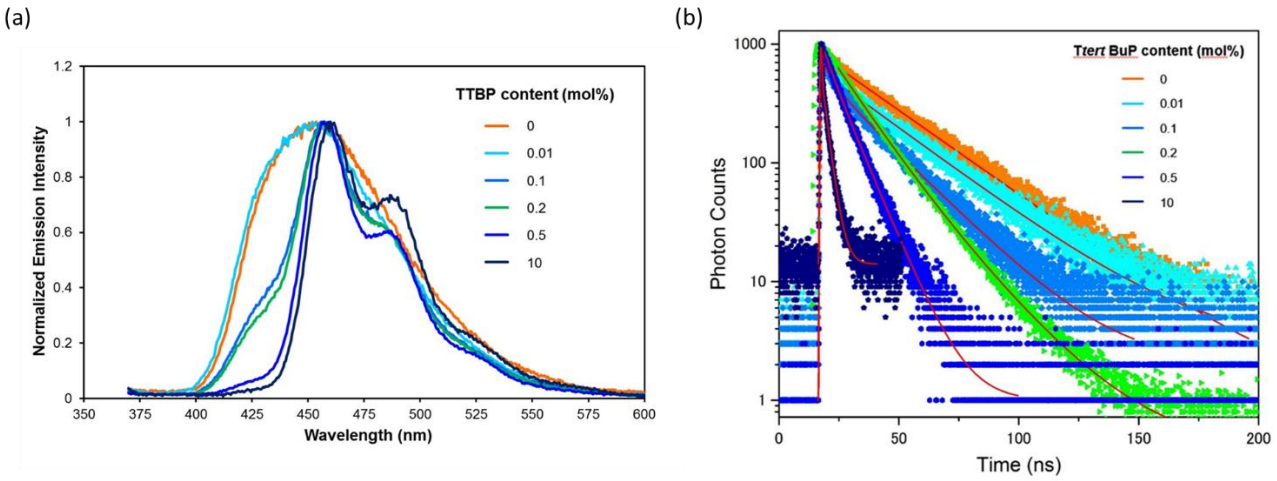

Figure 5-3-7. (a) Emission spectra of **A2**/TTBP blend films with various TTBP contents. The excitation wavelength was selected as λ_{ex} =350 nm. (b) PL decays of **A2**/TTBP blend films with various TTBP contents. The excitation wavelength was selected as λ_{ex} =350 nm and decays were obtained at 425 nm.Fitting lines are indicated as red lines.

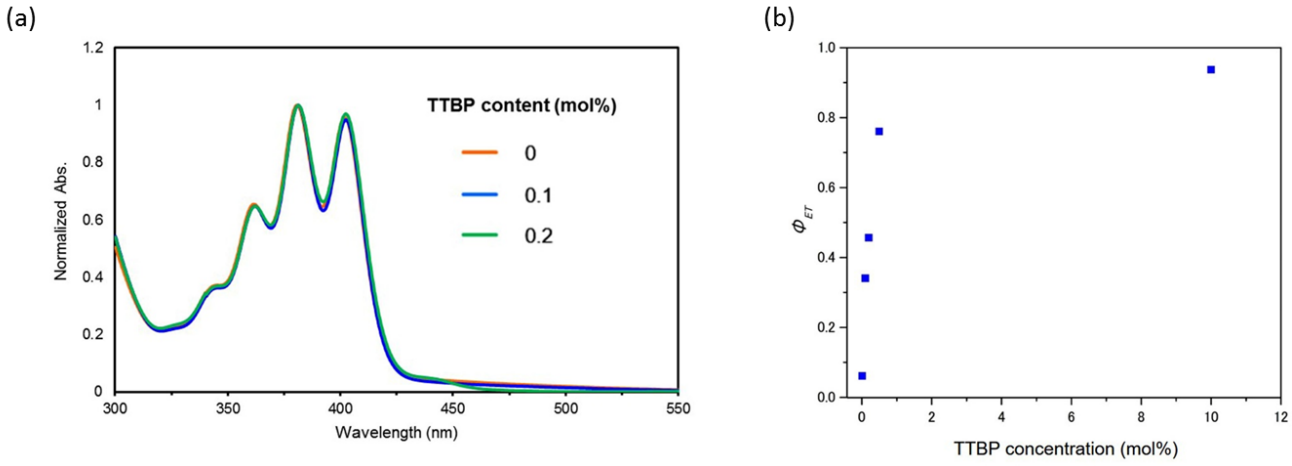

Figure 5-3-8. (a) UV-vis absorption spectra of **A2**/TTBP blend films with various TTBP contents. (b) Φ_{ET} values as a function of TTBP content for **A2**/TTTBP blend films.

Table 5-3-1. Average fluorescence lifetime τ, singlet energy transfer efficiency Φ_{ET} and fluorescence quantum yield Φ_{FL} of **A2**/TTBP blend films at various TTBP contents.

TTBP [mol%]	τ [ns]	Φ_{ET} [%]	Φ_{FL} [%]
0	29.7	-	34
0.01	27.9	6	45
0.1	19.6	34	57
0.2	16.1	46	63
0.5	7.12	76	71
10	1.87	93	28

Fluorescence quantum yield of **A2**/TTBP blend films, Φ_{FL}, was measured by using an integrating sphere (Table 1). As expected, the Φ_{FL} value gradually increased with increasing the amount of TTBP. The highest fluorescence quantum yield of 71% was observed at 0.5 mol% of TTBP, which is more than two times higher than that of **A2** pristine film. Note that most of the TTBP molecules in the blend films are considered to be dispersed homogeneously up to the mixing ratio of 0.5 mol% since the emission spectrum the **A2**/TTBP blend film at 0.5 mol% TTBP is close to that in diluted solution of TTBP (Figure 5-3-9). The drop of Φ_{FL} at the higher TTBP content of 10 mol% would be due to the aggregation of TTBP, as the pristine TTBP spin-coated film showed a low fluorescence quantum yield of 12%. At the TTBP content of 0.2 mol%, where about the half of **A2** singlet energy is collected to TTBP, the distance from a TTBP molecule to the farthest **A2** molecule is estimated to be about 5.8 nm by using the density of **A2** film. This distance is not directly correlated with the singlet diffusion length of 26.1±3 nm in **A2** films obtained by the fluorescence quenching method. The reason for this discrepancy is not clear but probably related to different rate constants of singlet energy quenching/collection, or unfavorable TTBP position/orientation in **A2** films. Nevertheless, the Φ_{FL} value was significantly improved by the synergistic effect of long-range diffusion of delocalized **A2** singlet excitons and the high fluorescence quantum yield of molecularly dispersed TTBP in the blend films.

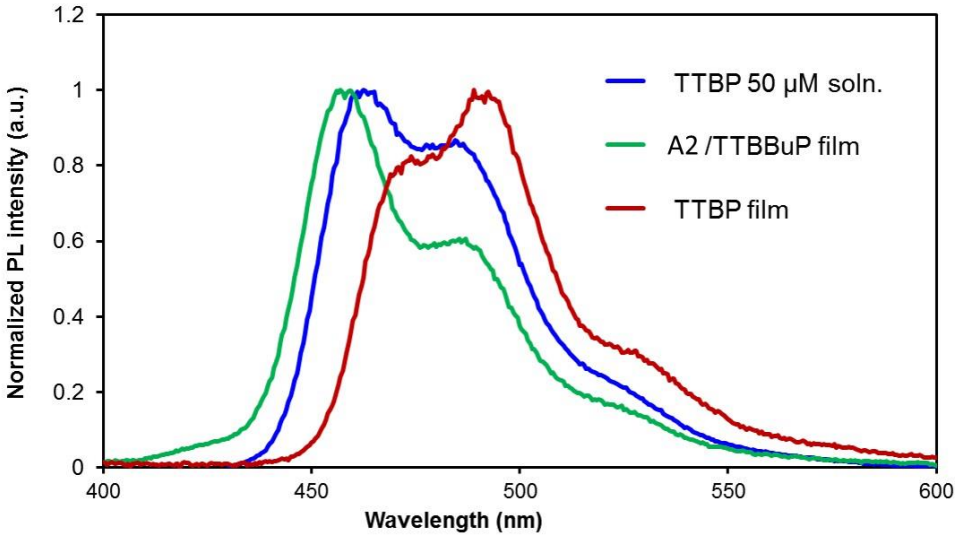

Figure 5-3-9. (a) PL spectra of TTBP in 50 μM Chloroform solution (blue), **A2**/TTBP blend film at 0.5 mol% TTBP (green) and spin-coated film of TTBP (red). Excitation wavelength was selected as λ_{ex} =350 nm.

5-3-4 Suppressed back energy transfer and upconverted energy collection in PtOEP/ A2/TTBP ternary films

For the realization of upconverted energy collection, PtOEP/**A2**/TTBP blend films were prepared by spin-coating. In these films, PtOEP, **A2** and TTBP act as triplet donor, triplet acceptor and energy collector/emitter, respectively. We confirmed that the photophysical properties of spin-coated **A2** films were not affected by adding 0.1 mol% of PtOEP (Figure 5-3-10). Interestingly, in our previous report, we used the drop-cast instead of spin-coating to make solid samples, and we observed that the addition of the same amount of PtOEP completely changed the absorption and emission spectra of **A2**. Thus the spin-coating is found to be the effective method to maintain the original photophysical properties in the presence of additives.

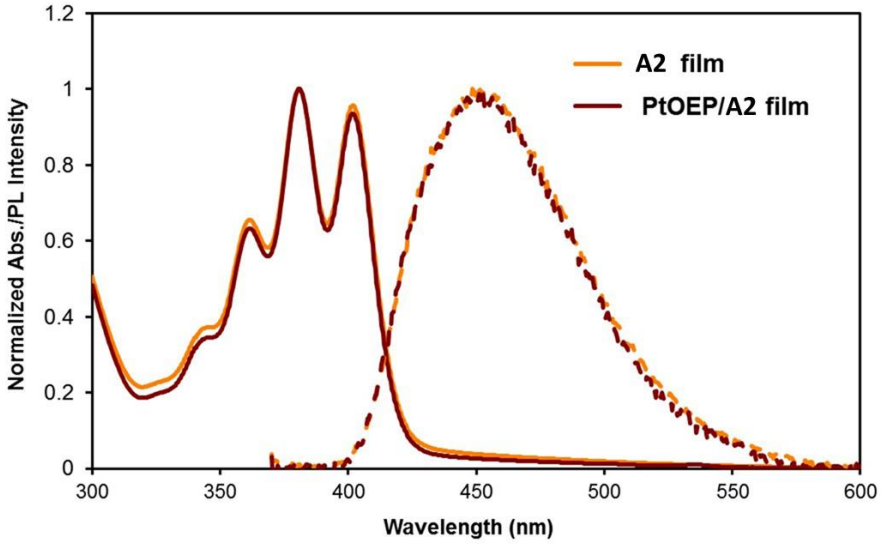

Figure 5-3-10. UV-vis absorption spectra (solid lines) and emission spectra (dashed lines) of **A2** films with (deep red) and without (orange) 0.1 mol% PtOEP. The excitation wavelength was selected as λ_{ex} =350 nm.

To improve the UC efficiency in condensed systems, it is important to suppress the back energy transfer from upconverted singlet state to donor molecules. We evaluated this factor by measuring prompt fluorescence decay curves of spin-coating films prepared by using different components. Figure 5-3-11a shows the comparison of fluorescence decays of **A2** and **A2**/PtOEP films. The decay became apparently faster by the addition of PtOEP, and the average lifetime decreased from 29.7 ns to 17.8 ns by adding 0.1 mol% PtOEP. A certain amount of reduction in lifetime after adding PtOEP indicates the presence of back energy transfer. A back energy transfer efficiency Φ_{BET} is quantified by a similar manner as equation (5). For the **A2**/PtOEP blend films, Φ_{BET} is estimated as 40%, showing the major adverse effect. On the other hand, in the case of the PtOEP/**A2**/TTBP ternary film, a negligible effect of back energy transfer was observed (Figure 5-3-11b). The average lifetime of TTBP in the PtOEP/**A2**/TTBP films (8.93 ns) was almost similar to that of **A2**/TTBP films (8.44 ns).

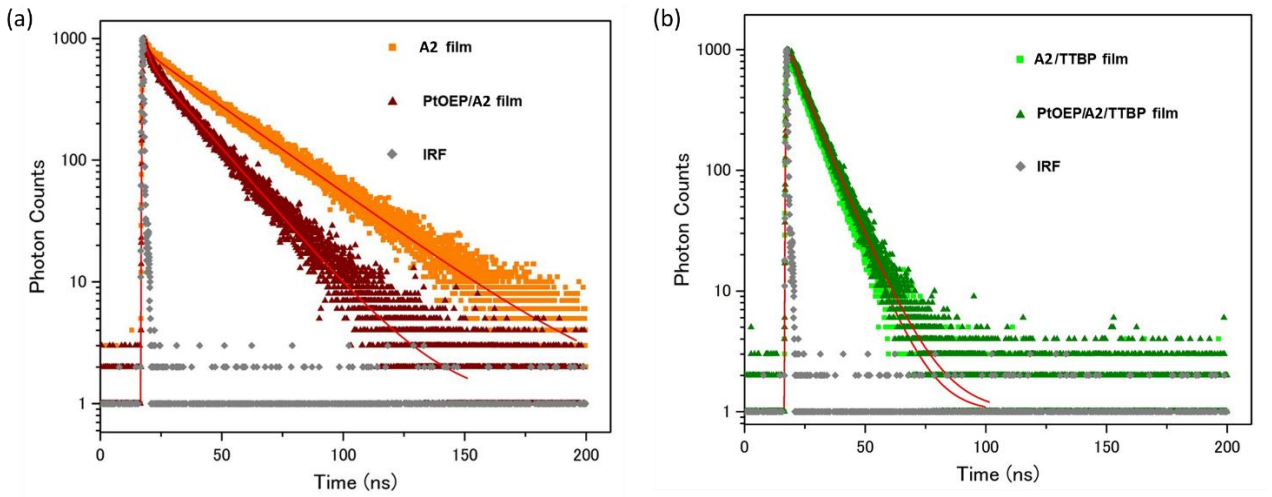

Figure 5-3-11. (a) PL decays of **A2** films with (deep red) and without (orange) 0.1 mol% PtOEP. (b) PL decays of **A2**/0.5 mol% TTBP films with (deep green) and without (light green) 0.1 mol% PtOEP. The excitation wavelength was selected as λ_{ex} =365 nm and PL decays were detected at 460 nm. Fitting lines are indicated as red lines.

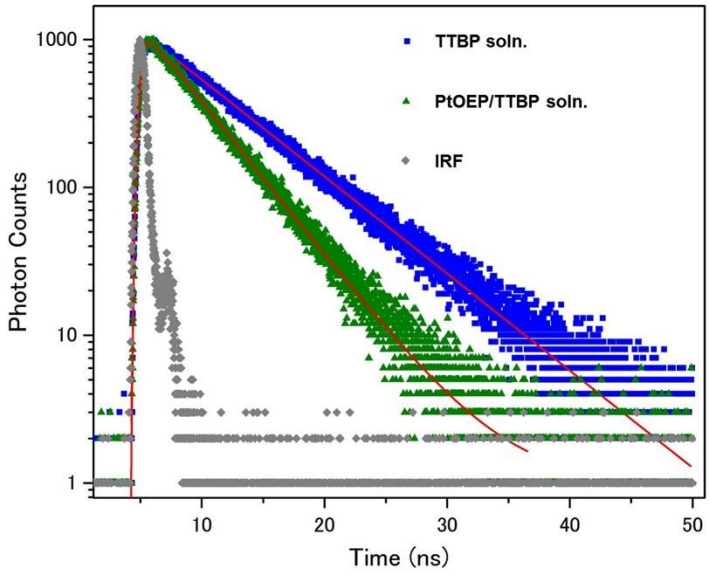

Figure 5-3-12. PL decays of 10 mM TTBP solution with (green) and without (blue) 2 mM PtOEP. The excitation wavelength was selected as λ_{ex} =365 nm. Fitting lines are indicated as red lines.

To our interest, a considerable back energy transfer from TTBP to PtOEP (Φ_{BET} = 37%) was observed in a chloroform solution of TTBP and PtOEP when the concentration of these molecules is same as that in **A2** films (Figure 5-3-12). These results clearly demonstrate that the unfavorable back energy transfer, inevitable in the molecular diffusion system, can be effectively suppressed by the appropriate spatial control of multiple chromophores in the diffusion-free solid-state architecture.

Finally, the effect of the energy collector TTBP upon TTA-UC performances was evaluated. Under excitation with a 532 nm laser, an upconverted emission was clearly observed from both the PtOEP/**A2** and PtOEP/**A2**/TTBP blend films (Figure 5-3-13). The difference in spectral shape of upconverted emission between these two samples reflects the effect of energy collection to TTBP as observed in the fluorescence spectra (Figure 5-3-7a).

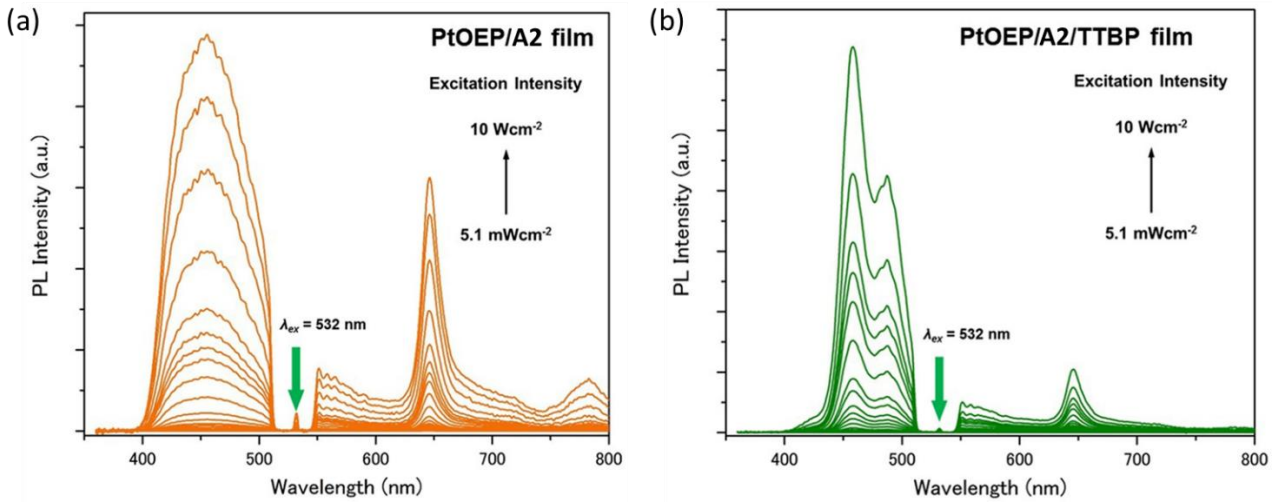

Figure 5-3-13. PL spectra of (a) PtOEP/**A2** films (0.1 mol% PtOEP) and (b) PtOEP/**A2**/TTBP films (0.1 mol% PtOEP, 0.5 mol% of TTBP) under Ar with various excitation intensities (λ_{ex} = 532 nm). The scattered incident light was removed by using a 532 nm notch filter.

The TTA-UC mechanism in these samples was confirmed by excitation power dependence of UC PL intensity and UC PL decay profiles. Generally, TTA-UC emission intensity shows a quadratic-to-linear transition with increasing the excitation intensity, and the transition point gives a threshold excitation intensity (I_{th}).[34-36] Above I_{th}, the TTA becomes the main deactivation channel for the acceptor triplets. The excitation intensity dependence of UC PL intensity of the blend films showed the quadratic-to-linear transition, and similar I_{th} values of 207 mWcm^{-2} and 195 mWcm^{-2} for PtOEP/**A2** and PtOEP/**A2**/TTBP films (Figure S5-3-14a). From the tail part of the UC PL decay curves shown in Figure 5-3-14b, we estimated similar triplet lifetime τ_T of these samples (3.9 ms for PtOEP/**A2** film and 3.5 ms for PtOEP/**A2**/TTBP). These results provide the clue about chemical species responsible for TTA process. The similar I_{th} and τ_T values imply that the TTA process mainly takes place between **A2** molecules regardless of the presence of TTBP. Therefore, in the current system TTBP is considered to mainly act as energy collector of the singlet state formed after the TTA process (Figure 5-1-1).

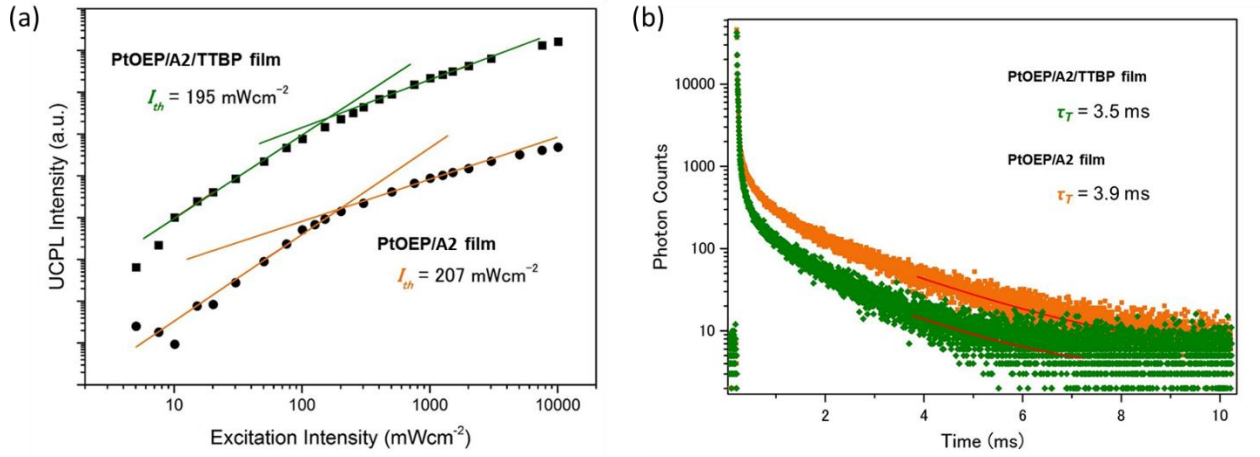

Figure 5-3-14. (a) Double logarithmic plots of the UC PL intensity as a function of the excitation intensity for PtOEP/**A2** films (orange) and PtOEP/**A2**/TTBP films (green) under Ar atmosphere. The linear fits with slope 2 and 1 in the lower and higher excitation intensity regimes are shown. (b) PL decays at 460 nm for PtOEP/**A2** films (orange) and PtOEP/**A2**/TTBP films (green) under Ar atmosphere. The red fitting curves were obtained by considering the known relationship of $I_{UC}(t) \propto \exp(-t/\tau_{UC}) = exp(-2t/\tau_T)$, where τ_{UC} is UC emission lifetime and τ_T is triplet lifetime.

In general, quantum yield is defined as the ratio of absorbed photons to emitted photons, and thus the maximum quantum yield of TTA-UC (Φ_{UC}) is 50%. However, many reports multiply this value by 2 to set the maximum efficiency at 100%. To avoid the confusion between these different definitions, the UC efficiency is written as Φ_{UC}' (= $2\Phi_{UC}$) when its maximum is normalized to be 100%. TTA-UC efficiency Φ_{UC}' of each film was determined by the relative method with Nile red as a standard. A relatively high Φ_{UC}' value of 4.2% was observed for PtOEP/**A2** film (Figure 5-3-15). The gradual decrease in the high excitation intensity regime might be due to the degradation caused by the strong laser excitation. Remarkably, the addition of TTBP increased the Φ_{UC}' value to 9.0%, which is one of the highest values among crystalline upconverters. This significant improvement of UC efficiency should originate from the synergistic effect of the enhancement in fluorescence quantum yield by the singlet energy collection to TTBP and the suppressed back energy transfer from TTBP to PtOEP.

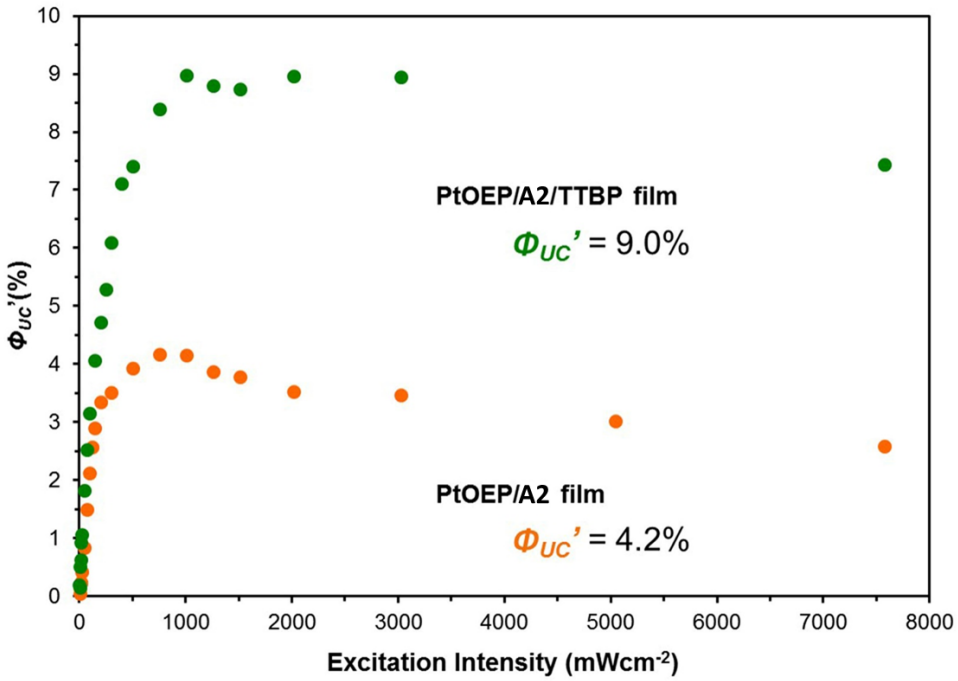

Figure 5-3-15. TTA-UC efficiency as a function of the excitation intensity of 532 nm laser for PtOEP/**A2** films (orange) and PtOEP/**A2**/TTBP films (green) under Ar atmosphere.

5-4 Conclusion

In this chapter, the UC efficiency in the solid-state has been improved based on the detailed understanding of exciton dynamics related to the energy collection process. Highly efficient singlet energy harvesting was realized thanks to the long-range diffusion of delocalized singlet excitons in the assembled state. The introduction of the energy collector not only improved the fluorescence quantum yield, but also suppressed the back energy transfer to the donor, both of which have been the serious problems of triplet energy migration-based UC in solvent-free condensed systems. In terms of device fabrication, the simple and scalable solution-based process has a significant advantage. While our current study focused on the benchmark green-to-blue TTA-UC, this strategy would be able to be generalized to other wavelength conversions. The NIR-to-visible TTA-UC is extremely important for energy and biology applications, and recent research efforts have enabled this by developing new types of triplet sensitizer such as inorganic semiconductor nanocrystals and S-T absorption metal complexes.[11,25-30] However, the broad absorption of these triplet donors extensively overlaps with acceptor emission, where the back energy transfer is the apparent issue even in solution systems. The singlet energy collection approach could also solve this issue by suppressing the back energy transfer. The singlet energy migration and collection would become a crucial strategy to realize an ultimately efficient TTA-UC in the solid-state.

References

(1) S. Baluschev, T. Miteva, V. Yakutkin, G. Nelles, A. Yasuda and G. Wegner, *Phys. Rev. Lett.*, 2006, **97**, 143903.

(2) T. N. Singh-Rachford and F. N. Castellano, *Coordin. Chem. Rev.*, 2010, **254**, 2560-2573.

(3) J. Z. Zhao, S. M. Ji and H. M. Guo, *Rsc Adv.*, 2011, **1**, 937-950.

(4) A. Monguzzi, R. Tubino, S. Hoseinkhani, M. Campione and F. Meinardi, *Phys. Chem. Chem. Phys.*, 2012, **14**, 4322-4332.

(5) Y. C. Simon and C. Weder, *J. Mater. Chem.*, 2012, **22**, 20817-20830.

(6) J. H. Kim and J. H. Kim, *J. Am. Chem. Soc.*, 2012, **134**, 17478-17481.

(7) V. Gray, A. Dreos, P. Erhart, B. Albinsson, K. Moth-Poulsen and M. Abrahamsson, *Phys. Chem. Chem. Phys.*, 2017, **19**, 10931-10939.

(8) J. Zhou, Q. Liu, W. Feng, Y. Sun and F. Y. Li, *Chem. Rev.*, 2015, **115**, 395-465.

(9) M. Haring, R. Perez-Ruiz, A. Jacobi von Wangelin and D. D. Diaz, *Chem. Commun.*, 2015, **51**, 16848-16851.

(10) T. F. Schulze and T. W. Schmidt, *Energy Environ. Sci.*, 2015, **8**, 103-125.

(11) N. Yanai and N. Kimizuka, *Acc. Chem. Res.*, 2017, **50**, 2487-2495.

(12) S. P. Hill and K. Hanson, *J. Am. Chem. Soc.*, 2017, **139**, 10988-10991.

(13) Z. Y. Huang and M. L. Tang, *J. Am. Chem. Soc.*, 2017, **139**, 9412-9418.

(14) R. R. Islangulov, J. Lott, C. Weder and F. N. Castellano, *J. Am. Chem. Soc.*, 2007, **129**, 12652-12653.

(15) J. H. Kim, F. Deng, F. N. Castellano and J. H. Kim, *Chem. Mater.*, 2012, **24**, 2250-2252.

(16) F. Marsico, A. Turshatov, R. Pekoz, Y. Avlasevich, M. Wagner, K. Weber, D. Donadio, K. Landfester, S. Baluschev and F. R. Wurm, *J. Am. Chem. Soc.*, 2014, **136**, 11057-11064.

(17) S. H. Lee, D. C. Thevenaz, C. Weder and Y. C. Simon, *J. Polym. Sci. A Polym. Chem.*, 2015, **53**, 1629-1639.

(18) S. Baluschev, V. Yakutkin, G. Wegner, B. Minch, T. Miteva, G. Nelles and A. Yasuda, *J. Appl. Phys.*, 2007, **101**, 023101.

(19) R. Vadrucci, C. Weder and Y. C. Simon, *J. Mater. Chem. C*, 2014, **2**, 2837-2841.

(20) H. Goudarzi and P. E. Keivanidis, *J. Phys. Chem. C*, 2014, **118**, 14256-14265.

(21) M. Hosoyamada, N. Yanai, T. Ogawa and N. Kimizuka, *Chem.-Eur. J.*, 2016, **22**, 2060-2067.

(22) N. Yanai and N. Kimizuka, *Chem. Commun.*, 2017, **53**, 655-655.

(23) K. Kamada, Y. Sakagami, T. Mizokuro, Y. Fujiwara, K. Kobayashi, K. Narushima, S. Hirata and M. Vacha, *Mater. Horiz.*, 2017, **4**, 83-87.

(24) T. Ogawa, N. Yanai, H. Kouno and N. Kimizuka, *J. Photon. Energy*, 2017, **8**, 022003.

(25) C. Mongin, S. Garakyaraghi, N. Razgoniaeva, M. Zamkov and F. N. Castellano, *Science*, 2016, **351**, 369-372.

(26) M. F. Wu, D. N. Congreve, M. W. B. Wilson, J. Jean, N. Geva, M. Welborn, T. Van Voorhis, V. Bulovic, M. G. Bawendi and M. A. Baldo, *Nat. Photon.*, 2016, **10**, 31-34.

(27) Z. Y. Huang, X. Li, M. Mahboub, K. M. Hanson, V. M. Nichols, H. Le, M. L. Tang and C. J. Bardeen, *Nano Lett.*, 2015, **15**, 5552-5557.

(28) Z. Y. Huang, D. E. Simpson, M. Mahboub, X. Li and M. L. Tang, *Chem. Sci.*, 2016, **7**, 4101-4104.
(29) K. Okumura, K. Mase, N. Yanai and N. Kimizuka, *Chem. -Eur. J.*, 2016, **22**, 7721-7726.
(30) Y. Sasaki, S. Amemori, H. Kouno, N. Yanai and N. Kimizuka, *J. Mater. Chem. C*, 2017, **5**, 5063-5067.
(31) O. V. Mikhnenko, H. Azimi, M. Scharber, M. Morana, P. W. M. Blom and M. A. Loi, *Energy Environ. Sci.*, 2012, **5**, 6960-6965.
(32) O. V. Mikhnenko, J. Lin, Y. Shu, J. E. Anthony, P. W. M. Blom, T. Q. Nguyen and M. A. Loi, *Phys. Chem. Chem. Phys.*, 2012, **14**, 14196-14201.
(33) O. V. Mikhnenko, P. W. M. Blom and T. Q. Nguyen, *Energy Environ. Sci.*, 2015, **8**, 1867-1888.
(34) A. Monguzzi, J. Mezyk, F. Scotognella, R. Tubino and F. Meinardi, *Phys. Rev. B*, 2008, **78**, 195112.
(35) Y. Y. Cheng, T. Khoury, R. G. C. R. Clady, M. J. Y. Tayebjee, N. J. Ekins-Daukes, M. J. Crossley and T. W. Schmidt, *Phys. Chem. Chem. Phys.*, 2010, **12**, 66-71.
(36) A. Haefele, J. Blumhoff, R. S. Khnayzer and F. N. Castellano, *J. Phys. Chem. Lett.*, 2012, **3**, 299-303.

Chapter 6 Conclusion and future remark

In this thesis, rational designs for triplet energy migration-based photon upconversion system by introducing molecular self-assembly concept have been proposed. The issues that have been achieved for each study are summarized below.

In chapter 2, the occurrence of TEM-UC in the self-assembled system in solution media was have been proved for the first time. In this system, all the advantages of the TEM-UC proposed in Chapter 1, namely diffusion of fast triplet excitons, low I_{th} value, and oxygen stability of UC luminescence, could be expressed. Although more specific strategies are required in more condensed and molecular diffusion-suppressed media, these high performances in solution succeeded in showing the high potential of TEM-UC strategy.

In chapter 3 and 4, guidelines to achieve homogeneous dispersion of donor molecules in the acceptor crystals are shown, which has been one of the outstanding problems for the realization of TEM-UC in condensed materials. In chapter 3, kinetically-controlled crystallization concept was the key to overcome this issue. In chapter 4, more sophisticated strategy, to achieve the homogeneous dispersion of donor molecules in acceptor crystals by keeping the highly-ordered crystal structure was developed. It takes advantage of the electrostatic interactions in ionic networks, which accommodate donor molecules without phase sgregation. The impact of the crystal defects to the Φ_{UC}' was also firstly described in this chapter.

In chapter 5, a solution to overcome the issue of reabsorption or back energy transfer of the upconverted energy to donor molecules has been developed. this approach introduced a singlet energy collector as the third component. Efficient singlet energy harvesting of the upconverted singlet energy was realized thanks to the long-range diffusion of delocalized singlet excitons in the assembled state.

In this thesis, two types of approaches for efficient solid-state TEM-UC have been proposed; one is to introduce the ionic interactions between donor and acceptor in order to form aggregation-free dispersion of donor molecules in acceptor ionic crystals without losing the high crystal regularity, and another is the upconverted singlet energy collection by the introduction of the third component, highly fluorescent singlet energy collector, for improving the fluorescence quantum yield and avoiding the back energy transfer to the donor. For further development of this topic, to combine these two strategies should be examined. Considering the fact that a certain amount of back energy transfer and/or reabsorption have been observed in the current ionic crystal system, the introduction of the third ionic component, which is act as an energy collector, to the ordered ionic crystal will induce the further improvement of Φ_{UC}' value.

In another point of view, our current systems have shown moderately low I_{th} value, but for the practical applications, this value should be further improved. In order to achieve lower I_{th} value, the key parameters are, as we mentioned previously, the triplet lifetime and triplet diffusion constant. For the elongation of triplet lifetime compared to our proposed system, we synthesized DPA dicarboxylic acid-based acceptor ionic crystals (referred as to DPA ionic crystals, Fig. 6-1). In this system, introduced phenyl rings that have the twisted configuration of the anthracene aromatic plane are considered to act effectively to elongate the triplet lifetime because of the suppressed vibrational motion of. Actually, about two times longer triplet lifetime (7.6 ms) compared to the current ionic crystal system ($(DCA)_2ADC$) has been observed for DPA ionic crystals. Thus, if the triplet diffusion constant is sufficiently large, this system will work with better I_{th} value. However, judging from the crystal structure of DPA ionic crystals, the small diffusion constant of triplet excitons would be expected due to the quite limited overlap between chromophore orbitals. In order to improve this situation, we propose to apply diphenyl amine as a counter cation for ionic composite. If the triplet energy can migrate by utilizing the π orbitals of cations, larger triplet diffusion coefficient and subsequent low I_{th} value for TEM-UC would be expected.

This proposed concept would be widely applicable to a variety of chromophore combinations, including the recently-developed precious metal-free S-T absorption systems and NIR-to-visible UC systems.

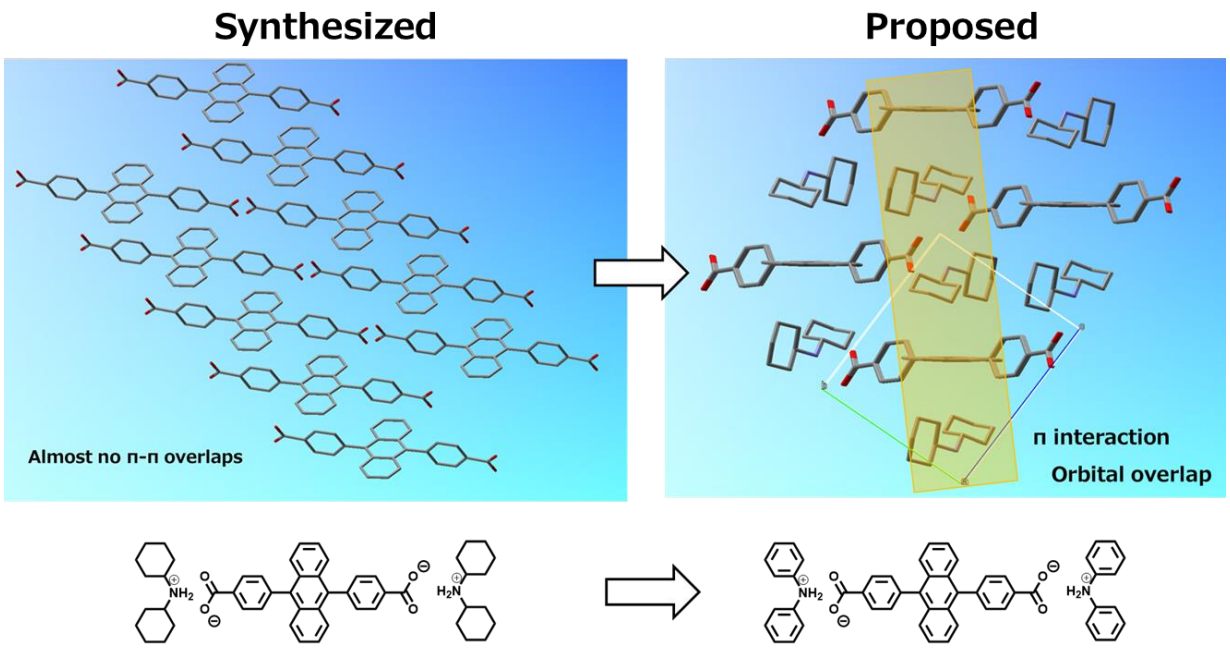

Figure 6-1. Crystal structure of synthesized DPA ionic crystals and proposed novel ionic crystal with utilizing DPA dicarboxylic acid and diphenylamine. The crystal structure of the novel ionic crystals is anticipated from the structural analysis of DPA ionic crystals.

Acknowledgments

The study in this thesis has been carried out under the direction of Professor Nobuo Kimizuka during April 2012 – March 2018 at the Department of Chemistry and Biochemistry, Graduate School of Engineering, Kyushu University.

The author would like to express his sincerest gratitude to Professor Nobuo Kimizuka for his great guidance, precious suggestion, and warm encouragement throughout this work. The author is greatly indebted to Associate Professor Nobuhiro Yanai for his helpful suggestion, continuous encouragement, and valuable discussion. The author wishes to express his gratitude to Associate Professor Teppei Yamada for his precious suggestion and support. The author is greatly indebted to Associate Professor Shigenori Fujikawa for his valuable advice and warm encouragement. The author wishes to express his gratitude to Assistant Professor Masa-aki Morikawa for his valuable support and warm encouragement. The author would like to thank Technical Staff Kazumi Matsuno, Azusa Suematsu, Chihoko Fukakusa, and Ryo Maeda for their warm encouragements and supports.

The author sincerely appreciates Professor Yoshiki Katayama and Professor Takuma Yasuda for reviewing this thesis.

The author expresses great gratitude to Assistant Professor Angelo Monguzzi at Dipartimento di Scienza dei Materiali, Università Milano-Bicocca for his helpful suggestion and valuable discussion. The author would like to his sincerest gratitude to Professor Thuc-Quyen Nguyen, Associate Professor Takashi Okubo (Kindai University) and Mr. Brett Yurash their valuable suggestion and warm acceptance of my stay during October 2016 – December 2016 at Department of Chemistry & Biochemistry University of California, Santa Barbara.

The author wishes to express his gratitude to Professor Pengfei Duan (National Center for Nanoscience and Technology, China), Assistant Professor Shigesaburo Ogawa (Seikei University), Assistant Professor Hiroaki Iguchi (Tohoku University), Assistant Professor Shogo Amemori (Kanazawa University), Dr. Keita Ishiba, Dr. Joseph Ka Ho Hui, Dr. Kouta Masutani, Dr. Deepak Asthana, Dr. Rakesh Kumar Gupta, Dr. Pankaj Bharmoria, Dr. Biplab Joarder, Mr. Hisanori Nagatomi, Mr Kazuma Mase, Mr. Daisuke Kichise, Mr. Yuya Nagao, Mr. Masaya Matsuki, Mr Masanori Hosoyamada, Mr. Shota Hisamitsu, Mr. Taro Wakiyama, Ms. Rina Yoshida, Mr. Yimin Liang, Mr. Tsubasa Kashino, Mr. Hironori Kouno, Mr. Kanji Shiraishi, Mr. Ryosuke Yamamoto, Mr. Keisuke Kanakogi, Mr. Yuta Kubo, Mr. Tomoya Shimono, Ms. Mariko Kozue, Mr. Keisuke Okumura, Mr. Shinya Uchino, Mr. Hirotaka Ohara, Mr. Yoichi Sasaki, Ms. Hanyu Yang, Mr. Toshiki Eguchi, Mr. Yuki Nagai, Ms. Nao Hirakawa, Mr. Saiya Fujiwara, Mr. Junji Miyano, Mr. Yusuke Kawashima, Ms. Fan Gao, Ms. Risa Okeda, Ms. Mika Kinoshita, Mr. Takashi Kobayashi, Mr. Tetsuro Kobayashi, Mr. Keisuke Hayashi, Ms. Rena Haruki for warm supports and discussion.

Finally, the author wishes to offer special thanks to his parents Hideaki Ogawa and Chie Ogawa, his brother Shota Ogawa for constant financial supports and warm encouragement.

Taku Ogawa

Department of Chemistry and Biochemistry

Graduate School of Engineering, Kyushu University

March 2018